Instituto Tecnológico y de Estudios Superiores de Monterrey

Campus Monterrey

School of Engineering and Sciences

"Role of rheological properties in near field electrospun fibers morphology"

A thesis presented by

Domingo Ricardo Flores Hernández

Submitted to the
School of Engineering and Sciences
in partial fulfillment of the requirements for the degree of

Master of Science
In
Manufacturing Systems

Monterrey Nuevo León, May 16th, 2017

Instituto Tecnológico y de Estudios Superiores de Monterrey

Campus Monterrey

School of Engineering and Sciences

The committee members, hereby, certify that have read the thesis presented by Domingo Ricardo Flores Hernández and that it is fully adequate in scope and quality as a partial requirement for the degree of Master of Science in Manufacturing Systems

_____

Dr. Jaime Bonilla Ríos
Tecnológico de Monterrey
School of Engineering and Sciences
Principal Advisor

_____

Dr. Sergio Omar Martínez Chapa
Tecnológico de Monterrey
Committee Member

_____

Dr. José Antonio Sánchez Fernández
Tecnológico de Monterrey
Committee Member

_____

Dr. Rubén Morales Menéndez
Director Nacional de Posgrados
Tecnológico de Monterrey

Monterrey Nuevo León, May 16th, 2017

Declaration of Authorship

I, Domingo Ricardo Flores Hernández declare that this thesis titled, 'Role of rheological properties in near field electrospun fibers morphology' and the work presented in it are my own. I confirm that:

- This work was done wholly or mainly while in candidature for a research degree at this University.
- Where any part of this thesis has previously been submitted for a degree or any other qualification at this University or any other institution, this has been clearly stated.
- Where I have consulted the published work of others, this is always clearly attributed.
- Where I have quoted from the work of others, the source is always given. With the exception of such quotations, this thesis is entirely my own work.
- I have acknowledged all main sources of help.
- Where the thesis is based on work done by myself jointly with others, I have made clear exactly what was done by others and what I have contributed myself.

_____

Domingo Ricardo Flores Hernández

Monterrey Nuevo León, May 16th, 2017

Dedication

A mis padres Alicia y Hermenegildo

Por hacer lo que hacen mejor, ser ellos mismos. No hay fuente mayor de fortaleza y amor que la que viene del ejemplo.

To my sister Blanca for giving me the pleasure of reading and Miguel for always being there

To my cousin Arely, because I want to be a good example for you

To my daughter

Adamari

You always push me to be better without knowing

To my fiancée

Ximena

You trust in my more than I do. Only you can see what I am capable of even when I myself want to give up.

Acknowledgements

I want to thank all those who have been side by side with me. For all those who taught patience, empathy and courage.

To Dr. Jaime Bonilla Ríos

Thank you for all your advices in and out of class, for sharing your knowledge and for supporting me during this whole travel.

To Cesar Ibarra

For showing me what two chemical engineers are capable of.

To Braulio Cárdenas

For all his help, patience and time during the experiments

I want to thank Tecnológico de Monterrey support on tuition and CONACyT with the support for living

Role of rheological properties in near field electrospun fibers morphology

by

Domingo Ricardo Flores Hernández

ABSTRACT

In electrospinning process, polymer nanofibers are formed with diameters in the submicron scale when a drop of viscoelastic polymer solution is subjected to a high voltage electrostatic field, when the charge force overcomes the surface tension of the solution, a beam is projected onto a collector. Among other parameters, the rheological properties of the polymer solution can significantly influence fiber formation during the electrospinning process, although this is well known, there is still no clear understanding of the effect of these properties to form fibers with morphology and structure consistent and controlled.. The study was conducted for a system of SU-8 2002 (an epoxy-based negative photoresist) dissolved in cyclopentanone with poly(ethylene) oxide, PEO, and tetrabutylammonium tetrafluoroborate, TBATFB, as additives. The fibers were electrospun in an Electro Mechanical Spinning, EMS, platform. The rheological properties of the polymer solution were studied under shear conditions and combined with oscillatory data to get uniaxial deformation behavior using the Wagner constitutive equation. The elongational viscosity, η_e, in the projected beam is estimated by using data from oscillatory tests. For this purpose, solutions of SU-8 2002 were tested and then electrospun systematically over a range of concentrations. It was found that the variation in concentration of the additives modifies the viscoelastic properties of the solutions and, therefore, the electrospinnability. As PEO concentration is increased the complex, elongational and shear viscosity also increases. For concentrations of TBATFB, the variation of the viscosities has not a clear behavior pattern. The most regular and thinnest fibers were those obtained from a concentration of 99.5, 0.25 and 0.25 wt%. of SU-8 2002, PEO and TBATFB respectively. With the acquired information, process variables for the EMS such as fabrication velocity, voltage and tip-to-collector distance were improved.

NOMENCLATURE

%γ	Amplitude gamma
$\dot{\varepsilon}$	Extensional rate
|G*|	Complex modulus
|η*|	Complex viscosity
°	Angular degrees
°C	Celsius degrees
A	Cross section area of a polymer thread
a_i	Weighted factor for memory function and for relaxation spectra
AS	Amplitude sweep
b	inter-bead length
c	Concentration
*c**	Critical concentration
CaBER	Capillary breakup extensional rheometer
C-MEMS	Carbon micro electromechanical systems
CP	Cone-and-plate geometry
Cp	Heat capacity
CST	Coil stretch transition
C_t^{-1}	Finger strain tensor for unidirectional shear flow
D	Diameter of a die
D	Diffusion coefficient
$D_{mid}(t)$	Measured diameter in CaBER
D_R	Global diffusion coefficient
ES	Electrospinning
F	Uniaxial pulling force
f_1	Weighted factor for Wagner model
FC	Flow curve
F_{DO}	Down ward force in polymer jets
F_R	Resultant force in polymer jets
FS	Frequency sweep
F_{UO}	Outward force in polymer jets
g	gravity
G(t)	Linear viscoelastic relaxation modulus
G’	Storage modulus
G’’	Loss modulus
$h(I_1,I_2)$	Damping function
I_1, I_2	Tensor invariants
IDE	Interdigitated electrodes
k	Fluid conductivity
k	Thermal conductivity
L	Longitude
LVER	Linear viscoelastic region
MEMS	Micro electromechanical systems
Mn	Number average molecular weight
Mv	Viscosity average molecular weight
Mw	Weight average molecular weight
MWD	Molecular weight distribution
N	Number of beads in Rouse model

N1	First normal stress difference
n1	Fitting parameter in Wagner model
n2	Fitting parameter in Wagner model
NFEMS	Near field electromechanical spinning
NLVER	Non-linear viscoelastic region
p	Scalar pressure
PEO	Poly(ethylene) oxide
Q	Polymer flow rate
R	Approximated radius of a polymer chain
r	Polymer jet radius
rpm	Revolutions per minute
SEM	Scanning electron microscope
T	Temperature
t	time
TBATFB	Tetrabutylammonium tetrafluoroborate
TTCD	Tip-to-collector distance
V	Voltage
υ	Velocity of the jet
v_{air}	Air velocity
wt%	Concentration in weight percentage
Z	Average number of polymer chains
z	Axial distance along the fiber axis
δ	Delay time
ε	Dielectric constant of the fluid
$\dot{\gamma}$	Shear rate
γ	Strain
$\gamma(t-t')$	Relative shear strain between any two times t and t'
η	Shear viscosity
η_0	Zero shear viscosity
η_e	Elongational viscosity
λ_i	Time constant for relaxation spectra
λ_{max}	Maximum length of a polymer chain
$\mu(t-t')$	Memory function
θ	Polymer jet angle
ρ	Density
σ	Stress
σ_e	Elongational stress
τ_d	Longest relaxation time
τ_r	Rouse longest relaxation time
ω	Angular frequency, rad/s or s^{-1}
ξ	Friction of beads in Rouse model

LIST OF FIGURES

LIST OF TABLES

Table of Contents

CHAPTER I INTRODUCTION

1.1 MOTIVATION

The Electrostatic spinning or Electrospinning (ES) is a technique where submicron fibers can be obtained by applying an electrostatic field to a polymer melt or solution. This micro and nanofibers have a large number of applications from filtration, batteries, and protective clothes to tissue engineering, controlled drug delivery and, in recent years, carbon micro electromechanical systems (C-MEMS). In the ITESM sensors and devices group, it is wanted to create interdigitated electrodes, IDE's, with suspended nanofibers between electrodes by using Near Field Electromechanical Spinning method to be used further in high sensibility gas sensors. This technique has been widely studied by this group; nevertheless, consistent depositions of nanofibers with controlled geometry are not achieved yet. Process variables such as process parameters, ambient parameters and solution properties have been broadly studied. However, there is a lack of information about the rheological properties of the solution in the bulk and during fiber formation. Understanding how these properties affect the final characteristics of the fibers can reduce time of experimentation and make a better selection of the process variables.

1.2 PROBLEM STATEMENT

Even when the electrospinning technique is capable of create fibers with a high aspect ratio, generate meshes with controlled patterns is difficult, usually random or semi-aligned fibers are obtained. In some applications, as it is the case of C-MEMS, the alignment of the fibers is crucial to have the adequate performance of the dispositive. Nowadays, a variation of the electrospinning process is gaining attention due to the ability of create controlled patterns with micro and nanofibers; this technique is called Electro Mechanical Spinning, EMS (In literature it can be also found as Near Field electromechanical spinning, NFESM). In EMS, short distances from the tip to the collector and a low voltage are used to avoid the bending instabilities present in far field electrospinning. Also, a three axis platform is used to create high resolution patterns. Although it seems to be a straightforward technique, a wide number of variables can

affect the final properties of the fibers. Process variables such as flow rate, applied voltage, distance from tip to collector, speeds of pattern fabrication, UV light, conductivity of the solution, etc., must be fairly well controlled in order to produce high quality fibers, see Figure 1.2-1. However, understanding the process of elongation of the polymer during fiber formation and the rheological phenomena involved could help in the selection of the optimal parameters for fibers production.

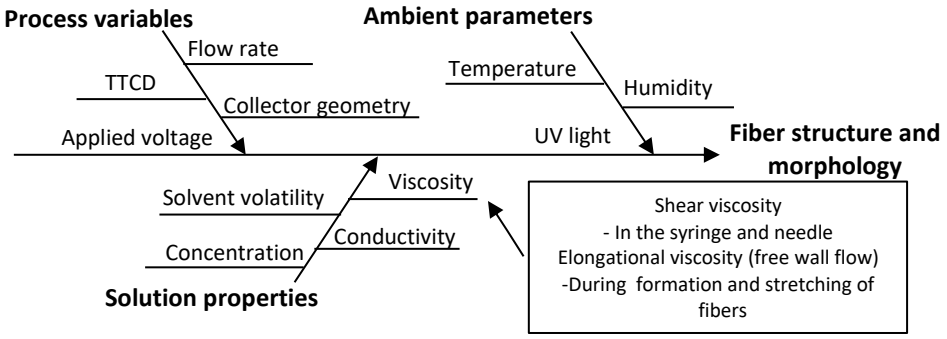

Figure 1.2-1 Process parameters involved during electrospinning process

In the sensors and devices group, a polymer solution of SU-8 2002 dissolved in cyclopentanone with poly(ethylene) oxide and tetrabutylammonium tetrafluoroborate as additives was electrospun in a ESM platform. The University of California in Irvine research group found that the best formulation to get the thinnest fibers was 99:0.5:0.5 wt%. of SU-8 2002:PEO:TBATFB. Nonetheless, neither a rheological characterization nor an elongational flow study was presented for this system.

In this work, a series of polymer solutions with different concentrations of PEO and TBATFB were prepared, rheologically characterized and then electrospun in order to correlate the rheological properties of the solution with the final geometry of the fibers and also to propose the best parameter conditions for the depositions. Since the nature of the flow process is a free wall flow at different extensional rates (rate of deformation due to the stretching of the fibers), the viscoelastic properties of the solution are the major factor to understand the behavior of the fibers during its formation; for this reason

a deep study of the viscoelastic properties of the solution is presented, focusing on the transition from viscous to elastic behavior and the elongational viscosity.

1.3 Research Questions

- How the variation of PEO and TBATFB affect the rheological properties of the solution?
- What is the relation between the viscoelastic properties and the spinnability of the solution?
- Is the 99:0.5:0.5 % wt ratio the best composition to obtain the smallest and most consistent fibers?
- It is necessary to use PEO or TBATFB as additives?
- Can the process variables be improved by knowing the viscoelastic properties of the solution?

1.4 Solution Overview

The anticipated results are that the PEO will increase the viscosity of the solution as its concentration increases. A similar effect is expected for the variation of TBATFB in the solutions but less obvious than the effect of the PEO, since the salt is used to increase the conductivity of the solution. It is expected that higher concentrations of PEO will produce thick fibers while in some point, in lower concentrations, continuous fiber will not be produced. The effects of the salt are expected to improve the electrospinnability of the solution at lower voltages. The typical polymer solution may or not be the optimal, however it is expected to fine tune the additives to have smaller fibers. Once the rheological behavior of the solutions is understood, improvements to the process might be applied such as velocities of deposition, flow rate, voltage, etc.

1.5 Main Contributions

It is expected to improve the stability and geometry of the deposited fibers on inter digitated electrodes by modifying the process variables of EMS according to the adequate elongational process of the fibers by knowing its behavior based on the viscoelastic analysis of the polymer solution.

1.6 Dissertation Organization

The rest of the dissertation is organized as follows. In Chapter II, a review of the electrospinning process is presented. The process parameters such as process variables, ambient parameters and solution properties and their influence in fibers formation are studied. Furthermore, an overview of the polymer jets and their process of elongation, electrospinning models that attempt to describe and predict the fiber diameter and morphology from the process parameters, and the EMS process are presented. The rheological phenomena involved during electrospinning are described in Chapter III. The chapter begins with an introduction of polymer solutions and the elemental rheological tests amplitude sweep, flow curve and frequency sweep are explained. Moreover, the elongational flow and its features in polymer solutions are examined. Finally, are studied different equipment to measure the elongational viscosity and also an alternative way to obtain the elongational viscosity through mathematical modeling is defined. Chapter IV corresponds to the experimental section. In first place, the process for the selection of the parameters for the rheological characterization is explained. The materials and parameters used in rheological tests are presented. Also, a replicate of experiments of PEO solutions from literature is used as an experimental control. Besides, the materials and equipment for the preparations of the electrodes where the fibers are going to be deposited is depicted. Finally, the process variables used during the fiber deposition in the EMS platform are shown. Chapter V presents the results of the rheological characterization of the different sets of polymer solutions, and finally the fiber characterization using a scanning electron microscope, SEM, is depicted. A discussion of the results and the correlation between the rheological results and the resultant fibers is made. In Chapter VI the conclusions of this work and the considerations to future works are presented.

CHAPTER II ELECTROSPINNING

INTRODUCTION

The electrostatic spinning or electrospinning is a technique by which polymer nanofibers with submicron-scale diameters are formed when a droplet of a viscoelastic polymer solution is subjected to a high voltage electrostatic field [1]. When the surface tension is overcome by the electrical charge, an electrically charged polymer beam (jet) is projected onto a collector. This technique was first observed in 1897 by Rayleigh, widely studied by Zeleny in 1914 on electrospraying and finally patented by Formhals in 1934. However no further relevant studies are presented until 1969 in Taylor's work on electrically driven charged jets which provides the basis for further studies on the subject, but not until the late eighties and early nineties that takes interest from the scientific community through the work of Darrel H. Reneker [2].

Figure 2.1 a) Number of patents published yearly and b) Number of items published yearly from 2001 to 2011. Adapted from Persano (2013) [3].

In recent years the electrospinning has gained industrial and scientific interest. In Figure 2.1 the increasing number of patents and publications over the last years is shown. This increasing interest from researchers and industry comes from the numerous applications that nanofibers may have, like tissue engineering, water and air filtration, controlled drug delivery, protective clothing, microelectromechanical systems (MEMS),

carbon microelectromechanical systems (C-MEMS) among others. Besides the applications, another attractive feature about ES is that it is relatively cheap and straightforward process compared with other techniques for fiber fabrication.

In ES, the main process variables are the applied voltage, the feed rate of the solution, types of collectors, distance from the tip to the collector, TTCD, polymer solution parameters such as the polymer molecular weight, surface tension and conductivity [4]. These parameters have been extensively studied to establish a relationship between them and the morphology of the resulting fibers, although there is a certain understanding of the phenomenon, there is not a clear comprehension of the role played by the rheological properties during the formation of nanofibers and how these affects the morphology of the fibers.

The study of the rheological properties of the solution in the bulk and in the interface (at the exit of the nozzle and until the polymer jet reach the collector) may reduce the time of laboratory experimentation (usually done by trial and error) by predicting in advance how this properties influence the formation of the jet and the subsequent formation of fibers [5]. In literature there is not enough information about the viscoelastic properties of polymer solutions in the interface, where takes place the jet formation.

In this work a constitutive model is used to calculate the elongational viscosity of the polymer solution and the variation thereof during formation of the jet in electro-mechanical spinning process (EMS). A study is performed for the system of SU-8 2002 (an epoxy-based negative photoresist) dissolved in cyclopentanone for the production of C-MEMs. The solution of SU-8 2002/cyclopentanone is mixed with polyethylene oxide (PEO) to modify the viscoelastic properties of the polymer solution, and tetrabutylammonium tetrafluoroborate, (TBATFB) to enhance the conductivity. It is expected that the results will help to reduce the experimentation time in EMS processes and generate knowledge applicable to future research in electrospinning.

2.1 FUNDAMENTAL ASPECTS

In the electrospinning process a high voltage is used to create an electrically charged jet of a polymer solution that leaves a pipette or syringe tip. Before the jet reaches the collector, the solvent, in which the polymer is dissolved, evaporates; being then when the fibers are accumulated in the form of an interconnected web in the collector [4].

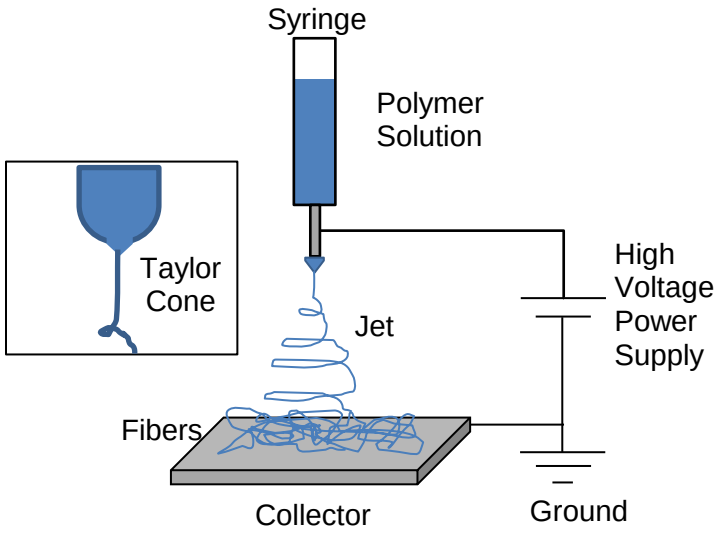

Figure 2.1-1 Typical setting for electrospinning process

One electrode is placed into the polymer solution or melt and the other one is attached to the collector or simply grounded as it shown Figure 2.1-1. The electric field is located at the end of the capillary tube or direct in the syringe tip that contains the solution fluid held by its surface tension. This induces a charge on the surface of the liquid. Mutual charge repulsion and the contraction of the surface charges cause a force directly opposite to the surface tension. As the intensity of the electric field is increased, the surface of the fluid at the tip of the capillary tube elongates to form a conical shape known as the Taylor cone [6]. When the electric field reach a critical value, the repulsive electrostatic force overcomes the surface tension and the charged jet of the fluid is ejected from the tip of the Taylor cone. The polymer solution jet undergoes an instability and elongation process, which allows the jet to become very long and thin. Meanwhile, the solvent evaporates, leaving behind a charged polymer fiber. In the case of melt

polymers the discharged jet solidifies when it travels in the air [7]. Even though there are variations of the electrospinning process like near field electrospinning, low voltage near Electro-Mechanical spinning, etc. the principle of the process remains the same.

2.2 Process Parameters

Several parameters influence fiber formation during electrospinning. These parameters are: i) process variables for example the polymer solution flow rate, electric potential at the tip of capillary tube, collector geometry and tip-to-collector distance (TTCD), ii) environmental parameters such as solution temperature, humidity and air velocity in the chamber electrospinning and iii) the solution properties such as viscosity, elasticity, conductivity and surface tension [8]. There are studies that relate the parameters mentioned and the role of these played during the electrospinning, in these works, researchers have changed the distance from tip to collector, applied voltage, flow rate of the solution, polymer concentration, polymer molecular weight among others, resulting in equations that combine these parameters to predict the morphology of the fibers [1].

2.2.1 Process Variables

There are basically four components to carry out the ES process: A capillary tube or needle, a polymer solution, a fiber collector and a power supplier [7]. Process variables are those that can change the final properties of a fiber by varying one or more of the components aforementioned. Table 2.2-1 shows the major process variables, their function and the effect on the process.

Table 2.2-1Major Process variables and their influence in electrospinning

Variable	Action	Effect
Polymer flow rate	Influence the speed of the jet and the mass flow of the solution.	If it is too small, there is not enough material to form a continuous fiber. Also, it has been observed that the final diameter of the fiber increases as the flow rate increases too [1], [9], [10].
Collector Geometry	Establish the orientation of the fibers	Depending on the shape and movement of the collector, the fibers could be oriented as random, aligned uniaxial, biaxial or as a pattern [4], [11].
Tip-to-collector distance	It allows the polymer jet to dry on its path to the collector.	At short distances flatter fibers are obtained. By increasing the distance the fibers begin to show a rounded shape. An optimal distance between the tip and the collector is required to promote the solvent evaporation and control the fiber formation [12], [13].
Applied voltaje	Induces the necessary charge on the electric field solution to initiate the process of electrospinning	In many cases, high voltages promotes the stretching of the solution due to Coulomb forces on the jet and therefore the reduction in diameter in the fibers and higher rate of evaporation the solvent in the fibers [1], [14]–[16].

2.2.2 AMBIENT PARAMETERS

Besides the process and solution variables, there are also parameters such as humidity, temperature, presence of ultraviolet light, etc., that can modify the final properties or morphology of electrospun fibers. Studies have been conducted to examine these environmental parameters during electrospinning. Mitt-Uppatham et al. investigated the effect of temperature during electrospinning of nylon 6 over a temperature range of 25 to 60°C and found that with the increase in temperature there is a decrease in fiber

diameter. He conclude that this effects are caused by the inverse relationship between temperature and viscosity [17].

Variation of humidity during electrospinning polystyrene solutions have been studied and show that increasing the environmental moisture forms small circular pores on the fiber surface [18]. This work shows that at very low percentages of moisture, a volatile solvent may evaporate too quickly. In some cases the evaporation is so rapid that problems arise at the tip of the syringe, so electrospinning can only be carried out few minutes before that the nozzle gets clogged by the dried polymer. Ultraviolet light naturally does not usually affect the electrospinning of conventional polymers, however during the electrospinning of solutions containing SU-8; this factor must be controlled. The SU-8 is an epoxy-based negative photoresist; this means that reacts in the presence of ultraviolet light creating polymer interlinked chains from SU-8 monomers, this change the rheological properties of the solution and the final properties of the fiber. Studies were carried out on solutions electrospinning SU-8, however, exposure to ultraviolet light is performed after the electrospinning [19].

2.2.3 SOLUTION PROPERTIES

Although electrospinning can be performed with melted polymers, in most cases, a polymer solution is preferred due to its easier preparation and wider number of systems that could exist. In principle, almost all polymers, natural or synthetic may be electrospun through judicious selection of solvents and or electrospinning process parameters. Besides, nano-particles or salts can be added to the solution to modify the desired properties of the fibers or to monitor the effect of any process variable [20]. For the preparation of the polymer solution usually pellets are added to a solvent contained in a glass vessel and the mixture is agitated until the polymer is completely dissolved. The resulting solution has features intrinsic to the polymer and solvent used, as well as any other additive in some cases [21], [22].

Properties such as surface tension and conductivity have been studied extensively for a large number of solvent/polymer systems [10], [23]–[26]. Nevertheless, there is not enough information about the properties such as viscoelasticity or surface

rheology, an important reason for this to happen is because of the complexity and difficulty of measure these properties on diluted polymer solutions. Some of the major properties are presented in Table 2.2-2 and their effects on final deposited fibers.

Table 2.2-2 Major Solution properties and their influence in electrospinning

Variable	Action	Effect
Surface Tension	Determines the formation of the jets	Generally, the high surface tension of a solution inhibits the electrospinning process because of the instability of jets this generates sprayed droplets [1], [27], [28].
Conductivity	Increases the capacity of the jet to be affected by voltage by the applied electric field	By increasing the conductivity of the solution there is a substantial decrease of the diameter of the electrospun fibers, whereas with low conductivity of the solution results in insufficient elongation of the jet by the electric force to produce uniform fibers and beads may be formed [16], [29], [30].
Molecular weight	Affects the final morphology of the fibers by modifying the viscosity, conductivity and surface tension of the solution	It has been observed that solutions with low molecular weight tend to form beads instead of fibers and high molecular weight solutions produce fibers with larger diameters [23], [31], [32].
Solvent Volatility	Controls the jet solidification	Solution prepared from solvents with very low volatility may result in wet fibers, fused fibers or even no fiber collection. On the contrary, a high volatility may result in intermittent spinning due to solidification of the polymer at the spinneret tip [8], [17], [18].
Shear Viscosity	Controls the fracturability of the polymer jets	In low viscosity solutions, surface tension is the dominant factor and just beads or beaded fibers are formed. An increase in the solution viscosity or concentration gives rise to a larger diameter and more uniform fiber [11], [34], [35].

2.3 Electro-mechanical spinning and Carbon Micro Electro Mechanical Systems

2.3.1 Electro-Mechanical Spinning, EMS

As it was explained in previous chapters, the typical electrospinning process is capable to produce long continuous fibers mats not only at laboratory scale but also, nowadays, is scaling up to industrial production [3]. However, for some applications a single fiber deposition or a controlled pattern is necessary. To avoid the whipping instabilities caused by the electric charges in non-deposited fiber, a novel method was developed using very short distances from tip-to-collector where the polymer jet is still straight, this technique is called Near-Field Electrospinning [36]. Modifications to this method have been made in order to control de accuracy of the fiber deposition. The collector is placed in a micro-controlled stage that can be programed to follow high controlled patterns; this variation is called Electro-Mechanical Spinning, EMS, (or low voltage near field electro-mechanical spinning). In Figure 2.3-1 the setting of EMS is depicted.

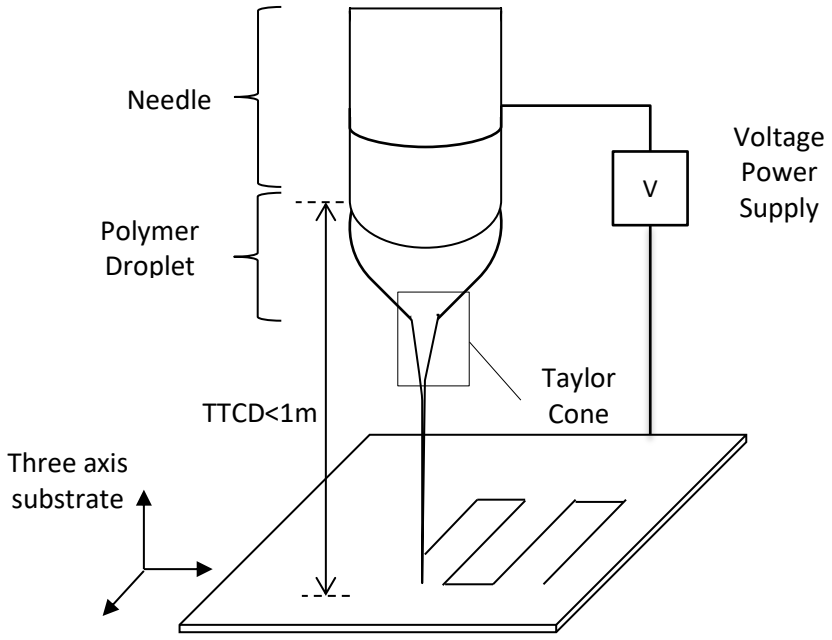

Figure 2.3-1 Setting up for Electro-Mechanical Spinning. Short distances from tip to collector and a three axis collector as major modifications from typical Electrospinning. Adapted from M. J. Madou (2011) [15].

This technique requires a reasonable less voltage than its counterpart, while in ES the applied voltage varies from 10 to 15kv in EMS, voltage is usually smaller than 500v. Also, the distances from tip-to-collector are reduced from 5 to 20 cm in ES, to less than 1 mm in EMS. The capacity of operate in low voltages improves the control over thickness of the micro and nanofibers. Coupled with this, the ability of control the speed of the stage, allows creating very fine fibers up to 20nm [3], [37]. Nevertheless, because of the short distances, in some polymer systems there is no enough distance to stretch adequately the fiber and only micro fibers can be obtained [38].

EMS is gaining attention in the field of C-MEMS where, in some applications, isolated fibers or highly controlled fiber depositions are required. Although there are several methods to produce this kind of carbon nanofibers such as vapor growth, discharge, laser ablation and chemical vapor deposition, etc., these techniques are often expensive and hard to be scaled up to a volume production [39], [40].

2.3.2 Carbon Micro Electro Mechanical Systems, C-MEMS

The two main stages for C-MEMS production are i) Polymer patterning, where technologies such as ES, EMS, photolithography, molding, laser writing, etc., are used; and ii) Carbonization, that results in an isometric reduction or shrinking of the original polymer pattern into a final carbon structure [41], see Figure 2.3.2-1.

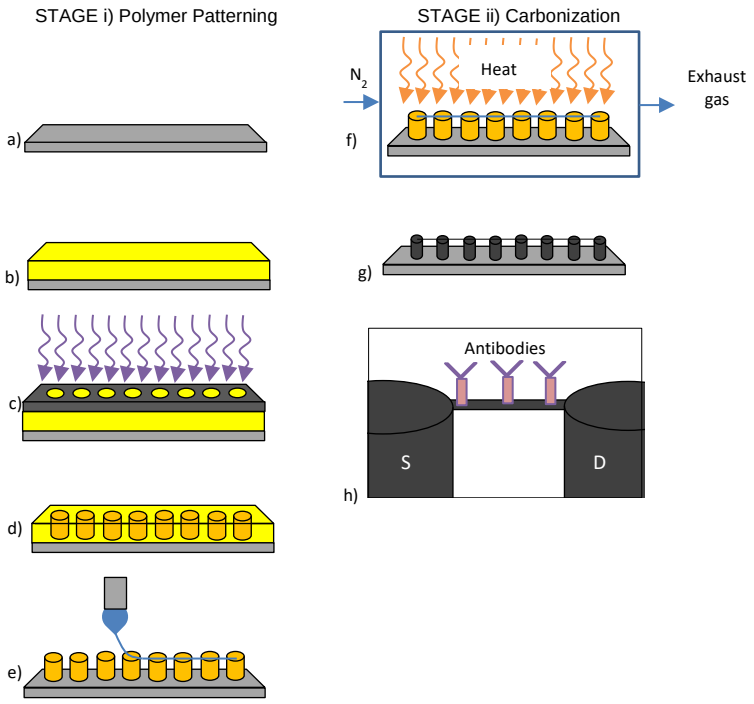

Figure 2.3-2. STAGE i: a) Silicon wafer. b) Spin coating of SU-8. c) UV exposure through a mask. d) SU-8 crosslinked and uncross linked posts to be developed. e) Developed wafer with posts of SU-8 crosslinked and fiber deposition by EMS.STAGE II): f) Carbonization via pyrolizis. g) Carbonized structure with reduced dimensions. h) Antibody functionalization of the fiber to work as a transistor.

In this figure all the steps required for this investigation are depicted with the exemption of the fiber functionalization that is out of the scope of this work. The sensibility of this kind of devices is enormous and can be used in a variety of applications such as high sensitivity gas sensor, transistors, supercapacitors, etc. [42]–[44].

2.4 Electrospinning Jets

When the electrostatic field overcomes the surface tension, a polymer jet is projected and follows a path from the tip of the syringe to the collector, where the fibers are deposited. In the beginning, the jet follows a straight path of a tapering cone, then through a series of successively smaller electrically driven coils. Each coil increases

their radius with each bending coil and finally it is deposited as a solid or semisolid fibers [45].

Before the jets are formed, when there is no flow rate and no electric field is applied, a droplet of polymeric fluid is formed at the tip of the needle or dispenser. This droplet is suspended only by surface tension and viscoelastic stresses. Once the electric field is applied, below a critical value, a steady state shape is formed with no jet ejection and this conical form is called Taylor cone [6].

When the electrostatic field exceeds the surface tension of the polymer a jet is formed. It is possible to observe three zones during the formation of the jet (i) Taylor cone (ii), the transition zone and (iii) the jet, as it shows Figure 2.4-1. There have been studies on the rheological properties in these areas and developed new methods for measuring the speed of the jet at any point after it leaves the nozzle until it reaches the collector, nevertheless these methods are in initial phases and numerous improvements have to be done [46]. For the case of electrospinning, the cone-jet regime is of particular importance since it represents the initial stage of formation of the fiber.

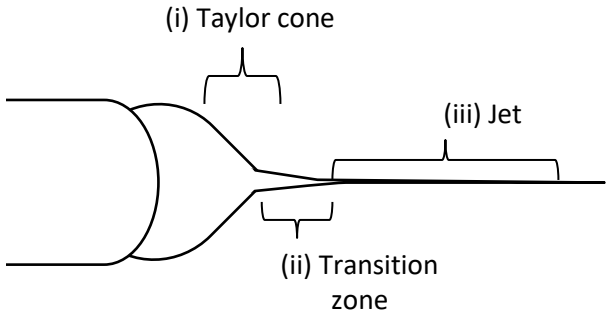

Figure 2.4-1. Jet formation zones. Adapted from Han (2008) [46]

The polymer jet usually follows a straight path followed by an increasing diameter coil. At the beginning of the jet, electric instabilities start to form coils. This coils become smaller as new electrical bending instabilities are formed, this process continue until the elongation stops, typically by solidification of the thin jet. At this point, if the variables of the whole process are the optimal, a slender and continuous liquid filament of nanometric scale is formed [47].

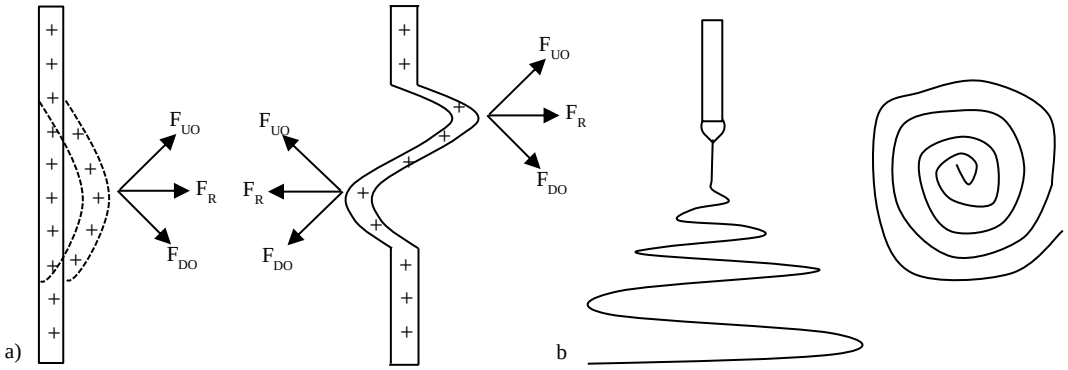

Figure 2.4-2. a) Instabilities in the tapered jet; F_{DO} is the downward force, F_{UO} is the outward force and F_R is the resultant force. Adapted from Reneker & Yarin (2008) [45]. b) Tapered jet with conical shape adapted from Thompson et. al (2007) [48].

Due to these electrical instabilities the jet begins to form a path in an inverted cone shape. It is started when a segment of an electrospinning jet starts to be perturbed; then, the segment begins to grow in response to the repulsive electric forces between the uniformly distributed charges carried with the jet. The charge carried with the perturbed segment is forced downward and outward by the charges above the perturbed region, at the same time this perturbed segment is forced upward and outward by the charge below the perturbation. The resultant of these forces is in a radial direction with respect to the straight jet and grows exponentially in time as the radial displacement of the segment increased as it shown Figure 2.4-2 [45]. At the same time, the repulsion of adjacent charges moving with the jet caused all the bent and straight segments of the jet to continue to elongate along their local axes. The elongation increased more rapidly in the bending segment [46], [49].

However and since these instabilities are suppressed by the NFEMS characteristics, a different approach has to be done to understand the phenomenon. The whole system, showed in the previous section of this chapter, consist in a metallic syringe where the polymer flows until it reaches a free space surrounded by air. The polymer then flows out of the syringe and form a jet that goes downwards, with gravity. It is remarkable to mention that, in EMS unlike far field ES, even when voltage is not applied, a fiber can be formed if the droplet get touched by the substrate (collector). In fact, in EMS there is an extra step called initialization, where the charged droplets have

to be punctured to start the formation of fibers, this is because of the low voltages used don't overcome completely the surface tension [15]. When the fiber is touching the substrate this can be moved in three axis, see Figure 2.4-1.

The experimentally adjustable parameters during fiber deposition are the applied voltage, V, the polymer flow rate, Q, tip-to-collector distance, TTDC, and the velocities of the stage (collector). The parameters of the fluid are: conductivity, *K*, dielectric constant, ε, mass density, ρ, kinematic viscosity at the bulk, η, elongational viscosity on the jet, η_e. Other parameters to take into account are the coefficient of interfacial tension between the fluid and the air.

Some assumptions to study the process are that the surrounding fluid is air that provides a uniform external pressure and has no effect on the jet. The temperature of the fluid and in the whole system is constant. The fluid has a Non-Newtonian viscoelastic behavior and is very sensible to deformation.

Another major parameter to be considered is the relaxation of free charge in the system, τ_e. This is the timescale for the local relaxation of bulk charge density within a conducting medium and is of primary importance during electrospinning modeling [50].

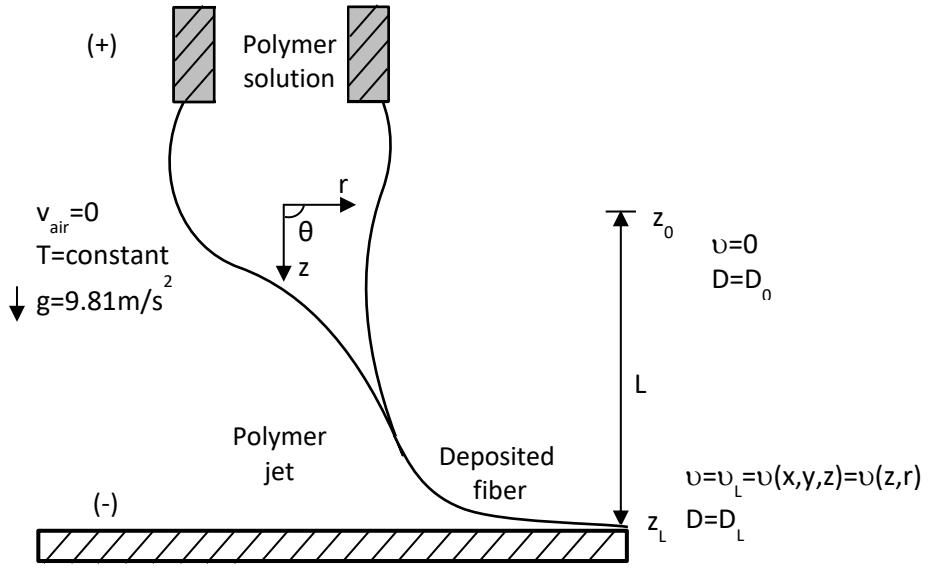

Figure 2.4-1 Analisis on EMS jet

In order to explain the whole process it is possible to follow the method proposed by J. Eggers. He assumes that the jet is a long, slender object and then uses a perturbative expansion in the aspect ratio. This element obeys the conservation of mass and charge. Also, because of viscous dissipation and external forces such as gravity, it does conserve neither energy nor momentum [50], [51]. Nevertheless, the work of Eggers and Hohman assumes a Newtonian Fluid as a study element and the elongational flow of viscoelastic materials differs drastically for this assumption. Since there are no walls restricting the flow of the polymer jet, the flow must be considered as an elongational one. Subsequently there are no shear forces acting on the jet, it means that the restriction of the flow is intrinsic to the molecular structure of the polymer, molecular weight, additives among others.

Another approach that can be made is that one done by Han et al. for fiber spinning. In this analysis the forces due to rheological properties, inertia, air drag, surface tension and gravity are taken into account as (2.4-1) shows, for this case the force due to the electric field has to be added to original equations. The research done by Han et al. demonstrates that for fiber spinning the rheological forces are up to 90% of the total force during the process [52].

$$F = F_{rheo} + F_{drag} + F_{inert} + F_{grav} + F_{surface} + F_{volt} \qquad (2.4\text{-}1)$$

$$F_{rheo} = \frac{[\tau_{zz}(z) - \tau_{rr}(z)]}{\pi R(z)^2} \qquad (2.4\text{-}2)$$

$$F_{inert} = \dot{m}\left(\upsilon_L - \upsilon_z(z)\right) \qquad (2.4\text{-}3)$$

$$F_{drag} = \int_z^L 2\pi\left(\frac{\rho\upsilon_z(z)^2 C_D}{2}\right)R(z)dz \qquad (2.4\text{-}4)$$

$$F_{surface} = 6\pi\wp\left(R(z) - R_L\right) \qquad (2.4\text{-}5)$$

$$F_{grav} = \int_{z}^{L_T} \rho g \pi R(z)^2 dz \qquad (2.4\text{-}6)$$

The force due to the voltage has to be defined for this method; however the modeling of the process is out of the scope of this work where only the calculations for the elongational viscosity are made. In order to have a better understanding of the flow process of the polymer jet, this phenomenon is studied in Chapter III. Nevertheless, in the next section several models are presented that aim to predict and explain the ES process.

2.5 Electrospinning Models

Nanofiber properties can vary dramatically given the many variables that may influence the process. Theoretical prediction and understanding of the parameter effects on jet radius and morphology could significantly reduce experimental time by identifying the most likely values that will yield specific qualities prior to production. An accurate, predictive tool using a verifiable model that accounts for multiple factors would provide a means to run many different scenarios quickly without the cost and time of experimental trial-and-error.

Mathematical description of the thinning liquid jet can be formulated within the context of conventional electro hydrodynamics. One such exposition is that presented by Hohman et al. for Newtonian fluids, which makes use of the slender body approximation to write perturbative expansions in the aspect ratio of the jet for the relevant jet characteristics. For highly conductive fluids, convergence of the equations to a solution was found to be laborious, a problem associated with specifying the initial surface charge density on the fluid jet exiting the spinneret [27]. Further assuming Newtonian fluid does not take into account the viscoelastic behavior of the jet. In electrospinning, stretching and viscoelastic relaxation both are present. The longitudinal stress level is determined by the competition between the stretching and the relaxation. Some models of electrified and electrospun jets and their key features are presented in Table 2.5-1.

Table 2.5-1 Brief list of several mathemtical analysis and models of electrified and electrospun jets and some of their key features. Adapted from Yarin (2007) [28]

Reference	Features
Spivak (1998) [30]	Straight electrified jet, viscous Newtonian or shear-thinning power-law liquid
Hohman (2001) [27], [50]	Linear stability analysis of small capillary and bending perturbations of electrified viscous Newtonian jet
Fridrikh (2003) [53]	Analysis of terminal diameter of a thinning electrified jet at the last stage of bending. The model does not account for viscoelasticity, solvent evaporation and polymer surface tension.
Feng (2003) [22]	Straight electrified jet of viscoelastic liquid
Reneker (2000); Theron (2005); Yarin (2001)[6], [49], [54]	Linear and nonlinear model (small and large perturbations) of the dynamics of single and multiple bending jets in electrospinning of polymer solutions. The model accounts for solution viscoelasticity, electric forces, solvent evaporation and solidification, surface tension and jet-jet interactions. It explains the physical mechanism of electrospinning and describes all the stages of the process

By far, the model presented by Reneker et al., is the most complete of all. Nevertheless, there still is a lack of accuracy on its predictions. A profound study on the elongational viscosity can provide tools to enhance this or other models.

CHAPTER III RHEOLOGY AND PHENOMENA INVOLVED IN ELECTROSPINNING

INTRODUCTION

Rheology is the science of deformation and flow of matter. It is a branch of physics and physical chemistry, where the most important variables come from the field of mechanics: forces, deflections and velocities

All kinds of flow behavior, which can be described rheologically in a scientific way, can be viewed as being in between two extremes: A flow of perfect viscous fluids and deformation of perfect elastic solids. Even though, most materials present a viscoelastic behavior, sited between these two extremes, these materials are called viscoelastic [55].

To analyze and understand how viscoelastic materials behave, different methods have been developed along the years. This methods have become more sophisticated with the introduction of new technologies to process the information and to measure forces in a very precisely way.

In this chapter is presented an introduction to polymer solutions, an overview of rheometry and the most used tests to characterize viscoelastic materials. Further, a study of the elongational flow and the various phenomena involved are presented. Finally, the different methods to characterize the rheological properties during elongational flow are studied.

3.1 POLYMER SOLUTIONS

Polymer solutions are present in everyday situations; they display interesting viscoelastic properties that have attracted the attention in many fields of investigation and production. The exceptional properties of polymers are due to their macromolecules. Their chains are long and entangled; they are small enough to be subjected to Brownian motion that tend to randomize their configuration giving the linear chains a ball-shaped arrangement [56]. When a shear or stretching force is applied, it creates a large interaction between the molecules that persist to high shear or elongational rates. Also, in the case of linear polymers, when the fluid is stretched, their exclusive configuration allows the transition to highly aligned chains in the strain

direction. Therefore a high resistance to be stretched is present and is related to a property called extensional viscosity.

The viscosity of polymer solutions depends not only on temperature, shear or elongational rate but also in molecular weight distribution and concentration [57], see Figure 3.1-1. The solvent properties are also important because its quality could be from “god” to “bad”, and the effects on viscosity could be significant.

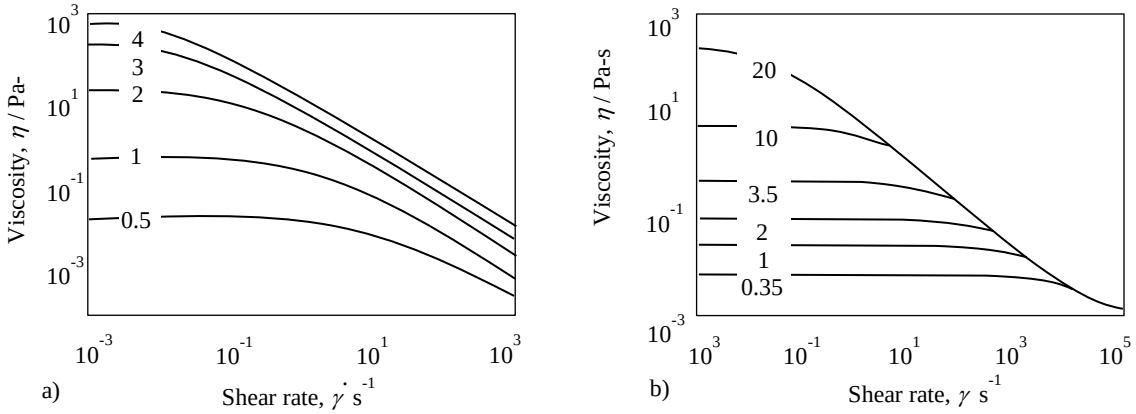

Figure 3.1-1 a) Effects on shear viscosity due to concentration. Flow curve for poly styrene in toluene, Mw=20M, for different concentrationsof polymer, shown as wt%. b) Effects on shear viscosity due to molecular weight, shown in millions gr/mol. Adapted from M. Kulicke (1984) [58].

Figure 3.1-2 shows how the quality of a solvent can promote an intertwined configuration or a ball-shaped for a good and a bad solvent respectively. Moreover, the appropriate selection of the solvent can modify drastically the parameters to process a polymer solution into a final product [59], [60].

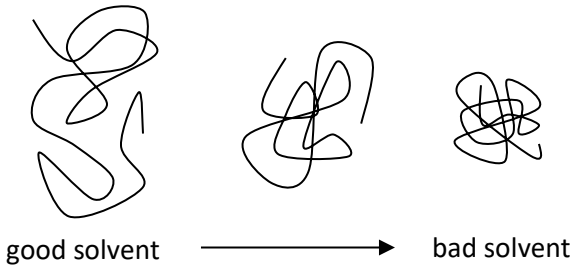

Figure 3.1-2 Effects in polymer chains dimensions due to solvent quality.

Another factor that modifies the structure of the coils is the presence of electrolytes. In nonionic solvents when an electrolyte is added, the charges are distributed along the chains and their own repulsion stretches the coil into a more aligned configuration. On the other hand, in some aqueous systems, the chains are first in a stretch-like configuration because the charges are unshielded. When an electrolyte is present, this charges start to become more shielded, promoting the shrinkage of the chains as it can be seen in Figure 3.1-3 [21].

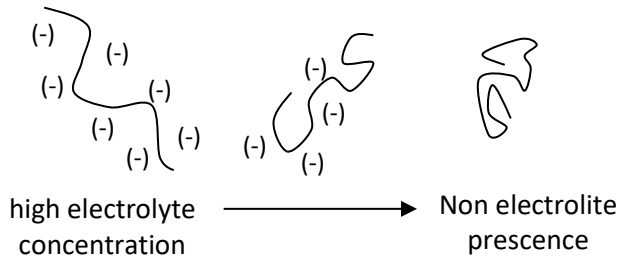

Figure 3.1-3 Effects of electrolyte in polymer chain dimensions.

As in polymer melts, there is a point at which entanglement take place in polymer solutions. Nevertheless, this point can be controlled in polymer solutions by modifying the concentration or using polymers with different molecular weights.

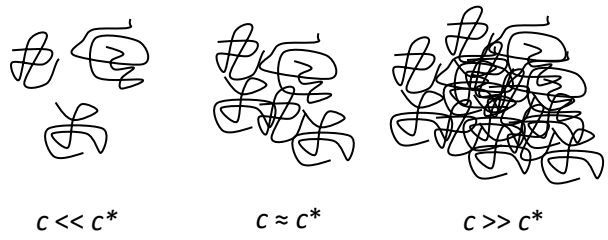

Figure 3.1-4 Molecules and entanglements from values of concentration below, same and higher than critical concentration. Adapted from Barnes (2000) [55]

From this, is possible to calculate the critical concentration, c*, at which the entanglements can change drastically the viscosity see Figure 3.1-4 [7], [15], [34], [61]. In order to understand the rheological behavior of polymer solutions, it is necessary to

perform different experiments in specialized equipment. A general view of this technology is presented in next section.

3.2 Rheometry

Rheometry is the measuring technology used to determine rheological data. There are different measuring systems, instruments and analysis methods. Both, liquids and solids can be investigated using rotational and oscillatory rheometers. Rotational tests are performed to characterize viscous behavior. In order to evaluate viscoelastic behavior, creep tests, relaxation tests and oscillatory tests are performed. A summary is presented in Table 3.2-1where, depending on their flow behavior, rotatory or oscillatory tests are recommended.

Table 3.2-1 Bheavior of materials and characterization techniques

Liquids		Solids	
(ideal-) Viscous Flow behavior Newton's law	Viscoelastic Flow behavior Maxwell's law	Viscoelastic Deformation behavior Kelvin/Voigt's law	(ideal-) Elastic Deformation behavior Hooke's Law
Flow/viscosity curves	Creep tests, Relaxation tests, oscillatory tests.		

3.2.1 Amplitude Sweep

Materials such as polymers exhibit viscoelastic behavior which is directly related to molecular structure and formulation differences. Very often, samples are under conditions of non-linear viscoelastic flow i.e. conditions were high rates of deformation are applied. These conditions are present in production processes such as coating, spraying and extruding. For these processes the elastic behavior of high molecular weight polymers such as melts or solutions is often more important than their viscous response to shear. Elasticity is often the governing factor for flow anomalies which limit production rates or cause scrap material [3], [60].

An amplitude sweep is a typical test used when the behavior of a polymer solution or polymer melt is not well known. In this basic test a constant angular frequency is settled. An increasing or decreasing deformation or strain is applied, Figure 3.2-1 a). The obtained results are the storage and loss moduli, G' and G'', along the values of percentage of strain applied. The amplitude is the maximum of the oscillatory motion. Usually at low frequencies the viscoelastic material presents a linear behavior, this is when the viscoelastic properties are independent of the strain or stress imposed because the structure of the material remains undisturbed. Nevertheless, as the amplitude is increased at some at some point this linear trend changes suddenly. Once this critical amplitude value is reached the material becomes more elastic or viscous depending of its initial state, Figure 3.2-1 b).

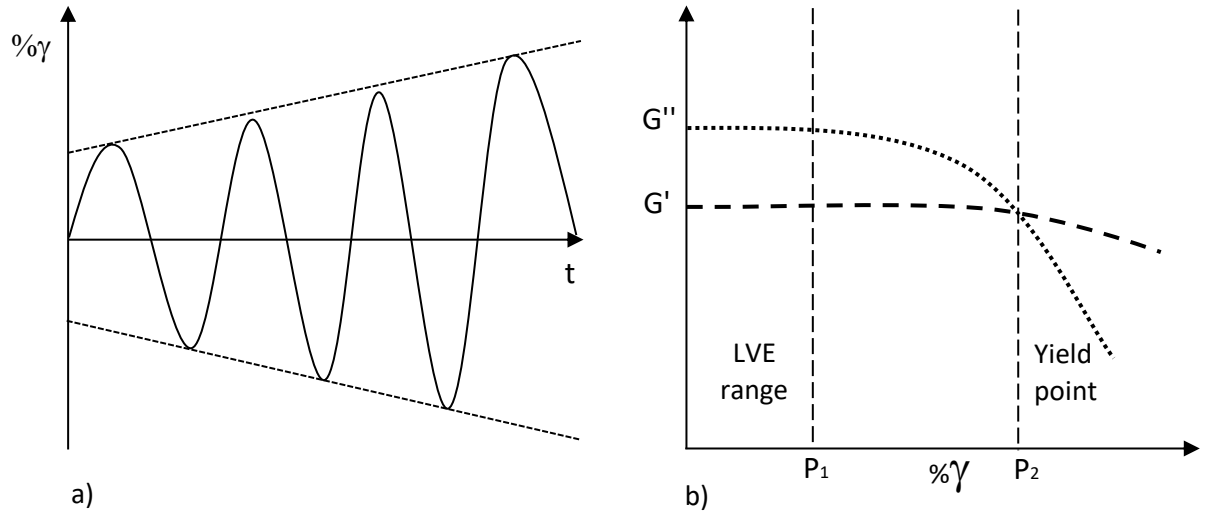

Figure 3.2-1a) Imposed amplitude along time with constant frequency. b) Results for an amplitude sweep showing the LVE range, P_1, and yield point P_2.

The limiting value of the linear viscoelastic range applies for the given test conditions, i.e., at the preset angular frequency. In Figure 3.2-1 it is shown a material that presents a gel-like structure and G''>G' at low percentage of strain, P_1, but once the crossover point is reached, G'>G'' that means that the material becomes more solid-like after the LVE region, P_2. With the amplitude sweep also the yield point can be

determined. Therefore two special points can be used: the end of the LVE-region and the intersection of the curves for G' and G''. In most cases the intersection of G' and G'' is of more practical importance.

3.2.2 FREQUENCY SWEEP

A frequency sweep, FS, is a common oscillatory test useful to understand the rheological behavior of complex fluids, it measure the time dependency of viscoelastic properties. During FS a decreasing or increasing frequency has to be imposed while the amplitude is kept constant, Figure 3.2-2.

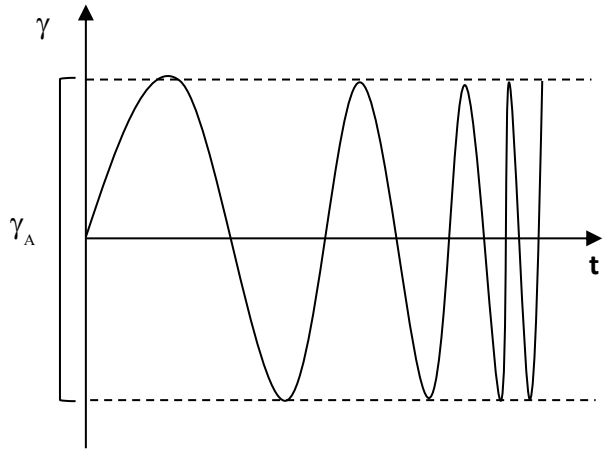

Figure 3.2-2 Increasing frequency with constant amplitude, %γ_A, in a frequency Sweep.

FS is considered a viscoelastic spectrum, generally speaking, the shorter the timescale the more elastic the material behaves. These results are related to the molecular structure of the sample. Figure 3.2-3 shows typical data for a polymer melt where different regions are observed. From lower to higher angular frequency there is a) a range of imposed strain or stress where the material structure dissipates the applied force, this is the zero shear viscosity region and b) after the yield point, there is a zone where the material becomes more elastic, this is the rubbery plateau.

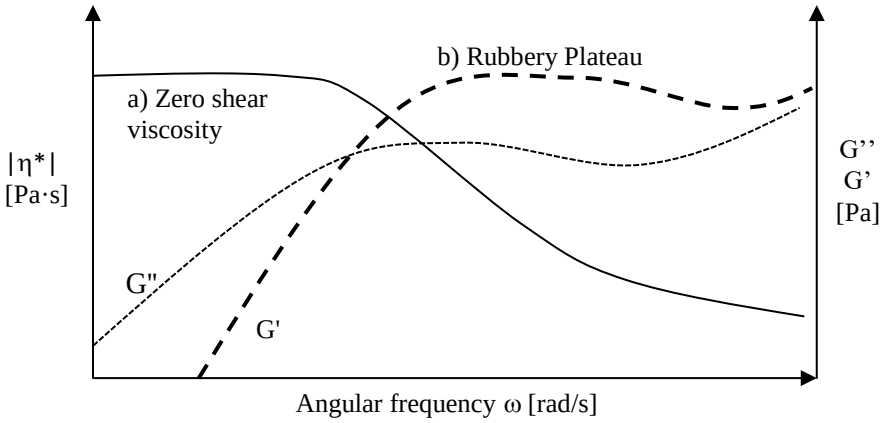

Figure 3.2-3 Typical results for a frequency sweep, angular frequency, ω, is increasing. G', G'' and complex viscosity, |η*|, are plotted. a) Zero shear viscosity region b) Rubbery plateau region

Another important of FS's is that it is possible to estimate the molecular weight distribution, MWD, and the molar mass, as shown in Figure 3.2-3. Furthermore, characteristics such as glass transition, rubbery-elastic characteristics, entanglement density, and processability can be obtained. The measurement results can be superposed to create master curves.

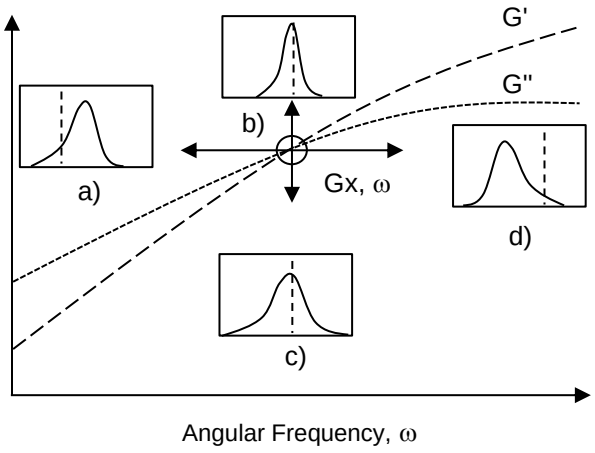

Figure 3.2-4 Estimation of the molecular weight distribution (MWD)/molecular structure of a polymer according the crossover pont in a frequency sweep. a) Higher average molecular weight/ long or branched molecules. b) Narrow MWD. c) Wide MWD. d) Lower average molecular weight/short or linear molecules [62].

In Figure 3.2-5, there is a schematic representation of an oscillatory rheometer. There are two main elements, the element that imposes a force and the one that is the measuring element. With both information there is possible to define the equations that describes the phenomenon present in a frequency sweep.

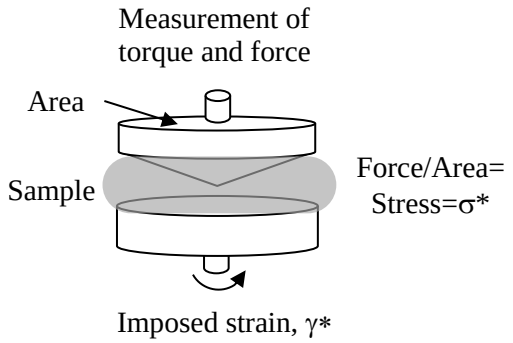

Figure 3.2-5 Schematic representation of an oscillatory rheometer and the operation principle

With the stress and the strain it is possible to find a relation for a viscoelastic modulus from

$$G^* = \frac{\sigma^*}{\gamma^*} \tag{3.2-1}$$

The strain is imposed with an angular frequency, for this reason both, strain and stress are dependent on frequency and time. The stress also has a delay time, δ, because of the offset of the response of viscoelastic materials.

$$\gamma = \gamma_0 \sin(\omega t) \tag{3.2-2}$$

$$\sigma = \sigma_0 \sin(\omega t + \delta) \tag{3.2-3}$$

From response of the moduli presented in (3.2-1) to a rotatory strain, it is possible to clear for σ_0 as follows

$$\sigma_0 = \gamma_0 G \tag{3.2-4}$$

However G has now to be defined in terms of the oscillatory forces as follows

$$G = \mathrm{G}\sin(\omega t)\cos(\delta) + \sin(\omega t)\cos(\delta) = \mathrm{G}'\sin(\omega t) + \mathrm{G}''\cos(\omega t) \tag{3.2-5}$$

Now the modulus has two elements, one for the viscous response, G(w)=G*cosδ, and one for the elastic response, iG''(ω)=G'sinδ, given by

$$G^* = G'(\omega) + iG''(\omega) \tag{3.2-6}$$

Then is possible to define the equations and data obtained by the frequency sweeps like the complex modulus that is the absolute value of the summation of the squares of both the elastic and viscous response

$$|G^*| = [G'(\omega)]^2 + [G''(\omega)]^2 \tag{3.2-7}$$

The ratio of G'' and G' known as tanδ, or tandelta, that indicates the response of the material at a given angular frequency, for values below 1 the response is elastic for values higher than 1 the response is viscous. Also δ, in degrees, indicate the behaviors aforementioned, for δ=90° there is a perfect elastic response and for δ=0° there is a perfect viscous response, nevertheless for polymeric materials 0°<δ<90°

$$\tan\delta = \frac{G''(\omega)}{G'(\omega)} \qquad (3.2\text{-}8)$$

Finally the complex viscosity is defined as follows

$$|\eta^*|(\omega) = \frac{\sqrt{|G^*(\omega)|}}{\omega} \qquad (3.2\text{-}9)$$

3.2.3 Flow Curve

A flow curve, FC, is used to determine the flow behavior of a sample. The viscosity is measured as a function of the shear rate in a rotational rheometer with different geometries according to the sample. Cup-and-bob is used when the sample has very low viscosity, cone-and-plate when the sample has low viscosity and weak structure and parallel plate when the sample has from medium to high viscosity and a strong structure. The results include values of shear viscosity, shear rate and shear stress. It is one of the most important rheological measurements. It shows the flow behavior for low and high shear rates.

Basically three types of behaviors could be found in FC, ideal viscous, shear thinning and shear thickening. Figure 3.2-6 shows three different materials and their response to an imposed shear rate. For the ideal viscous flow the viscosity is independent on the shear rate. This behavior is common for homogenous low molecular weight fluids like lubricating oil. For such samples it is sufficient to indicate one value for the viscosity at a certain temperature. Shear-thickening flow behavior shows up normally for highly filled dispersions at high shear rates. Shear thinning is often a result of the orientation of small non-spherical particles or chains in the direction of the flow, for example the pumping of slurries.

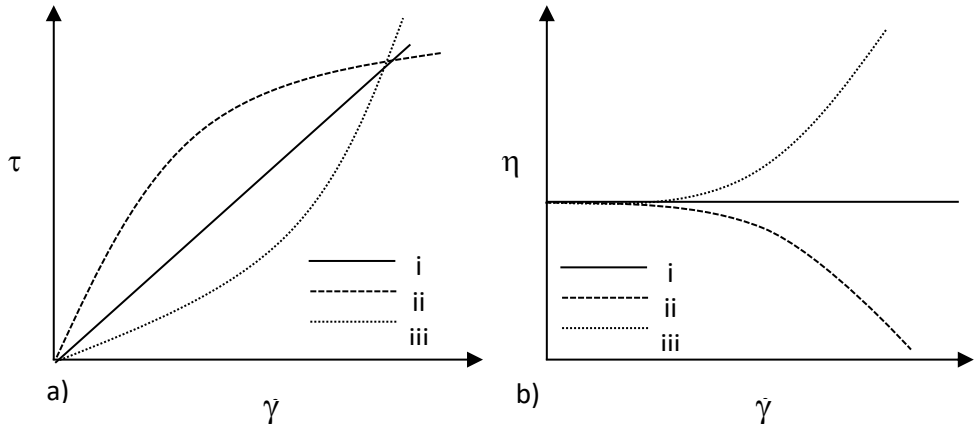

Figure 3.2-6 a) Flow curve stress vs stress. b) Flow curve strain vs shear viscosity. Both figures for i Newtonian fluid, ii Shear thinning fluid, iii Shear thickening fluid.

3.3 Extensional Flow

Introduction

Although several publications study only the rheological properties carried out in simple shear flows such as rotational viscometers [63]–[65]. During electrospinning a major, or more significant effect, is provided by an extensional flow. In extensional flow the element of a fluid is stretched or squeezed rather than sheared, and for some fluids there can be a large difference between their shear and extensional viscosities [66]–[68].

For a better understanding it is possible to assume that a test element is a large polymer molecule flowing in a barrel, at first is aligned to the flow lines. Assuming that the relation of diameter of the barrel and the flow rate are bigger enough, the element would be randomly flowing, but, if the element is forced through a diameter reduction, it will start to experience a stretching flow. As it enters to the small tube, the polymer chain will tend to align along the flow axis, and as it emerges from the smaller tube it would tend to move towards its off-axis angle again, see Figure 3.3-1. This phenomenon occurs also when the element is stretched out without walls.

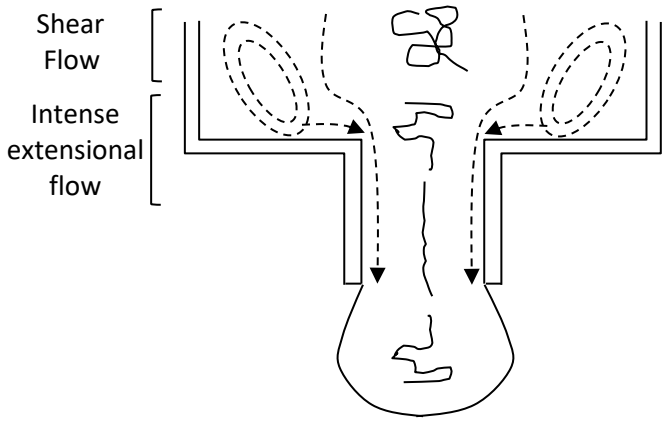

Figure 3.3-1 Polymer chain flowing through a contraction getting aligned with the flow lines. Extensional flow due to a diameter contraction.

The importance of the stretching and alignment of the molecular structure is based in how this alignment affects the flowing properties. For a better understanding it is precise to study the simplest form of extensional flow, the uniaxial extensional flow that indeed, is precisely the same flow present during electrospinning. The uniaxial extensional flow is the equivalent of pulling out a tread or filament of liquid, as it is shown in Figure 3.3-2. In this case the velocity gradient is in the same direction that the flow instead at the angles as it is in the case of shear flow [55].

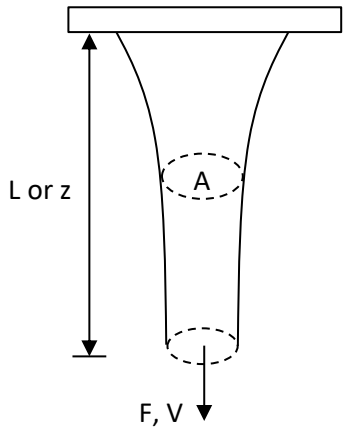

Figure 3.3-2 Uniaxial extensional flow. Pulling force, F, applied to a cross section area, A, at certain velocity, V.

As it is in the case of shear flow where a strain and stress are present, in uniaxial extensional flow there are their equivalents the extensional stress or tension, given by

$$\sigma_e = \frac{F}{A} = \tau_{11} - \tau_{22} \qquad (3.3\text{-}1)$$

and the extension or elongational rate, given by

$$\dot{\varepsilon} = \frac{dV}{dz} \qquad (3.3\text{-}2)$$

with the ratio of the stress and rate it is possible to calculate the uniaxial elongational viscosity, as follows

$$\eta_e = \frac{\sigma_e}{\dot{\varepsilon}} \quad (1) \qquad (3.3\text{-}3)$$

The estimation of the elongational viscosity is far from being trivial because of the measurement or estimation of the extensional stress. Sections 3.4 and 3.5 are devoted to the measurement and estimation of η_e.

3.3.1 Elongational flow at molecular level

The major difference between elongational and shear viscosity is best illustrated by considering a single fiber suspended in a Newtonian liquid. If this liquid with the fiber suspended is subjected to a shear flow, the fiber will align along the flow axis and this minimizes the effects or disturbances due to the liquid surrounding it [69]. On the other hand, if the same liquid with the fiber is subjected to an extensional flow, the fiber again will align along the flow axis, but now a higher resistance will be present because of the stretching of the fiber, in this case the stretched liquid tries in turn to stretch the fiber. In Figure 3.3-3 is plotted how both, elongational and shear viscosities, behaves as the elongational and shear rate are increased. While shear viscosity will decrease as fibers get align in the flow axis direction the elongational will increase. The eventual difference

between the shear and extensional viscosities at high deformation rates increases with increasing aspect ratio of the fibers [31].

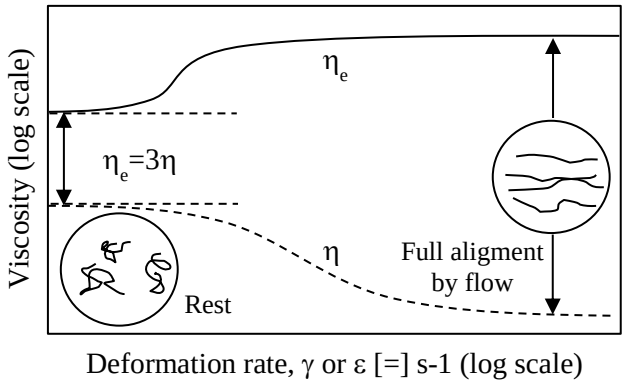

Figure 3.3-3 Both elongational and shear viscosities and the effects of the fiber alignment at comparable deformations.

For polymer solutions this effects are bigger than in the fictitious fiber solution because of the inter-fiber contacts now are intermolecular entanglements. For this reason it is of primary importance to understand the dynamics of this contacts and entanglements as a function of the extension rate.

At rest or a very low extension rates a transient network is formed as the fibers or chains become entangled and disentangled under the action of Brownian motion, that is just a simple diffusion motion [56]. The stretching interferes with the dynamic of this transient network. If the inverse of the extensional rate is bigger than the longest relaxation time of the molecules, τ_d, that is related to the average life of the entanglements of the network, the material acts like an elastic solid and the stress increases considerably until the entanglements would rupture, this rupture cause a decrease in the viscosity. If the average number of entanglements remains invariable, in a hypothetical case, it could be noticed that the extensional viscosity increases drastically while the shear viscosity remains constant. Nevertheless, in real processes, as the extension rate increases the entanglements after a sudden increase starts to decrease. This is well explained in Figure 3.3-4. A detailed work on this subject was

carried out by Bhattacharjee et al. where a well characterized solution an entangled polymer solution of nearly monodisperse (Mw/Mn = 1.01) polystyrene (Mw = 1.95 × 106 g/mol) in diethyl phthalate that was subjected to a extensional and shear step strain increases. They observed that the relaxation time is inversely proportional to the magnitude of deformation steps [70].

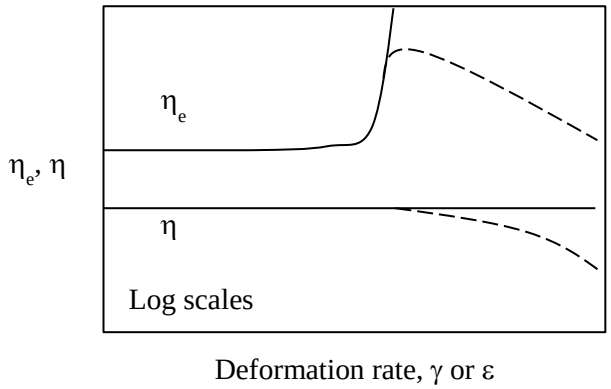

Figure 3.3-4 Both shear and extensional viscosities of a polymer network, network dynamics effects shown as solid lines, and the effect of loss of junctions shown as dotted lines.

In order to explain this, it is necessary to introduce some non-dimensional numbers and their meaning in rheology. The first one is the Rouse number, in pursuance to understand this element it is necessary to overview the Rouse model. This model aims to explain the behavior of short polymer chains in terms of entangled polymer hydrodynamics. It consists of a Gaussian worm-like chain which can exchange energy with its surroundings. Subdivide a real polymer into segments, each of which is sufficiently long to obey Gaussian statistics, which have end-to-end distances a_R, then, attach these segments together with imaginary springs, representing the entropic restoring forces on the chain as a whole, as can be seen in figure 3.3-5 [71].

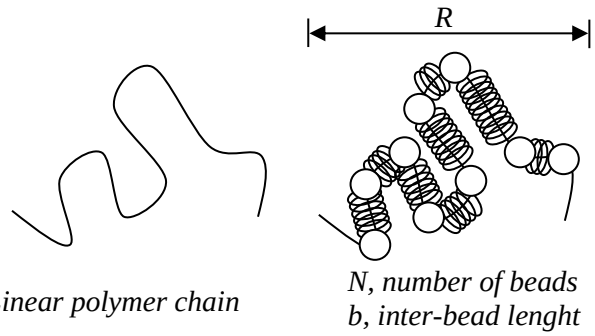

Figure 3.3-5 Representation a polymer chain with springs connecting beads.

The motion of the molecules at rest follows the Brownian motion

$$\langle\left[\vec{r}(t) - \overrightarrow{r(0)}\right]^2\rangle = 6Dt \qquad (3.3\text{-}4)$$

Were D is the diffusion coefficient and t is time, when a force is applied it leads a constant velocity

$$\vec{F} = \xi\vec{v} \qquad (3.3\text{-}5)$$

Each bead has its own friction, ξ, and the total friction is obtained the total number of beads, N, as follows

$$\xi_R = N\xi \qquad (3.3\text{-}6)$$

To obtain the global diffusion coefficient it is applied the Einstein relationship

$$D_R = \frac{kT}{N\xi} \qquad (3.3\text{-}7)$$

Where k is a diffusion constant intrinsic to the material and T is temperature. Now is possible to define the Rouse number

$$\tau_R = \frac{\xi N R^2}{kT} \qquad (3.3\text{-}8)$$

That is the longest relaxation time in function of the total nodes or beads, N, in the polymer chain, the friction ξ, the total radius, R, of the molecules assumed as a sphere, the temperature and the constant of diffusion. Finally, the Trouton ratio, Tr, was discovered by the experimental work of Trouton and is defined as the ratio of the viscosities, η_e/η, as measured at any particular shear rate and root-three $(3)^{1/2}$ times the equivalent extension rate. At very low deformation rates the extensional viscosity is three times the shear viscosity.

The work of Doi-Edwards studies the dynamics of entangled polymeric melts and solutions. They defined 4 regions region 1, when the strain rate is less than the inverse of the longest relaxation time of the chains ($\dot{\varepsilon} < 1/\tau_d$), region 2 where $1/\tau d < \dot{\varepsilon} < 1/\tau_R$, where $\tau_R = \tau_d/3Z$ is the Rouse time of the chain and Z is the average number of entanglements per chain at equilibrium, $\eta_e \sim \dot{\varepsilon}^{-0.5}$. In region 3, when $\dot{\varepsilon} > 1/\tau_R$, the extensional viscosity rises above $3\eta_0$, until the stretch-coil-transition is completed, and the extensional viscosity becomes independent of the applied strain rate in region 4. The level at which the extensional viscosity saturates depends on λ_{max} and Z where λ_{max} is the ratio to the maximum length of the polymer chain segments to its equilibrium length. Figure 3.3-6 shows a general flow curve for this [72].

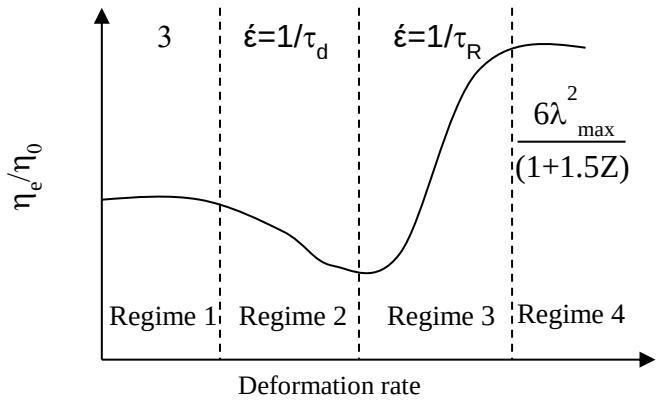

Figure 3.3-6 Shows the regions of the Trouton ratio at different deformation rates

Another major phenomenon takes part when the polymer solution is made of linear polymer chains of high molecular weight. In those cases the properties are dominated by isolated individual polymer ball-shaped coils. At low elongational rates the polymer chains are ball shaped, but at a critical elongational value is reached the polymer chains suddenly unwinds and in to a long stretched string in a phenomenon called coil-stretch-transition, CST.

In some polymer solutions both effects are present. In Figure 3.3-7 is showed the different zones and the behavior of the polymer chains in each one. In zone (1) the ball shaped chains are forming and breaking entanglements in a constant rate, when a low elongational rate is imposed (2) this forces the coils to increase the number of entanglements and also the η_e. As the extension rate is increased the entanglements starts to break apart diminishing the viscosity (3) finally at a critical elongational value the chains get unwounded and the viscosity increases dramatically (4). The work of Ferguson et al. with solutions of polybutadiene in decaline depict this precise phenomenon [34].

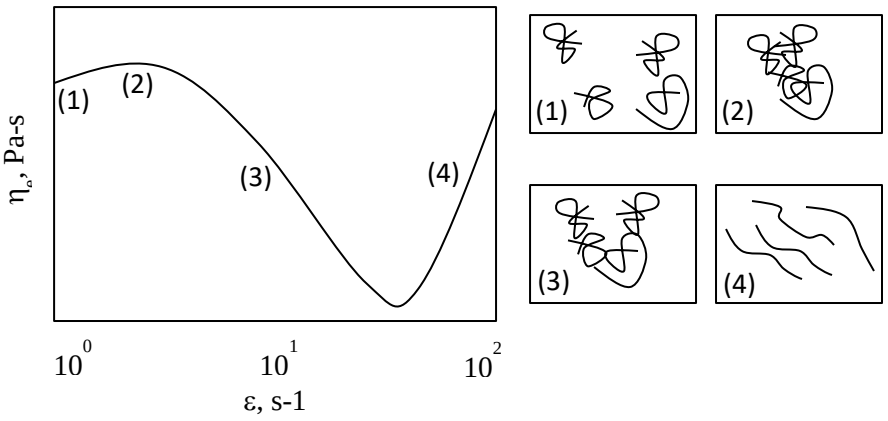

Figure 3.3-7 Extensional viscosity versus extension rate for a solution of polybutadiene in decalin, showing the extension/tension thickening, extension/tension thinning and coil stretch regions respectively. Adapted from Ferguson (1990) [34].

Nevertheless, to follow or measure these systems is not an easy work. A big effort has been made in order to estimate the rheological properties involved during elongational processes. Next section explains different methodologies to measure or estimate elongational viscosity.

3.4 Measuring the elongational viscosity

Despite some applications where it is possible to form filaments or sheets that can be pulled in one or two directions, measure the elongational viscosity is reasonable difficult. There are several problems that must be solved in order to make veracious measurements.

In the case when the sample can be clamped or attached, the nature of the elongational flow implies that the longitude of the sample has to increase exponentially to maintain a constant elongational rate. Another problem is that even when it is possible to measure the stress, the cross-section area decrease constantly and it must be followed through the whole process. Some ingenious methods have been developed to solve these troubles. Nevertheless, when the sample to be measured is a mobile solution, the aforementioned methods are impossible to perform.

Alternative methods have been created depending on the sample. If the fluid is “spinnable”, then a rotating drum wind up a liquid thread while a camera system is used to measure an average elongational rate [55]. When the sample is not spinnable, there are different techniques that could be used.

3.4.1 Opposed Jets Rheometer

One of the most common usage is the opposed jet technique, where two identically capillaries are immersed in a fluid, reasonably near to each other, but in an opposing direction as it show Figure 3.4-1. In this system when the fluid is sucked, a flow that is approximately to the uniaxial extension flow is formed between the two capillaries. Streamlines close to the stagnation point provide enough residence time for the fluid elements so that isolated flexible polymer molecules (such as PEO molecules) subjected to a high enough strain rate can undergo a coil–stretch transition. This state

can be followed and detected by using a laser beam passing through the stagnation point. Also, the pressure drops are measured. Using this information and the distances and diameters of the capillaries it is possible to estimate the elongational viscosity [73]. In is work, Saez et al., studied a polymer system of high molecular weight PEO in presence of surfactants by the technique of opposed jets demonstrating the efficiency of this technique. Nevertheless, a recurrent problem in this method is that it is very difficult to ensure a steady state of the flow [69]. Another problem is that a considerably amount of solution is required. This is a major issue when the solution to be tested is expensive or hard to obtain, for example SU-8 for C-MEMS fabrications or when a spider web solution has to be characterized.

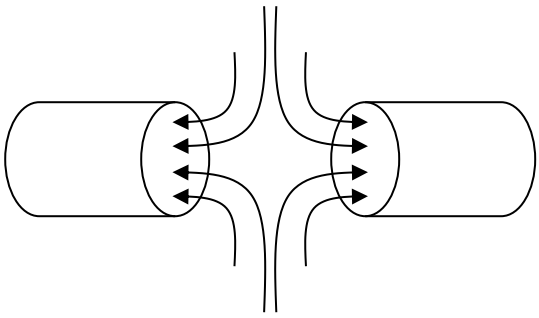

Figure 3.4-1Extensional flow in an opposed jet flow

3.4.2 Capillary Rheometer

Another system to estimate the elongational viscosity is the capillary rheometer. In this equipment a load is placed at the top of a barrel that pushes the sample. The sample, usually a polymer melt, is inside the barrel in which, at the end, there is a very short die ($L/D \approx 0$) that constrain the flow promoting then the elongational flow as it can be seen in Figure 3.2-1. By measuring the pressure drop at the entrance of the die it is possible to estimate the elongational viscosity through different mathematical models and corrections [74].

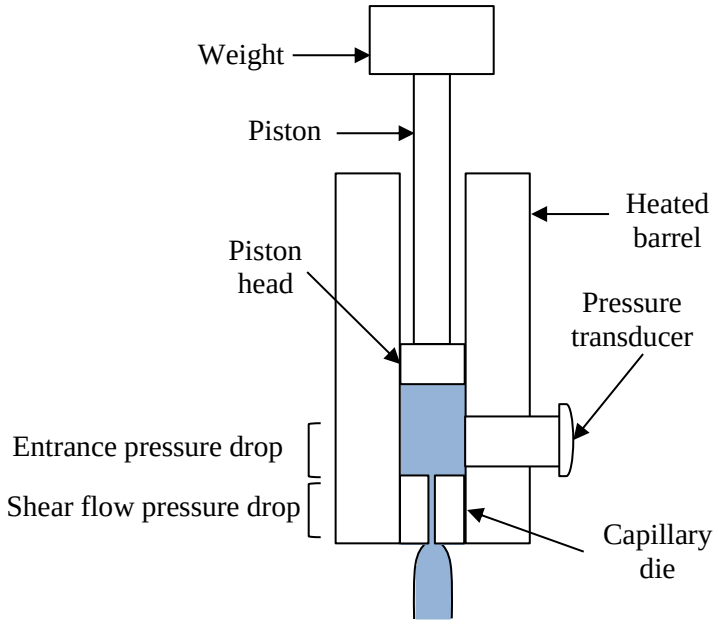

Figure 3.4-2 Operation scheme of a Capillary rheometer

However, this technique has to overcome some difficulties. Because of the physical assumptions and principles governing the system, the pressure drop due to the barrel walls has to be estimated and corrected in order to have the most accurate measurement of pressure at the entrance of the die. Besides, measuring the pressure at the entrance without affecting the flow is a non-trivial task. Another problem is that, as the case of opposed jets, it is necessary to know when a steady flow is reached. Because this is a closed system and big pressures can be reached (a glass or plastic material is not a good option due to its fragility), use a laser beam is not an easy option. Furthermore, this equipment ignores parameters such as normal stress difference and the total strain viscoelastic relaxation [75]. As is the case of the opposed jets that presents the problem of high amount wasted material.

3.4.3 Capillary Breakup Extensional Rheometer

A technique that uses lower amounts of the polymer melt or solution for an elongational characterization is the Capillary Breakup Extensional Rheometer, CaBER. The purpose of the CaBER is to impose a predominantly-uniaxial extensional step on a

liquid sample to extract information on its transient extensional properties [76]. By monitoring the dynamics of breakup of a fluid filament following a short, rapid extensional deformation, it is possible to obtain information about the relaxation time spectrum, the extent of non-Newtonian behavior, the time to breakup for the fluid and the apparent elongational viscosity. As opposed to conventional extensional rheometers, which impose a carefully prescribed velocity history on the fluid, a filament breakup rheometer imposes a rapid axial step strain of prescribed magnitude to induce a statically-unstable shape and then allows the stretched neck-shaped fluid sample to relax and breakup under the action of capillary forces [77]. In Figure 3.4-3 is presented the evolution of the sample through time. During the test, the evolution of the thread midpoint diameter is monitored usually by a near infra-red laser or a high speed camera; this measurement allows to observe the overall extensional behavior of the fluids as well as to extract rheological properties, if an appropriate constitutive equation is chosen to describe the fluid behavior [78].

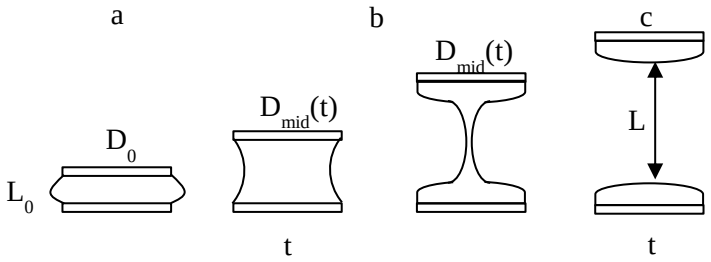

Figure 3.4-3 Operation scheme of a CaBER. a) Initial configuration of a liquid column. b) Imposed stretching deformation. c) Breakup of the column. During the whole process mid point thread is measured. Adapted from Briatico-Vangosa (2015) [78].

CaBER has shown to be a good option when an elongational characterization is required [79]–[81]. However, improvements have to be realized in order to increase the sensitivity of the equipment when low viscosity solutions are tested. Also, the major disadvantage against other methods is that it has a limited range of extensional rates to perform the analysis. In some processes like paint spraying, centrifugal spinning, electrospinning, etc., the extensional rates are far from those that CaBER can reach.

Since the aforementioned methods are difficult to carry out, it is reasonable to found just a small number of commercial equipment in the market. For this reason, is difficult to found reliable data of elongational viscosity. For most of the people interested

in characterize slow viscosity polymeric solution, a laboratory build up equipment is required. This is a reason of why, for the same solution, different researchers report rheological data, that in some cases differs in one or two orders of magnitude [82].

3.5 ESTIMATION THROUGH MATHEMATICAL MODELING

An alternative way to estimate the elongational viscosity is by using mathematical models. To study the polymer flow and the phenomenon involved during its processing it is indispensable to reflect the governing flow equations. For incompressible fluids, as it is the case of polymer solutions, the flow is governed by conservations equations of mass, momentum and energy: (3.5-1, 3.5-2, and 3.5-3) Computational polymer processing

$$\nabla \cdot \boldsymbol{\nu} = 0, \tag{3.5-1}$$

$$\rho \boldsymbol{\nu} \cdot \nabla \boldsymbol{\nu} = -\nabla p + \nabla \cdot \boldsymbol{\tau}, \tag{3.5-2}$$

$$\rho C_p \boldsymbol{\nu} \cdot \nabla T = k \nabla^2 T + \tau : \nabla \boldsymbol{\nu} \tag{3.5-3}$$

where ν is the velocity vector, p is the scalar pressure, τ is the extra stress tensor, ρ is the density, Cp is the heat capacity, k is the thermal conductivity, and T is the temperature. This system of conservation equations is the so called Navier-Stokes equations in fluid mechanics [51].

The adequate rheological constitutive equations have to be selected in order to accurately relate the stress tensor and the velocities and velocity gradients (kinematics). Several equations and models have been formulated to explain a wide variety of rheological phenomena. Two of the most widespread models are the empirical ones like Carreau given by (3.4-4) and the Cross models given by (3.4-5)

$$\eta(\dot{\gamma}) = \eta_\infty + \eta_0 [1 + (\lambda_C \dot{\gamma})^2]^{\frac{n-1}{2}} \tag{3.5-4}$$

$$\eta(\dot{\gamma}) = \eta_{\infty} + \frac{\eta_0}{1 + (\lambda_C \dot{\gamma})^{1-n}} \tag{3.5-5}$$

In these equations, η_0 is the zero shear rate viscosity, η_∞ is the infinite shear viscosity, λ_C is a time constant and n is a power law index. The magnitude of $\dot{\gamma}$ is given by

$$\dot{\gamma} = \sqrt{\frac{1}{2} II_{\dot{\gamma}}} = \sqrt{\frac{1}{2} (\dot{\gamma} : \dot{\gamma})} \tag{3.5-6}$$

$II_{\dot{\gamma}}$ is the second invariant of the rate-of-strain tensor. These models describe the shear viscosity at low and high shear rates of a wide number of polymer solutions and melts. Nevertheless, since the polymer solution and melts are complex materials they exhibit both viscous and elastic effects, for this reason more sophisticated and complete constitutive equations have to be considered to describe viscoelastic properties.

There have been different approaches of these equations such as differential types, integral types, molecular models and so on. From differential models one of the most eminent are those proposed by Wagner (Upper Convected Maxwell) and the Oldroyd-B, both presented in the early 1980s. Further, in the 1990s the Pan-Thien/Tanner and the Giesekus models were widely used by the scientific community and recently, the K-BKZ model has been vastly used [49], [68], [83].

However, some of these models require data usually hard to obtain or are difficult to solve. An alternative to this is achieved by the Wagner model (1977) that use rheological data easy attainable, and also it has been also tested for a wide number of polyolefins and its calculation is straightforward.

The Wagner model is a modification of the Lodge model given by (3.5-7) that could not predict fairly well the shear thinning behavior in the non-linear viscoelastic region (NLVER).

$$\sigma = \int_{-\infty}^{t} \mu(t-t', I_1, I_2) C_t^{-1}(t') dt' \qquad (3.5\text{-}7)$$

The NLVER region is reached when the shear rate is bigger than the inverse of the longest relaxation time. From startup experiments Wagner observed that the maxima of the shear stress (σ), and the first normal stress difference (N1), occurred at constant values of shear rate denoted by γ_s and γ_n respectively. The memory function $\mu(t\text{-}t', I_1, I_2)$, depends on the time difference and the invariants of the relative Finger strain tensor (C_t^{-1}). Due to the independence of γ_s and γ_n upon shear rate, he proposed to separate the memory function into a product of a time dependent memory function $\mu(t\text{-}t')$ and a strain dependent damping function $h(I_1, I_2)$ as follows

$$\mu(t-t', I_1, I_2) = \mu(t-t') h(I_1, I_2) \qquad (3.5\text{-}8)$$

The memory function can be obtained from data on the linear viscoelastic region (LVER) and can be also approximated by exponential expressions such as

$$\mu(t-t') = \sum a_i e^{\left(-\frac{(t-t')}{\lambda_i}\right)} \qquad (3.5\text{-}9)$$

Where a_i are weight factors and λ_i are time constants. In 1978 Laun demonstrated experimentally that the separation of the function memory was valid and present a way to obtain the memory function from measurements in both NLVER and LVER. The weighted factors and the time constants are obtained from the storage modulus, G', and the loss modulus, G'' in the LVER:

$$G'(\omega) = \sum a_i \lambda_i \left[\frac{\omega^2 \lambda_i^2}{1 + \omega^2 \lambda_i^2}\right] \qquad (3.5\text{-}10)$$

$$G''(\omega) = \sum a_i \lambda_i \left[\frac{\omega^2 \lambda_i^2}{1 + \omega^2 \lambda_i^2} \right] \quad (3.5\text{-}11)$$

In his work, Wagner specifies that a_i and λ_i does not have a physical meaning while a_i is fitted on experimental data, λ_i is fixed logarithmically between $1x10^4$ to $1x10^3$.

On the other hand, the damping function, $h(I_1,I_2)$, can be expressed in numerous ways. However, in this work a double exponential damping function proposed by Laun for creep and recovery response cases and the response to uniaxial deformation is used:

$$h(t,t') = f_1 e^{-n_1|\gamma|} + f_2 e^{-n_2|\gamma|} \quad (3.5\text{-}12)$$

Where n_1 and n_2 are fitting parameters sensitives to strain and f_1 is a weighted factor. Another important element in the Wagner model is the relative Finger strain tensor for unidirectional shear flow, given by

$$C_t^{-1}(t') = \gamma(t,t') \begin{vmatrix} 1+\gamma^2(t,t') & \gamma(t,t') & 0 \\ \gamma(t,t') & 0 & 0 \\ 0 & 0 & 1 \end{vmatrix} \quad (3.5\text{-}13)$$

where $\gamma(t\text{-}t')$ is the relative shear strain between any two times t and t'

$$\gamma(t,t') = \gamma(t) - \gamma(t') \quad (3.5\text{-}14)$$

and the invariants are given by

$$I_1 = I_2 = 3 + \gamma^2(t,t') \; and \; I_3 = 1 \; (Incompressibility \; assumed) \quad (3.5\text{-}15)$$

The model proposed by Wagner taking into account the elements aforementioned is the next:

$$\sigma(t) = \int_0^t \mu(t-t')\, h(t,t')\gamma(t,t')dt' + \gamma(t)h(t)\int_{-\infty}^0 \mu\,(t-t')dt' \qquad (3.5\text{-}16)$$

Where

σ(t) is the stress

μ(t-t´) is the memory function evaluated at t-t'

t is the time at which stress or strains is being evaluated

t' represents all the times previous to time t

h (t,t') is the damping function

γ is the strain and

$$\int_{-\infty}^0 \mu\,(t-t')dt' = G(t)$$

G(t) is the linear viscoelastic relaxation modulus

The elements of the relaxations spectra are calculated from oscillatory data, by using a fitting of the values of H(λ) with the loss and storage moduli with the next equations and (3.5-10) and (3.5-11)

$$G''(\omega) = \sum_{j=1}^{n} H(\lambda)_j \frac{\omega}{1+\omega^2\lambda_j^2} \qquad (3.5\text{-}17)$$

$$G'(\omega) = \sum_{j=1}^{n} H(\lambda)_j \frac{\omega^2}{1+\omega^2\lambda_j^2} \qquad (3.5\text{-}18)$$

The Wagner model in the form of (3.4-16) can be used to determine the shear viscosity and the first normal stress difference as a function of time at any given shear rate. The analytical solution of the model for viscosity is

$$\eta(t,\dot{\gamma_0}) = f_1 \sum_{i=1}^{n} \frac{a_i}{\alpha_i^2}\{1 - e^{-\alpha_i t}(1 - n_1\lambda_i\dot{\gamma_0}\alpha_i t)\} + (1 - f_1)\sum_{i=1}^{n} \frac{a_i}{\beta_i^2}\{1 - e^{-\beta_i t}(1 - n_2\lambda_i\dot{\gamma_0}\beta_i t)\} \quad (3.5\text{-}19)$$

And the analytical solution for N1 is given by

$$N1(t,\dot{\gamma_0}) = \dot{\gamma_0^2}\left\{f_1 \sum_{i=1}^{n} a_i\,\alpha_i^3\left[1 - e^{-\alpha_i t}\left(1 + \alpha_i t - \alpha_i^2\frac{n_1\lambda_i\dot{\gamma_0}}{2}\right)t^2\right]\right\} + (1 - f_1)\sum_{i=1}^{n} a_i\,\beta_i^3\left[1 - e^{-\beta_i t}\left(1 + \beta_i t - \beta_i^2\frac{n_2\lambda_i\dot{\gamma_0}}{2}\right)t^2\right] \quad (3.5\text{-}20)$$

When (3.4-17) and (3.4-18) are evaluated at t → ∞ the resultant equations are:

$$\eta(\dot{\gamma_0}) = f_1 \sum_{i=1}^{n} \frac{a_i}{\alpha_i^2} + (1 - f_1)\sum_{i=1}^{n} \frac{a_i}{\beta_i^2} \quad (3.5\text{-}21)$$

$$N1(\dot{\gamma_0}) = 2\dot{\gamma_0^2}\left\{\sum_{i=1}^{n} f_1\frac{a_i}{\alpha_i^3} + \sum_{i=1}^{n}(1 - f)_1\frac{a_i}{\beta_i^3}\right\} \quad (3.5\text{-}22)$$

Where t is time

$\dot{\gamma_0}$ is the shear rate at wich the function is evaluated

n_1, n_2 are the strain sensitive terms of the damping function obtained by fitting of the steady state shear viscosity curve

f_1 Is a weighted factor for the damping function

a_i is aweight factor for the exponential terms of the memory function

λ_i is the characteristic relaxation time of the memory function

And

$$a_i = \frac{1 + n_1 \lambda_i \dot{\gamma_0}}{\lambda_i} \tag{3.5-23}$$

$$\beta_i = \frac{1 + n_2 \lambda_i \dot{\gamma_0}}{\lambda_i} \tag{3.5-24}$$

Equation (3.4-16) can be also used to determine the extensional stress, $\sigma_e(t)$, by doing some modifications. For this calculations the Finger strain tensor for uniaxial deformation has to be used instead of the relative Finger strain tensor for unidirectional flow.

$$C_t^{-1}(t') = \gamma(t,t') \begin{vmatrix} \exp[2\dot{\varepsilon}(t't')] & 0 & 0 \\ 0 & \exp[-\dot{\varepsilon}(\dot{t't'})] & 0 \\ 0 & 0 & \exp[-\dot{\varepsilon}(\dot{t't'})] \end{vmatrix} \tag{3.5-25}$$

Also, to consider the stress under uniaxial extension, the extensional stress has to be equal to

$$\sigma_e(t) = \sigma_{11}(t) - \sigma_{22}(t) = \sigma_{11}(t) - \sigma_{33}(t) \tag{3.5-26}$$

As a consequence, the total strain change and becomes

$$\gamma(t,t') = \gamma_e(t,t') \tag{3.5-27}$$

$$\gamma_e(t,t') = C_{11}^{-1} - C_{22}^{-1} \tag{3.5-28}$$

$$\gamma_e(t,t') = \exp[2\dot{\varepsilon}(t't')] - \exp[-\dot{\varepsilon}(\dot{t't'})] \tag{3.5-29}$$

After the introduction of the new elements the elongational stress of the Wagner models is given by

$$\sigma_e(t) = \int_0^t \mu(t-t')\, h(I_1,I_2)(t,t')\{\exp[2\dot{\varepsilon}(t't')] - \exp[-\dot{\varepsilon}(\dot{t't'})]\}dt' + h(I_1,I_2)_t\{\exp[2\dot{\varepsilon}t] - \exp[-\dot{\varepsilon}\dot{t}]\}\int_{-\infty}^0 \mu\,(t-t')dt' \tag{3.5-30}$$

As in the previous case, there are different expressions for the damping function; however, in this work an exponential function for the damping function proposed by Wagner is used

$$h(I_1,I_2)_s = \exp[-(-2\delta)\sqrt{I_1-3} - \delta\sqrt{I_2-3}] \tag{3.5-31}$$

Where

$$I_1 = \exp[2\dot{\varepsilon}(t-t')] + 2\exp[-\dot{\varepsilon}(t-t')] \tag{3.5-32}$$

$$I_2 = \exp[-2\dot{\varepsilon}(t-t')] + 2\exp[\dot{\varepsilon}(t-t')] \tag{3.5-33}$$

The approach followed in this work use data obtained from shear measurements but using the elongational stress. It means that the values of n1 and n2 are used to calculate the finger strain tensor for uniaxial deformation. The elongational stress is calculated, then the elongational viscosity is calculed with

$$\eta_e = \frac{\sigma_e}{\dot{\varepsilon}} = \frac{\tau_{11}(t) - \tau_{22}(t)}{\dot{\varepsilon}} \qquad (3.5\text{-}34\ )$$

CHAPTER IV EXPERIMENTAL WORK

4.1 MATERIALS AND SAMPLE PREPARATION

The polymer system studied is SU-8 2002 dissolved in cyclopentanone with poly(ethylene) oxide and tetrabutylammonium tetrafluoroborate as additives, from now on SU-8, PEO and TBATFB. For the experiments, all reactants were used as they arrived. SU-8 was obtained from MicroChem(USA) while PEO and TBATFB 99% were obtained from Sigma Aldrich (USA). PEO has a viscosity average molecular weight, Mv~4,000,000 with less than 1000 ppm of BHT as inhibitor.

For preparing the samples, the adequate amount PEO and TBATFB were added to 5 mL of SU-8 in a 20mL vial and stirred at 160rpm during 1 hour at 75°C. The proportions are represented as SU-8:PEO:TBATFB in wt%. The samples with higher PEO concentration often needed more time of stirring to eliminate all the PEO lumps. In order to avoid any chance of cross-linking of SU-8, during the stirring step, all the samples were isolated from light. To extract the solution from the vial, a syringe of 5mL was used. To eliminate the bubbles from the solution, the syringe was placed upside down during 24 hours before the tests.

Table 4.1-1 Set of samples prepared to be characterized

	Serie A		Serie B		Serie C	
Sample	PEO	TBATFB	PEO	TBATFB	PEO	TBATFB
1	0.00	0.00	0.00	0.50	0.50	0.00
2	0.25	0.25	0.25	0.50	0.50	0.25
3	0.50	0.50	0.50	0.50	0.50	0.50
4	0.75	0.75	0.75	0.50	0.50	0.75
5	1.00	1.00	1.00	0.50	0.50	1.00

Note: Values are wt%. dissolved in SU8-2002

4.2 Rheological Tests

To determine the optimal parameters to obtain reproducible and accurate measurements during rheological tests, a set of pretest were made. This previous tests consist in amplitude sweeps (AS), Frequency Sweeps (FS) and Flow curves (FC).

For AS the recommended angular frequency, ω, is $10s^{-1}$. Nevertheless, a set of 1, 5, 10, 15, 20 and 30 s^{-1} angular velocities were tested for most representative samples, i.e. for lowest and highest concentrations of PEO and TBATFB. The results indicate that, indeed, an angular velocity $\omega=10s^{-1}$ had the best performance during all the tests; the amplitude gamma (%γ) was varied from 0.1 to 1000%.

During FS, different angular initial and final frequencies values were established. The initial frequency value was varied from 0.01 to 1 s^{-1} and the final value from 100 to 560 s^{-1}, being this the limit value of the rheometer. The tests pointed out that for the lowest values, the measurements were neither consistent nor accurate. For highest values, the equipment starts to miss measurement points or to present random pikes. The range for FS was established, then, from 0.1 to 100 s^{-1}.

In FC tests the initial and final shear rates, $\dot{\gamma}$, were verified from 0.001 to 1000 s^{-1}. A similar situation of FS tests was encountered. For lowest values the equipment was unable to make realistic measurements and when higher shear rate values were reached, the obtained data show no reproducibility. Lately was found, by looking at the sample during the test, that after $100s^{-1}$ the polymer solution starts to become more elastic. The solution, initially as a fluid, turn out to be like a rubber-like fluid escaping from time to time from the cone and plate and going back inside. Finally the range of shear rate was set from 0.1 to 100 s^{-1}.

According to literature, for low viscosity samples, the cone and plate (CP) geometry is the best option. Nevertheless, the geometry and equipment were compared with the experiments of Karim Bekkour. In his work, Bekkour performed rheological characterizations of PEO in water solutions. PEO concentration and molecular weight were examined through shear and oscillatory experimentations. Detailed information is presented in section 5.1 Geometry validation. Due to results of this comparison and also

to a more repeatability and accuracy during rheological tests, the geometry used along the rheological characterization was Cone-and-Plate.

As a summary, all tests were performed in a oscillatory rheometer (Physica MCR 301, Anton Paar) equipped with a cone-and-plate, CP, geometry (diameter 24.979mm, angle 4.014° and truncation of 249 μm). Experiments were conducted at 25 ± 0.1°C and 24 hours after polymer solution preparation. For amplitude sweeps the angular frequency was settled at 10 s^{-1}, and the amplitude gamma, %γ, was varied from 0.1 to 1000%. In flow curve tests, shear rate was applied from 0.1 to 100 s^{-1}. For frequency sweeps, the percentage of amplitude gamma, %γ, was determined according to the linear viscoelastic (LVE), region obtained from the amplitude sweep experiments previously made and the frequency was varied from 0.1 to 100s^{-1}.

To avoid solvent evaporation, the measurement chamber of the rheometer was saturated with cyclopentanone added to a cotton balls and positioned inside the chamber in order to saturate the atmosphere. Also, due to the sensitivity of PEO solutions to its previous states, all the samples were conditioned by applying a shear rate of 10s^{-1} during two minutes followed by two minutes of rest.

4.3 Electrodes preparation by photolithography

The electrodes were prepared according to the photolithography process guideline for SU-8 provided by MicroChem for a SU-8 layer of 20μm using SU-2015. For this procedure, 4 inches diameter wafers Si-SiO2 100were used. SU-8 2015 and SU-8 developer from MicroChem (USA). Deionized water, acetone and isopropanol from. High purity nitrogen by N_2. And as secondary equipment a Spin Coater, hot plate and UV lamp and EMS 78414-43WFG wafer tweezers.

A wafer was rinsed with deionized water, acetone, isopropanol and finally dried with N_2 in order to eliminate particles since there is no a clean room at the institution. After that, the wafer was placed in a hot plate at 120°C during 30 minutes to eliminate any residues from the rinsing process; the hot plate is inside an extraction hood. After the dehydration step the wafer is carefully placed and centered in the spin coater. Once the wafer is in the right position, the vacuum is activated to hold it. Following the

manufacturer procedure, 1 mL of SU-8 2015 is poured for each 25mm of wafer diameter, the pouring have to be done rapidly but with caution in order to avoid bubbles formation, also, the SU-8 has to be dispensed as uniform as possible on the wafer. When the SU-8 was in place, the spin coater used a program that follows, as a first step, 10s at 500rpm with an acceleration of 100 rpm/s followed by 30s at 2000rpm with an acceleration of 300rpm/s. Since a little amount of material is accumulated at the edge of the wafer, and this may cause an inadequate exposure of the material when the mask is placed, it is necessary to remove this excess with a wiper with acetone. After the edge removal, the wafer is placed in a leveled surface to rest during 1hr to eliminate any present bubble. Later, a soft bake is made at 95°C for 30 minutes to promote the activation of initializers of the crosslinking. When the soft bake is finished, the mask with the pattern of electrode is positioned on the wafer and this is placed in a chamber to be exposed to UV light for 1min to photo polymerize the material exposed through the mask. Afterwards, a post exposure bake is carried out at 95°C during 4 minutes. To develop the structure it is necessary to submerge the wafer in SU-8 developer during 4 minutes at room temperature, further a rinsing has to be done during 10s, after that an isopropanol rinsing is done and, if there is formation of salts evidenced for a white precipitated, the wafer is rinsed again with developer until the salt formation is null. Finally it is necessary to perform a hard bake during 1hr at 200°C.

4.4 Fiber Deposition

In order to understand the fiber deposition experimental explanation is necessary to explain three terms first. These are i) Fabrication speed, this speed is that one that the stage use to follow a programed pattern. ii) Inter-fabrication speed, this is required to move between patterns, for example, if you program two parallel lines the stage has to move from the first line to the second by using this inter-fabrication speed, also this speed is used to return to a zero position. iii) Acceleration, this parameter is necessary to reach the fabrication and inter-fabrication speeds.

In Figure 4.4-1 are presented the patterns of fiber deposited on the SU-8 electrodes. Fabrication speeds of 20, 40 and 60 mm/s were chosen. Since the total deposition longitude of the electrode is 1800μm, 10 lines were programed for each speed with a

separation of 50 μm and a separation of 100μm for each speed deposition. The inter-fabrication velocity and the acceleration used were v_i=500mm/s and a=500mm/s^2. In order to reach a steady flow of the fibers, the lines were programed with a length of 8500 μm even when the distance between the first and the las post is 1700 μm. The height from the substrate to the tip was settled at 200μm. Voltage was varied from 100v to 400v. For all samples was used 100v nonetheless the concentrated solutions required 400v to deposit the fibers. Flow rate was not measured because one droplet was enough to make more than 100 depositions.

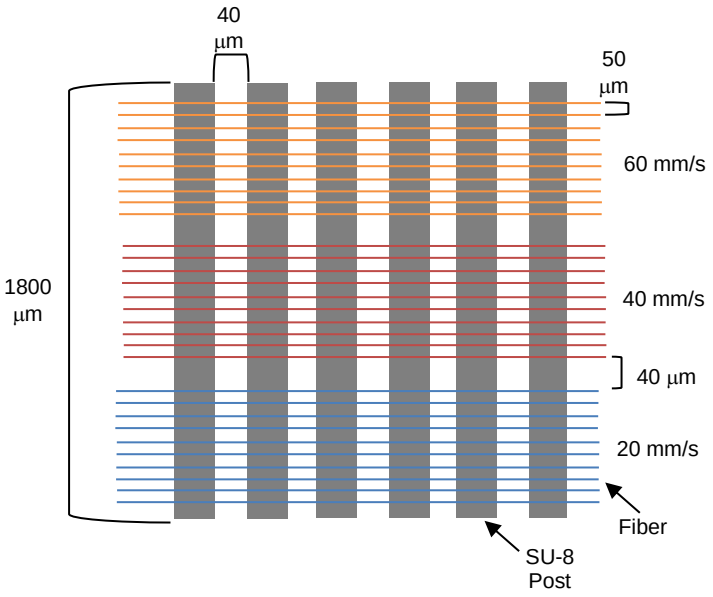

Figure 4.4-1Fiber deposition scheme

Since the fabrication speed used in the research done by The University of California in Irvine was 40 mm/s a second deposition method is used to compare results. The deposition consists in 30 fibers with the specifications aforementioned but using only the fabrication speed of 40mm/s.

The solutions to be deposited are those from Serie A because the amounts of additives increase equally, thus it is a more representative set of concentration. After deposition, all the devices were immediately exposed to UV light of ~360 nm wavelength during 10 min. Further, a gold layer of 5nm was deposited on each dispositive for SEM characterization.

CHAPTER V RESULTS AND DISCUSSIONS

5.1 GEOMETRY VALIDATION

Figure 5.1-1 shows the results for the experimentations following the methodology settled by Bekkour on its work with PEO solutions. Three concentrations were compared 2.5, 1 and 0.5 wt%. of PEO in D.I. water. As it can be seen, for all concentrations the experimental data fits practically flawlessly over literature data for γ>1 s^{-1}. A small discordance at lower shear rates for 1wt% and 0.5wt% is present. Nevertheless, these differences in results were expected since the PEO used in literature has a Mw=4x10^6 while the one used in the experiments has a Mv=4x10^6 and in a typical distribution curve, the average values are related to each other as follows: Mv< Mw. This means that the PEO used in literature has longer polymer chains and a slightly wider molecular weight distribution. However, since these results matches well done with the previous findings, these results give the required information to use the Cone-and-plate as the formal geometry for the rheological characterization experimentations due to its accuracy and reliability [84]

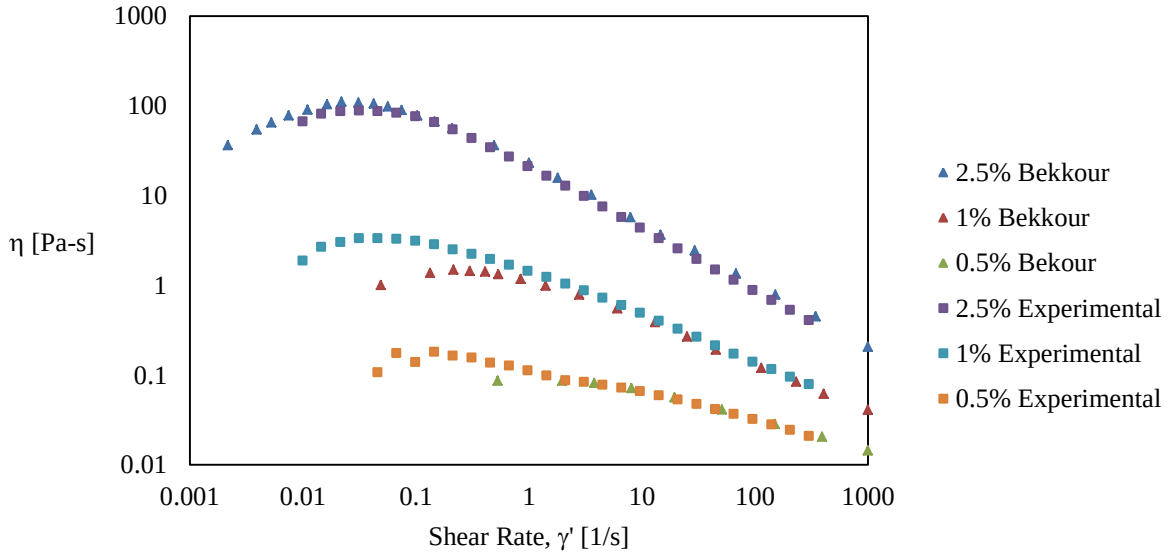

Figure 5.1-1 Flow Curve for PEO solutions in D.I. water. Comparisson between experimental data and literature (Bekkour) [31].

5.2 Rheological Characterization

5.2.1 Amplitude Sweeps

Figure 5.2-1 shows the results for amplitude sweeps (Constant angular frequency of ω=10 1/s) carried out on solutions of Serie A where both PEO and TBATFB are increased equally. For pure SU-8 2002 (0.0wt%. of PEO and TBATFB) the equipment was not capable of obtain data from the storage modulus, G'. And for the loss modulus, G'', at low shear rates there is a notorious variability of the data until a strain of 10% is reached. For the rest of the concentrations the storage modulus is smaller than the loss modulus. Both G' and G'' present a parabolic-like behavior, at low deformation the values of the moduli is increasing until it reaches a semi-stable linear behavior between 1 to 10 γ%, after this value is overcome both modulus start to decrease. As concentration increase the values of G' and G'' increase too, however for the two highest concentrations the magnitude of both moduli are closer in comparison with the rest of the concentrations.

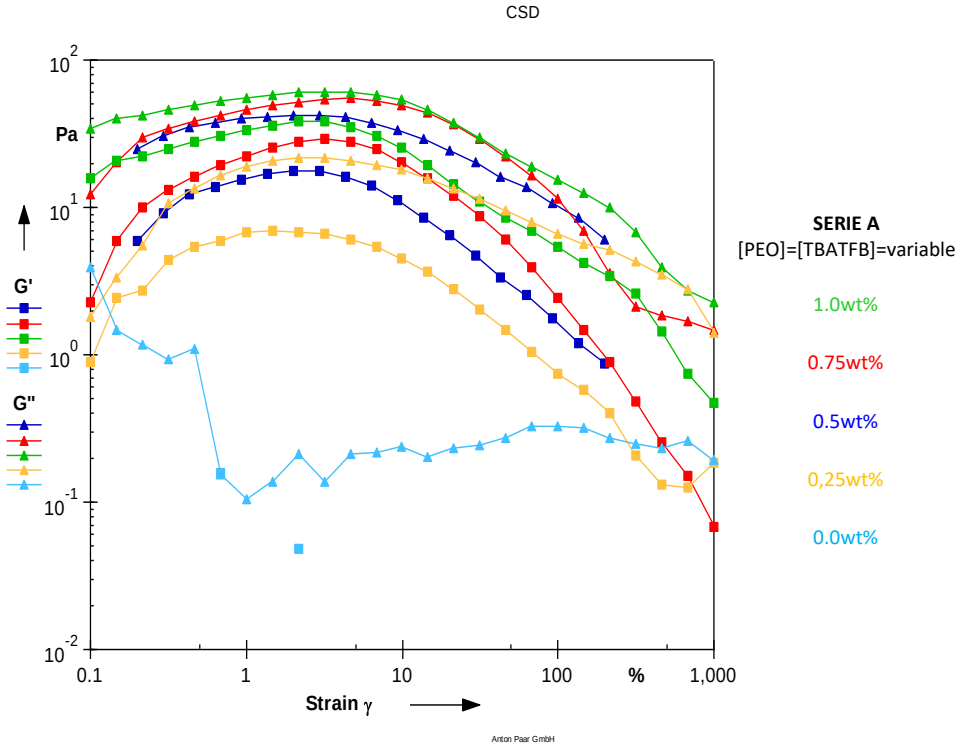

Figure 5.2-1 Amplitude Sweep for solutions from Serie A, where [PEO]=[TBATFB] varied from 0 wt% to 1wt%. Constant angular frequency, ω=10 s^{-1}.

These experiments show that there is no a clear Linear Viscoelastic Region, even for small deformations there is a response of the material, this means that the molecular structure of the material is high sensitive to external forces. Another particularity of the system is that there is no yield point, in fact as the deformation increase, both moduli separate from each other.

Figure 5.2-2 shows the results for amplitude sweeps (Constant angular frequency of ω=10 s^{-1}) carried out on solutions from Serie B where concentration of PEO varies from 0 to 1% and concentration of TBATFB=0.5wt% in SU-8 2002. For PEO=0wt%. there is virtually no measurements form G' and the viscous modulus is fairly constant on 0.2 Pa. Concentration of 2.5wt%. shows a similar behavior than zero percent of PEO but the semi-constant value for G' is of 2 Pa. For the rest of the concentrations there is a parabolic-like behavior as in Serie A.

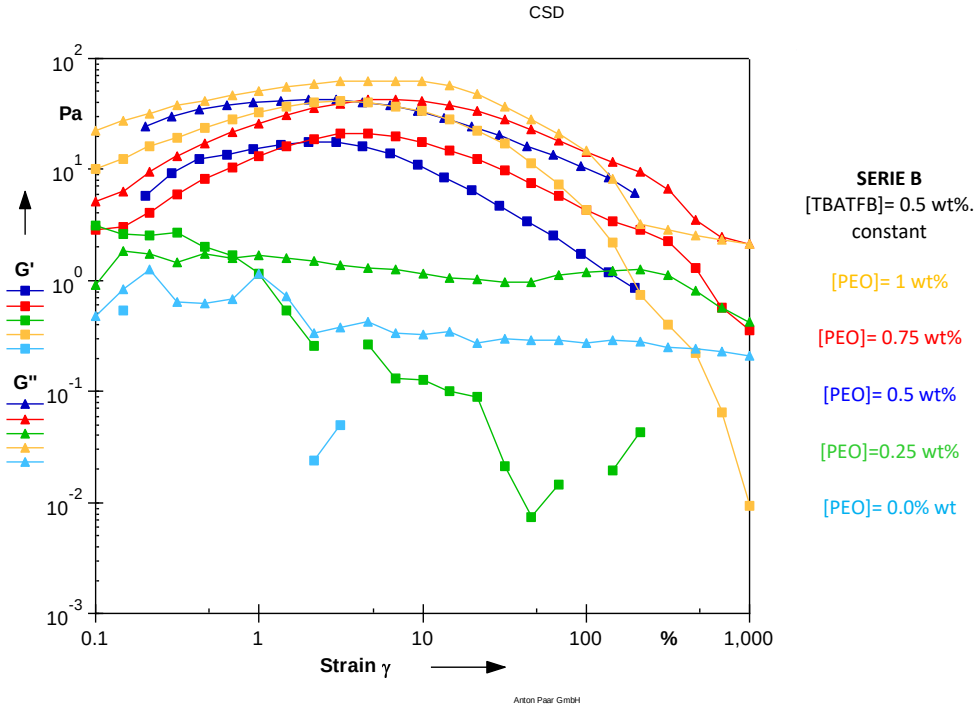

Figure 5.2-2 Amplitude Sweep for solutions from Serie B, where [PEO] varies from 0WT% to 1wt%. and [TBATFB]=0.5wt%. Constant angular frequency, ω=10s^{-1}

Figure 5.2-3 shows the results for amplitude sweeps (Constant angular frequency of ω=10 s^{-1}) carried out on solutions from Serie C where concentration of TBATFB varies from 0 to 1% and PEO =0.5wt%. in SU-8 2002. For the whole set of concentration the semi-parabolic behavior was present, G'<G''

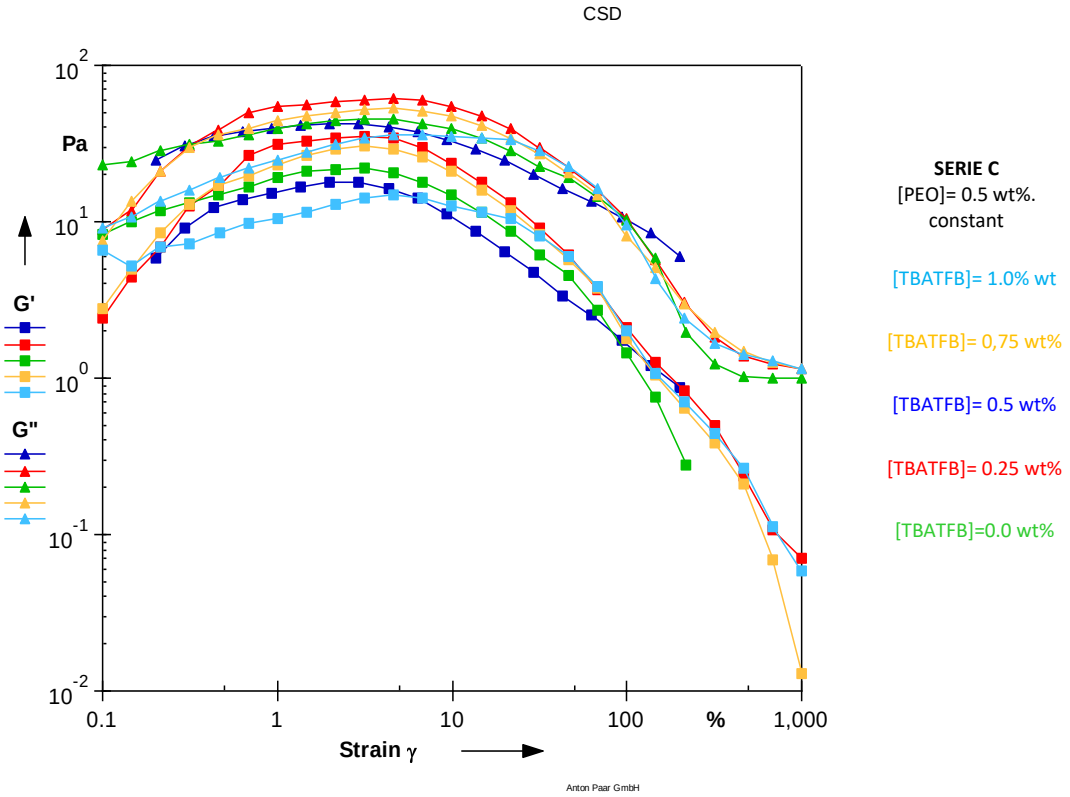

Figure 5.2-3 Amplitude Sweep for solutions from Serie C, where [TBATFB] varies from 0wt% to 1wt%. and [PEO]=0.5wt%. Constant frequency, ω=10 s^{-1}.

Table 5.2-1 Maximum and minimum values of G' and G'' for Serie A

		Serie A [PEO]=[TBATFB], wt%				
	Moduli, Pa	0.00	0.25	0.50	0.75	1.00
Low %γ	G'_{max}	0.16	6.95	17.70	28.90	38.2
	G''_{max}	3.90	21.70	42.20	54.80	60.80
	G'_{min}	0.00	0.89	5.86	2.29	15.90
	G''_{min}	0.11	1.80	30.20	12.20	34.30
High %γ	G'_{min}	0.00	0.13	0.87	0.07	0.48
	G''_{min}	0.20	1.42	6.06	1.49	2.28

Table 5.2-2 Maximum and minimum values of G' and G'' for Serie B

		Serie B [TBATFB]=0.5; [PEO]=variable, wt%				
	Moduli, Pa	0.00	0.25	0.50	0.75	1.00
Low %γ	G'_{max}	1.87	17.70	3.10	42.00	20.9
	G''_{max}	0.85	42.20	1.84	63.40	42.80
	G'_{min}	0.00	5.86	1.16	10.10	2.90
	G''_{min}	0.12	24.70	1.45	22.60	5.18
High %γ	G'_{min}	0.00	0.87	0.00	0.01	0.36
	G''_{min}	0.19	6.06	0.42	2.10	2.15

Table 5.2-3 Maximum and minimum values of G' and G'' for Serie C

		Serie C [PEO]=0.5; [TBATFB]=variable, wt%				
	Moduli, Pa	0.00	0.25	0.50	0.75	1.00
Low %γ	G'_{max}	21.80	35.40	17.70	30.40	14.9
	G''_{max}	45.30	61.90	42.20	52.90	36.30
	G'_{min}	8.24	2.44	5.86	2.80	5.16
	G''_{min}	24.40	8.86	30.20	7.54	9.10
High %γ	G'_{min}	0.00	2.12	0.87	0.01	0.06
	G''_{min}	0.99	10.40	6.06	1.14	1.15

From the AS graphs it is possible to three values for G' and G'', a minimum in the low %γ, a global maximum and a minimum in the high %γ. Tables 2.2 1-3 shows these values. For Series A and B all values increase as the concentration of additives increase, however for Serie C lower concentrations of TBATFB increase the values more than those of higher content of the salt, for example the maximum value of G' for 1wt% is of 14.9 Pa while 0.25wt%. has the highest value of the same Serie with 35.4 Pa. For all Series, values at low deformations are bigger than the values at the highest deformation.

The purpose of the AS is to determine the amplitude that has to be used in frequency sweeps; nevertheless this amplitude must be that one that keeps undisturbed the structure of the material, this is the linear viscoelastic region, but there is no LVER for any of the solutions tested. For these reasons, the amplitude selected was that one where the plots show less variation of the data, this is when 1%<γ<%10. However, when amplitude sweeps were tested using this amplitude, the system shows a high degree of variance and a complete lack of repeatability. Finally the amplitude gamma that gave the best performance of the equipment was %γ=20.

5.2.2 FLOW CURVE

Figure 5.2-4 shows the results of Flow Curves tests, FC, carried out on solutions from Serie A where both PEO and TBATFB are increased equally. There is an evident effect of the addition of both additives behavior of the solution under shear deformation. The values for shear viscosity increase as the concentrations of PEO/TBATFB are increased too. For concentrations from 1 to 0.25 wt%. there is a slightly increasing of η for lowest shear rates until a value of 0.3 s^{-1}. After this critical value, a shear thinning behavior is observed. This behavior is in agreement with literature. For the increasing values of shear rate, the ball-shaped molecules start to form entanglements, however after a critical value of $\dot{\gamma}$ (0.3 s^{-1}); these entanglements start to break apart, diminishing friction between chains and therefore the viscosity.

For higher concentrations there is a more pronounced slope while for 0.25wt% the viscosity practically remains constantly at 0.1 Pa·s. For pure SU-8, there is a lack of accuracy and repeatability in measurements below $\dot{\gamma}$=2 s^{-1}, after this value, it seems to be a minimum increasing in the values of shear viscosity, but it can be assumed as constant. The Newtonian-like behavior could be caused by the solvent (cyclopentanone), the small size of SU-8 molecules or the low concentration of SU-8 in the solution. It is known that the concentration of SU-8 molecules can modify the fluid dynamics, since SU-2000 series, like 2015 or 2050 are highly viscous.

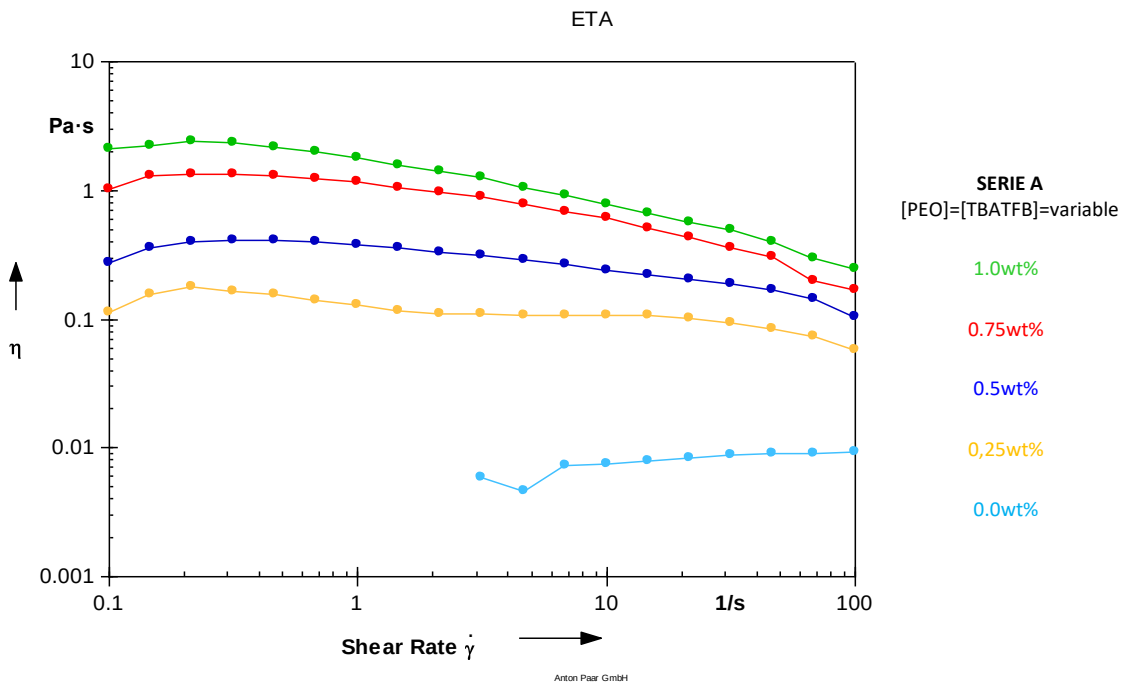

Figure 5.2-4 Flow Curve for solutions from Serie A, where [PEO]=[TBATFB] varied from 0 wt% to 1wt%.

From the FC graph it possible to observe that the minimum addition of additives (0.25wt%.) to pure SU-8 cause a change in one order of magnitude (from 0.01 to 0.1 Pa·s) on shear viscosity. While three times the same increment (increment of 0.25% wt. From 0.25wt% to 1% wt.) is necessary to cause the same effect in the viscosity (from 0.1 to 1 Pa·s). It is possible that the higher amounts of the additives are reaching a threshold for critical concentration, where the deformation rates have no longer effect on the viscosity.

Figure 5.2-5 shows the results of Flow Curves tests, FC, carried out on solutions from Serie B where PEO is varied from 0wt% to 1wt% and TBATFB=0.5wt%. is constant For these experiments there is not an obvious relation between the addition of PEO and the effects on shear viscosity. For PEO=1wt%., there is a small increase in η as $\dot{\gamma}$ is increased, but when $\dot{\gamma}$=1 the viscosity drops suddenly from 2 to 0.8 Pa·s, after this, a shear thinning behavior is present. For PEO=0.75 and 0.5 wt%. shear thinning behavior is present with a bigger slope for 0.75wt%. In fact, for the concentration of 0.5wt%, the

values of viscosity are in a range between 0.2 to 0.4 Pa·s, while for 0.75wt% the range of viscosities varies from 0.5 to 2 Pa·s. When PEO=0.25wt%, the shear viscosity decreases at lower shear rates and get stabilized at 0.1 Pa·s when 1%<$\dot{\gamma}$<20%. After this range the viscosity drops abruptly from 0.1Pa·s at $\dot{\gamma}$=20 s^{-1} to 0.02 Pa·s at $\dot{\gamma}$=100 s^{-1}. Finally, when PEO=0wt%, the values of viscosity at lower shear rates are negligible due to its variation, however as the shear rate reach the value of 2 s^{-1} the viscosity get stabilized and then start to present a minimum decrease on its values. It is remarkable that for Serie A this semi-constant value of viscosity is 0.01 Pa·s while for Serie B is of 0.02 when both PEO and TBATFB are 0.25wt%. It means that the presence of electrolytes caused a variation on the hydrodynamic of the solution, caused by the modification of the shape of the polymer chain due to the presence of charges.

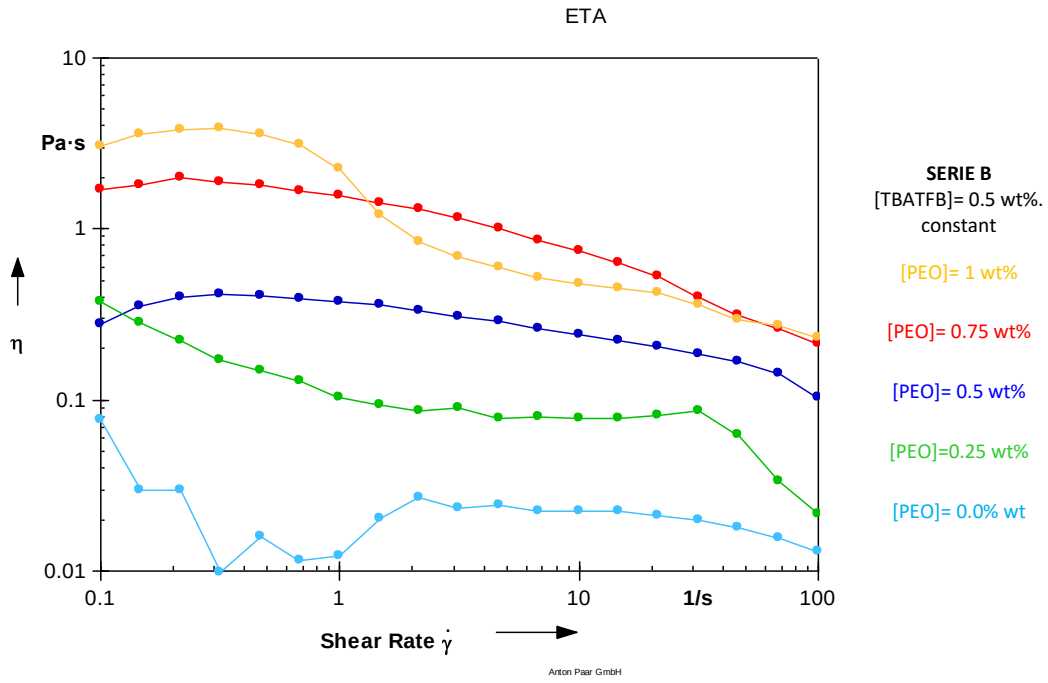

Figure 5.2-5 Flow for solutions from Serie B, where [PEO] varies from 0wt% to 1wt%. and [TBATFB]=0.5wt%.

Figure 5.2-6 shows the results of Flow Curves tests, FC, carried out on solutions from Serie C where TBATFB is varied from 0 to 1wt% and PEO=0.5wt%. is constant For TBATFB=1wt% there is a shear thinning behavior for shear rates from 0.1 to approximately 15 s^{-1}, after this value, a critical drop of the viscosity followed by a stabilization after shear rate reach 20 s^{-1} is present. A similar behavior is observed for concentration of 0.75wt%. and less evident for 0.0wt%. For concentrations of 0.5wt% and 0.25wt% the behavior of the shear viscosity is practically the same. The difference lies on the values of η at the lowest shear rates, where $\eta_{0.25\%}>\eta_{0.50\%}$ and highest shear rates, where $\eta_{0.25\%}<\eta_{0.50\%}$ with a crossover point at $\dot{\gamma}$=3 s^{-1}.

It is notorious that for TBATFB=0.0wt% the values of η are bigger than those for TBATFB equal to 0.25wt% and 0.5wt%. It has to be recalled that for Serie C there is always [PEO] at 0.5wt%, this means that the higher viscosity values for solution TBATFB=0.0wt% are caused by the PEO. It can be said that the effects of PEO are suppressed by TBATFB in small quantities. Perhaps only a small quantity of polymer chains is being modified in their structure changing from a ball-shaped to a semi-stretched chain reducing then the viscosity (under shear flow) because of the alignment of the chains with the flow lines. However as the concentration of TBATFB is increased over 0.5wt%, the values of shear viscosity overcome the values of the solution TBATFB=0wt%. It seems that there is a critical value of the salt that modifies the internal structure of the solution. Above this critical value, it is probable that almost all polymer chains get stretched promoting a higher number of entanglements and therefore an increment in η. Yet, when a value of shear rate of $\dot{\gamma}$=20s^{-1} is reached all the solutions have values of η around 0.2 Pa·s. At this rate of deformation, it is plausible that the hydrodynamics of the solutions are dictated majorly by the PEO.

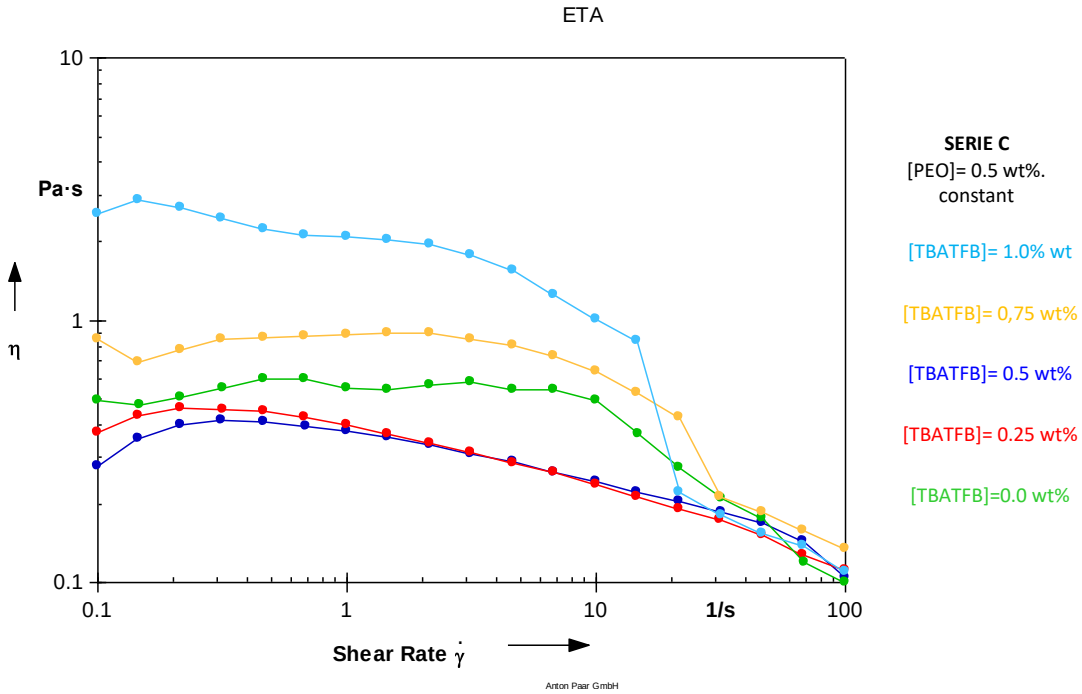

Figure 5.2-6 Flow Curve for solutions from Serie C, where [TBATFB] varies from 0wt% to 1wt%. and [PEO]=0.5wt%.

5.2.3 Frequency Sweep

In Figure 5.2-7 are presented the results for the frequency sweeps of solutions from Serie A ([PEO]=[TBATFB]). For the lowest concentration of PEO and TBATFB has a decreasing behavior of the complex viscosity and, after reaching a frequency of 3 s^{-1} start to increase. However, the G' was not measured by the equipment (See APPENDIX I), it is possible that $|\eta^*|$ its only representing the viscous behavior of this solution.

For solutions from 0.25wt% to 1wt% all the curves present the same shear-thinning like behavior. And there is a direct relation between the concentrations of the additives and the values of complex viscosity. An interesting behavior is encountered at the lowest angular frequencies of solution PEO=TBATFB=0.25wt% where a small drop of the complex viscosity is present. Probably at $\omega<0.1$ s-1 there is a previous state on the internal structure of the material, because both G' and G'' seems to show an increase at lowest angular frequencies, see APPENDIX I.

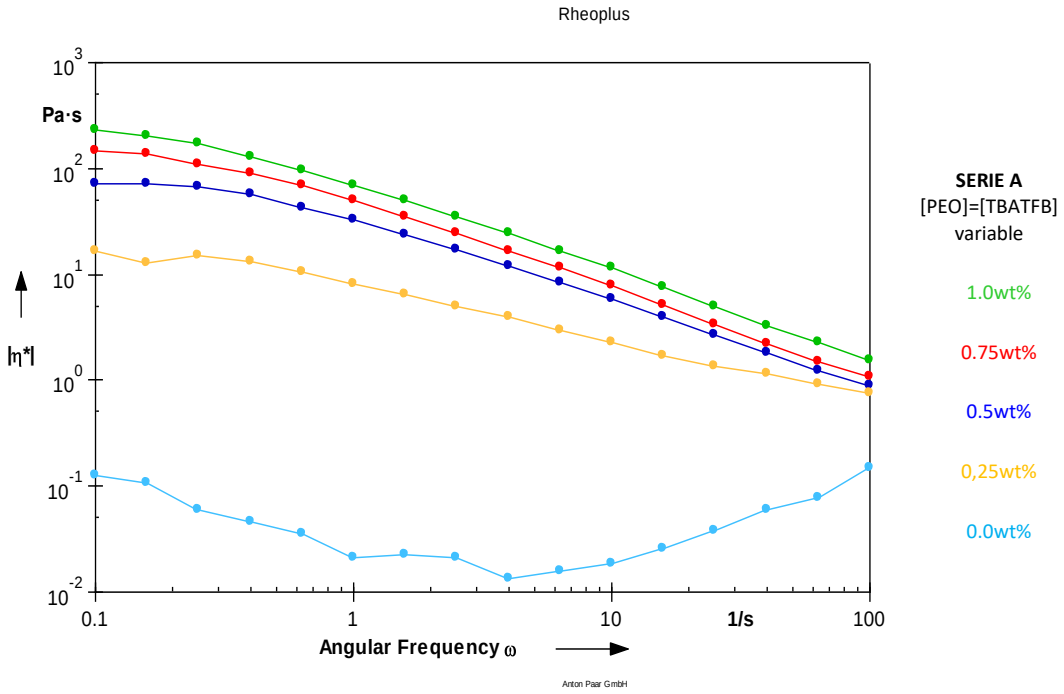

Figure 5.2-7 Frequency Sweep for solutions from Serie A, where [PEO]=[TBATFB] varied from 0 wt% to 1wt%. Constant ammplitude gamma, %γ=20

In Figure 5.2-8 are presented the results for the frequency sweeps of solutions from Serie B ([TBATFB]=constant, [PEO]=0%wt to 1wt%). The behavior of complex viscosity is very similar to those for the Serie A. For the lowest concentration of PEO, the equipment has not enough sensibility to make measurements of the storage modulus because this one is very low. When PEO=0.25wt% complex viscosity remains almost constant, $|\eta^*|$ =1Pa·s, for all the range of angular frequency, however the same effects is present in Serie A at 0.25wt%, a little variation of complex viscosity at the lowest values of ω. It is possible that lower concentrations of PEO interact with the salt and a transient state of the molecular structure is caused by the deformation forces.

Another particularity of this set of experimentations is that, for the higher concentrations, 0.5, 0.75, and 1wt%., the magnitude of complex viscosity is similar. At $\omega=100s^{-1}$, the three concentrations have a value $|\eta^*|\approx 2$ Pa·s. With this information it can be assumed that there is a critical concentration for this particular system of 0.5wt%. Under this concentration the system shows different behaviors as the molecules has enough space to diffuse and break entanglements. On the other hand when the critical

entanglement concentration is exceeded, the polymer chains overlapped and become highly tangled therefore is no longer possible to form more entanglements. The shear thinning behavior is due to the gradually rupture of entanglements and the consequent alignment of the chains. The invariable value of viscosity for the solution with concentration of 0.25wt% can be explained as a cancelation of the force applied and the Brownian motion that dissipates the energy in the transient network. It means that the rate of entanglements formation is equal to the rate of rupture thereof.

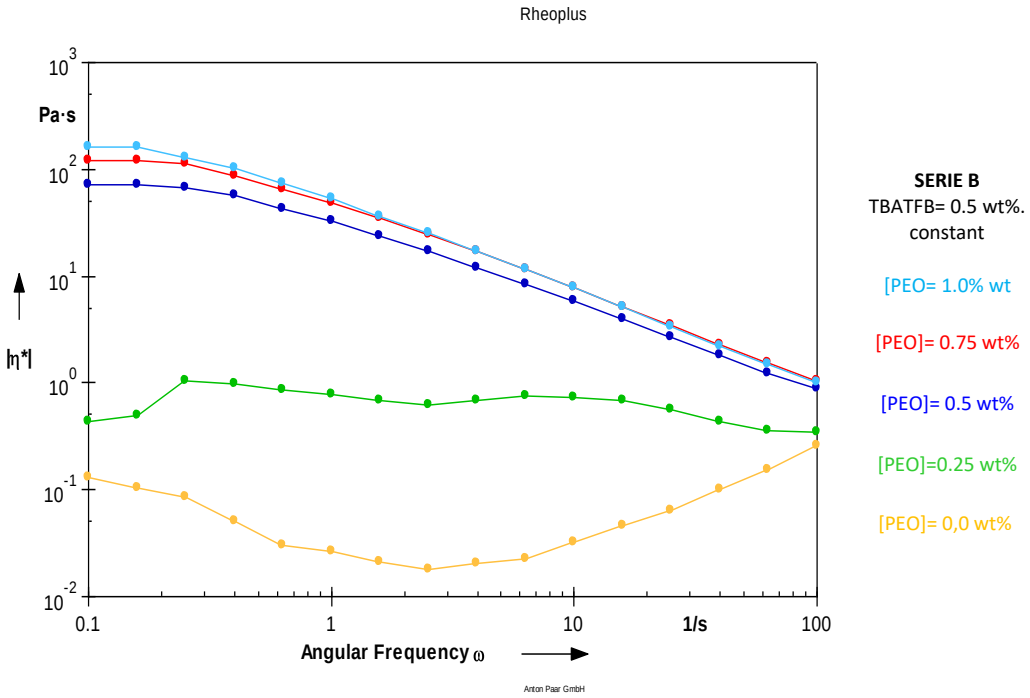

Figure 5.2-8 Frequency for solutions from Serie B, where [PEO] varies from 0wt% to 1wt%. and [TBATFB]=0.5wt%. Constant ammplitude gamma, %γ=20

Figure 5.2-9 presents the results for the frequency sweeps of solutions from Serie C ([PEO=0.5wt%, [TBATFB]=0wt% to 1wt%). The observations do not indicate a clear relation between |η*| and the addition of TBATFB. While concentrations of 1, 0.5 0.25 and 0 wt% have both behavior and magnitude alike, for solution with TBATFB=0.75wt% a non-uniform behavior is present. First, at lower angular frequencies there is an increasing of |η*|, later it remains almost constant at 20Pa·s until ω reach a value of $4s^{-1}$, then it drastically drops to 1 Pa·s, and again remains almost constant. It is noticeable

that concentration of 1% has a decreasing value of complex viscosity at higher angular frequencies and it reach a value similar to that one of TBATFB=0.75wt%.

Another interesting behavior of $|\eta^*|$ is present at the lowest values of ω (0.1, 0.2, and 0.3 s^{-1}) in this range of frequencies some concentrations change the magnitude of $|\eta^*|$ without a defined behavior. While some concentrations show a shear thickening behavior some other shows the opposite comportment, even TBATFB=0.5wt% remains undisturbed in this zone. It can be said that the addition of salt modifies hydrodynamics of the solutions in way difficult to be predicted and a further deep rheological characterization might be needed.

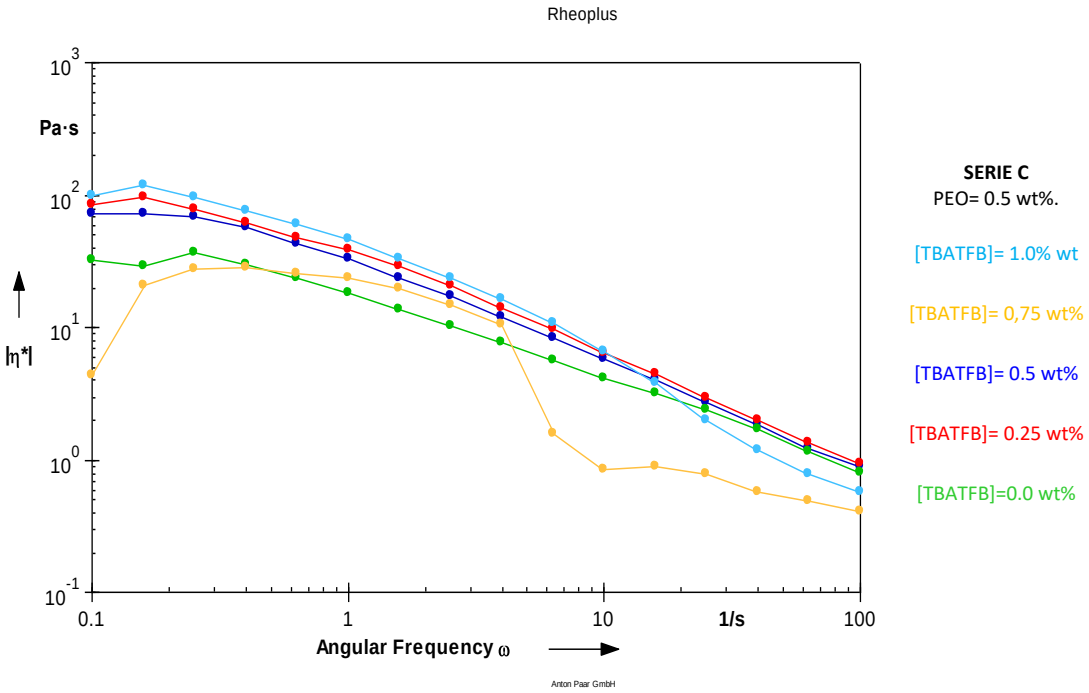

Figure 5.2-9 Frequency Sweep for solutions from Serie C, where [TBATFB] varies from 0wt% to 1wt%. and [PEO]=0.5wt%.Constant ammplitude gamma, %γ=20

5.2.4 ELONGATIONAL VISCOSITY

In Tables 5.2-1-3 are presented the values of the relaxation spectra, λ_i and a_i, and also the parameters n1 and n2 used to calculate the elongational viscosity for each set of concentrations. The terms of the relaxation spectra are obtained from a mechanical analog of a spring and a dashpot. Each set of spring and dashpot is a Maxwell element. λ_i is related to the dashpot (viscous behavior) and it refers to the time the polymer chains take to return to equilibrium after being disturbed, big values of λ_i dictates long times to return to equilibrium and vice versa. On the other hand a_i is related to the spring of the Maxwell element (elastic behavior), it means to the response as a solid of the fluid. The relaxation spectrum is the summation of the response of a determined number of elements.

For the tables 5.2-4 (Serie A) and 5.2-5 (Serie B) it is possible to observe that, for all the solutions, 5 elements were enough to determine the relaxation spectra. Besides, for each element, the values of a_i increase from left to right as the concentration of the additives increases too. This means that the elastic response of the material is directly related to the PEO and TBATFB quantity. The relaxation times are the same for all series because of all experiments were performed at the same range of angular frequencies.

For table 5.2-6 (Serie C) the values match with the information obtained from FC and FS, the elasticity of the material does not have a predictable relation with the amount of additives. However, since this values are obtained from oscillatory data (FS) it was expected to obtain this kind of behavior.

Finally, the parameters n_1 and n_2 have to be fitted from shear flow tests (FC) and the equation (3.5-21) that gives viscosity from the Wagner model for unidirectional shear flow. Nevertheless, this was not possible because of the values of a_i were not accurate and a minimizer factor was needed, yet, this factor was different for each solution and it did not have a physical meaning attributable. For this reason it was decided to fit the data for shear viscosity from the Wagner model with the complex viscosity. This procedure was realized without difficulties, but it is necessary to say that estimations of

elongational viscosity could have variations with real measurements due to this change in the original procedure.

Table 5.2-4 Relaxation spectra elements, λ_i and a_i. and strain sensitive terms of damping function, n_1 and n_2 for concentrations Serie A

Serie A				
	PEO=TBATFB wt%. In SU-8 2002			
	0.25	0.50	0.75	1.00
$\lambda_i[s^{-1}]$	Weight factors of memory function, a_i			
0.001	0.02	0.06	0.09	0.16
0.008	0.07	0.28	0.56	1.07
0.080	0.28	1.78	3.25	6.00
0.796	0.81	6.71	12.47	19.09
7.958	2.30	25.39	47.89	60.76
n1	0.01670	0.60260	0.20000	0.15169
n2	0.00118	0.00589	0.00900	0.00686

Table 5.2-5 Relaxation spectra elements, λ_i and a_i. And strain sensitive terms of damping function, n_1 and n_2. For concentrations Serie B

Serie B TBATFB=0.5wt%.				
	PEO wt%. In SU-8 2002			
	0.25	0.50	0.75	1.00
$\lambda_i[s^{-1}]$	Weight factors of memory function, a_i			
0.001	0.02	0.06	0.10	0.07
0.008	0.07	0.28	0.74	0.64
0.080	0.28	1.78	2.77	3.90
0.796	0.81	6.71	8.11	17.71
7.958	2.31	25.39	23.74	25.77
n1	0.08000	0.60260	0.04462	0.03542
n2	0.00013	0.00589	0.00405	0.00451

Table 5.2-6 Relaxation spectra elements, λ_i and a_i. and strain sensitive terms of damping function, n_1 and n_2. For concentrations Serie C

Serie C PEO=0.5wt%.					
TBATFB wt%. In SU-8 2002					
	0.00	0.25	0.50	0.75	1
$\lambda_i[s^{-1}]$	Weight factors of memory function, a_i				
0.001	0.04	0.04	0.06	0.00	0.02
0.008	0.27	0.41	0.28	0.03	0.07
0.080	0.61	2.26	1.78	2.00	0.28
0.796	3.58	6.14	6.71	143.63	0.81
7.958	20.91	16.71	25.39	-	2.31
n1	0.01937	0.04302	0.60260	0.04113	0.004446
n2	0.00146	0.00336	0.00589	0.00143	0.033736

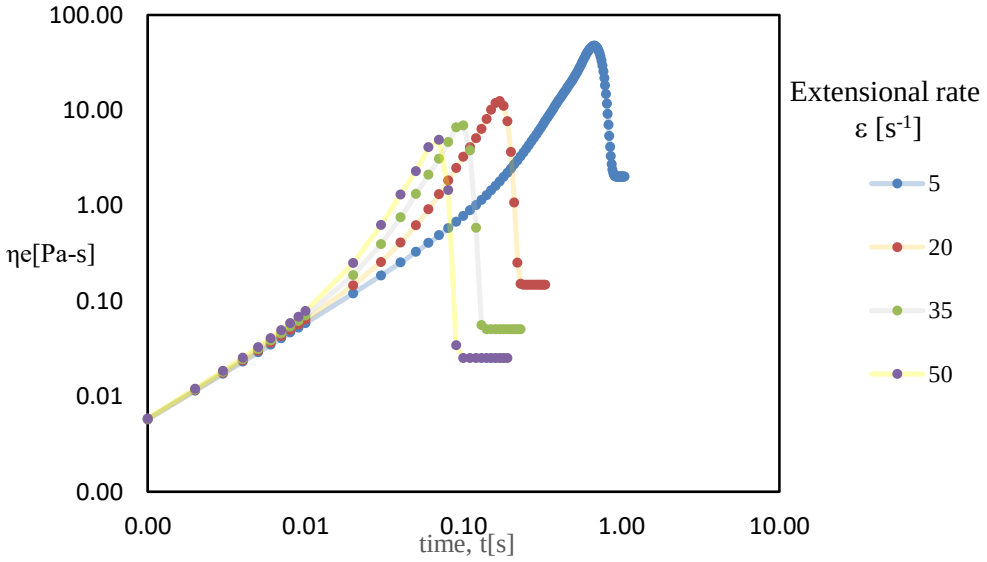

Figure 5.2-10 Elongational viscosities in function of time calculated at different extensional rates for Serie A 0.25wt%

In Figure 5.2-13 is plotted the data of the elongational viscosity in function of time at different shear rates until it reach a steady state for a solution from Serie A 0.25wt%. It can be seen that η_e for shear rate of $5s^{-1}$ present the largest time to reach the steady state. Also it is possible to observe that, as the extensional rates are increased the time

to reach the steady state of the ηe is reduced. This behavior is expected since the polymer chains has enough time to dissipate the low applied energy caused by the stretching by simply Brownian motion, but, when the extensional rate is the rate of entanglement of the polymer jet is so high that quickly reach an strong and unchanging internal structure of the solution.

From the data it is possible to observe that for all the curves there are an abrupt diminishing of the elongational viscosity just after the maximum was reached. This drop in η_e is followed by a steady state. This effect is caused by the rupture of the entanglements due to the high force applied at high deformation rates.

In order to compare the magnitude of η_e between the steady state and it maximum value in a transient state, it is possible to generate a new curve by taking the elongational viscosity (maximum or steady state) in function elongational rate at which η_e was calculated. Figure 5.2-14 shows the aforementioned graph.

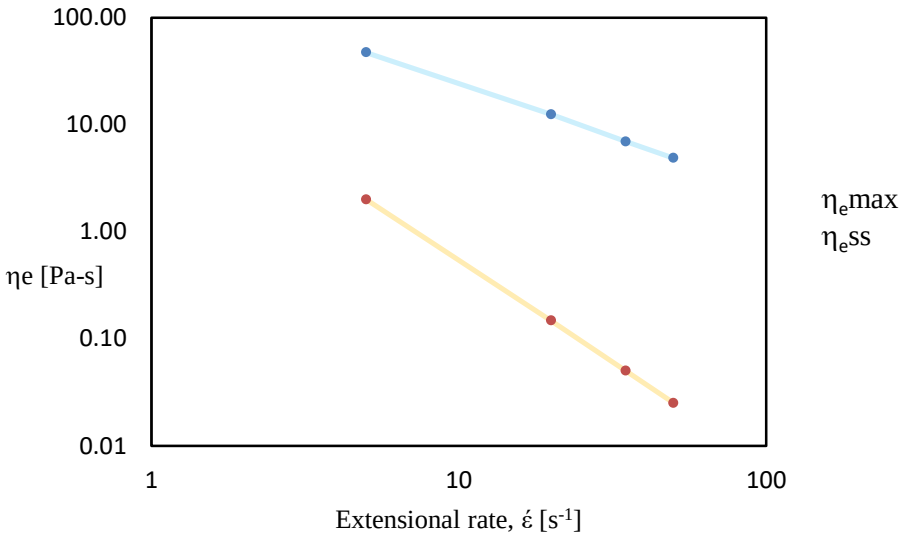

Figure 5.2-11 Elongational rate in function of elongational rate for the maximum, hemax (maximum elongational viscosity), and steady state values, hess (Steady state elongational viscosity). Solution A 0.25wt%

As it can be seen, the values of the maximum elongational viscosity are two orders of magnitude higher than those for the steady state. This means that for a given

system that works near to steady state flow, and therefore a steady extensional rate, if there is not enough time to get the steady state of the elongational viscosity, the properties of the product can present a large variation because the operation is taking place in this threshold.

The rest of the solutions were subjected to the same treatment and all of them present a similar behavior. For this reason from this point, there will be only presented the results of elongational viscosity as function of elongational rate. However all graphs of this section are presented in APPENDIX II. Observe that there is no results for pure SU8-2002 since this solution cannot analyze by this model.

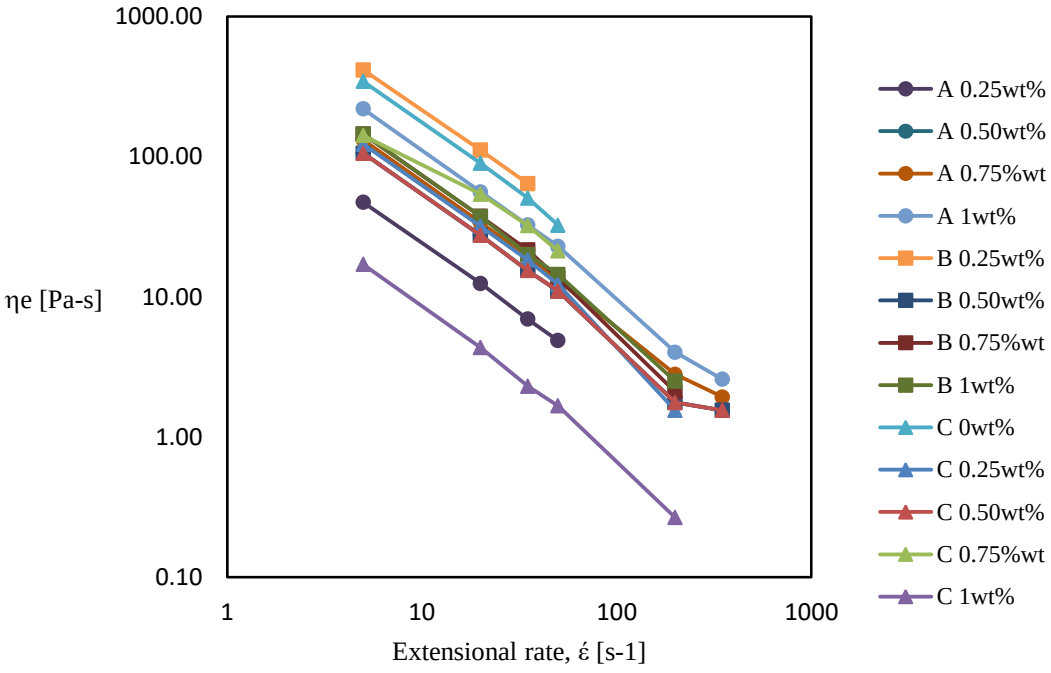

Figure 5.2-12 Maximum elongational rate vs extensional rate for the whole set of concentrations

Figure 5.2-15 shows the maximum values of the elongational viscosity for all the prepared solutions. Recalling that in Serie A concentration of PEO is equal to TBATFB, in Serie B TBATFB is constant at 5wt% and PEO varies from 0wt% to 1wt%, and in Serie C PEO is constant at 5wt% and TBATFB varies from 0wt% to 1wt%. Solution B 0.25wt% presents the highest values of η_e while the lowest is C1%wt. These result follow the same trend with those results for shear tests, where C1wt% shows a sudden

drop at high shear rates, it seems that the effect of the salt, at high concentrations, has big effect on the internal structure of the polymeric solution at high deformation rates. It is probably that the salt breaks the entanglements as higher deformations are applied by unfolding the polymer chains due to a solvation effect and the consequent repulsion of charges. The second lowest elongational viscosity values are those obtained from solution A 0.25wt%. A similar effect could be present in A 0.25wt%, but in this case, there is a considerably less amount of polymer chains, therefore the possibility of chain entanglement is reduced and, in doing so, the elongational and shear viscosity.

The second highest values are from A 1wt%. The rest of the concentrations have almost the same values of η_e. It is evident that all the curves have a decreasing behavior.

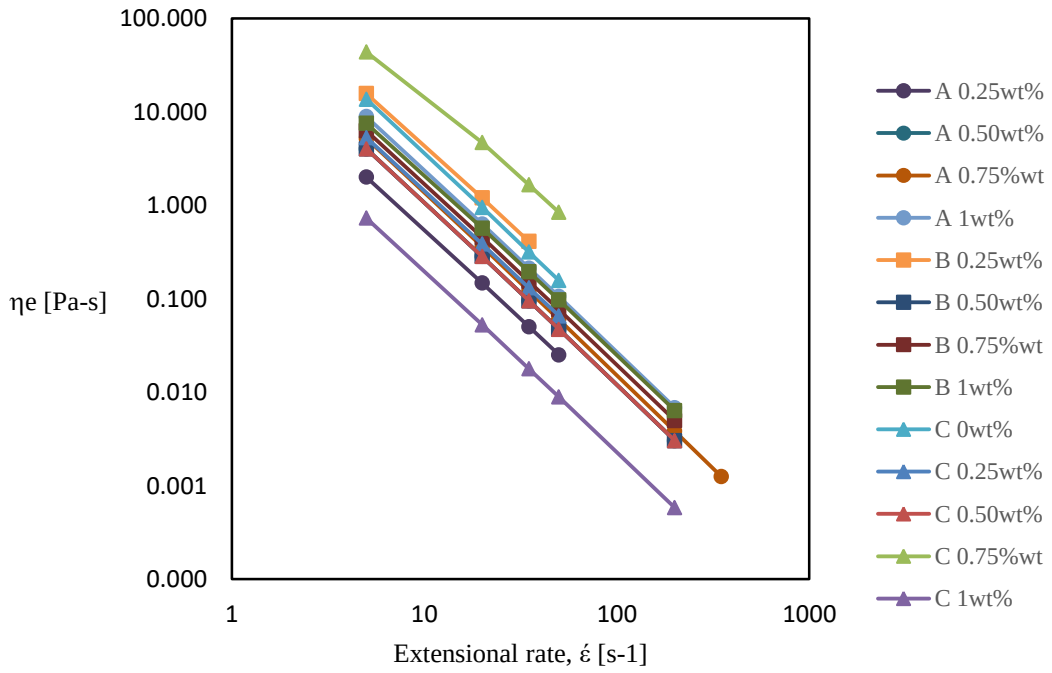

Figure 5.2-13 Steady state elongational rate vs extensional rate for the whole set of concentrations

Figure 5.2-15 shows the steady state values of the elongational viscosity for all the prepared solutions. Again in this graph the solution C1wt% has the minimum values of η_e and A 0.25wt% follows it. In this case the highest values of elongational viscosity are those obtained from the solution C 0.75wt%. The rest of the solutions have the same

range of values. It is important to mention that the thinning behavior is more pronounced in the steady state.

Since the fibers depositions were done with solutions from Serie A it is necessary to emphasize its elongational viscosity behavior. The elongational viscosity in function of elongational rate for Serie A is depicted in figure 5.2-15. As it can be seen, the amount of additives is directly related with the increase of the elongational viscosity. For solution 1wt% the initial value of η_e is around 200 Pa·s (at $\dot{\varepsilon} \approx 8s^{-1}$) while for 0.25wt% is approximately 60 Pa·s this is more than three times. For concentrations of 0.5wt% and 0.75wt% the initial value is close to 105 Pa·s, the half of the highest value and the double of the lowest. A marked thinning behavior is observable, however for solutions of 1wt%, 0.75 wt%, and 0.5 wt% there is a slight trend to a common value at $\dot{\varepsilon} \approx 400s^{-1}$. It is possible that at higher extensional rates the values of he of all the samples start to behave the same way as a result of the rupture of entanglements between polymer chains.

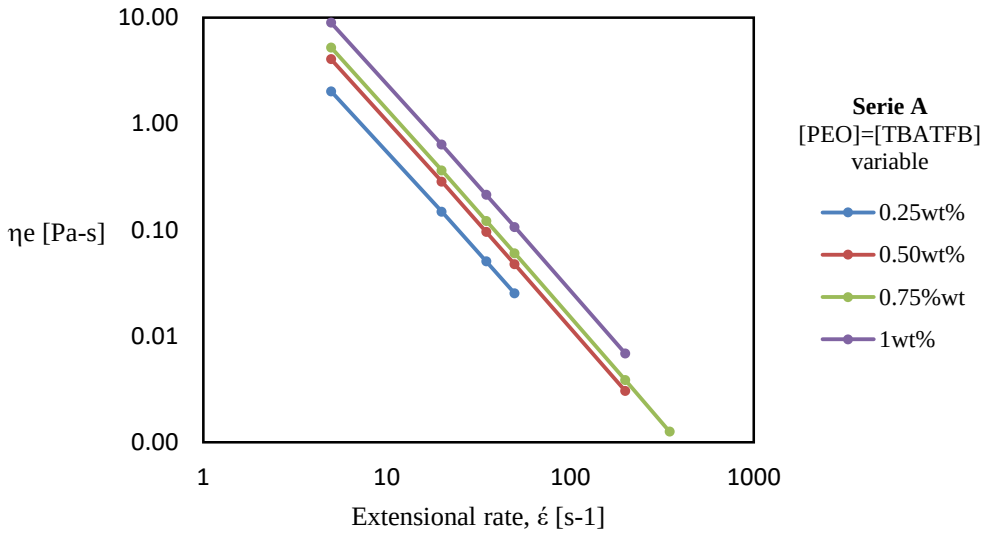

Figure 5.2-14 Steady state elongational rate vs extensional rate for Serie A ([PEO]=[TBATFB] variable)

With this information an important analysis can be done. Since it is known the distance from the tip-to-collector, TTCD, and also the velocity of deposition, now it can

be calculated the extensional rate of the process with as the ratio of the longitude, L, that is equal to TTCD, and the velocity of fabrication, v_f: $\dot{\varepsilon}=L/v_f$.

In table 5.2-4 there is a summary of the extensional rates present during fiber depositions. And the approximated time to reach the steady state from plots of APPENDIX II

Table 5.2-7 Extensional rates, approximated time to reach steady state and actual deposition time

Vf [mm/s]	έ [1/s]	L=TTCD [mm]	time to reach steady state, tss [s]	Deposition time, [s]
20	100	0.2	0.2	0.43
40	200		0.1	0.21
60	300		0.01	0.14

From table 5.2-7 is possible to observe that the steady state of the elongational viscosity was attained successfully. The steady state was reached by all the deposition velocities. The longitude of the depositions, l_d, is 8.5mm and the fabrication velocities were 20, 40 and 60 mm/s, the deposition times were calculated as $t_d=l_d/V_f$.

5.3 FIBER CHARACTERIZATION

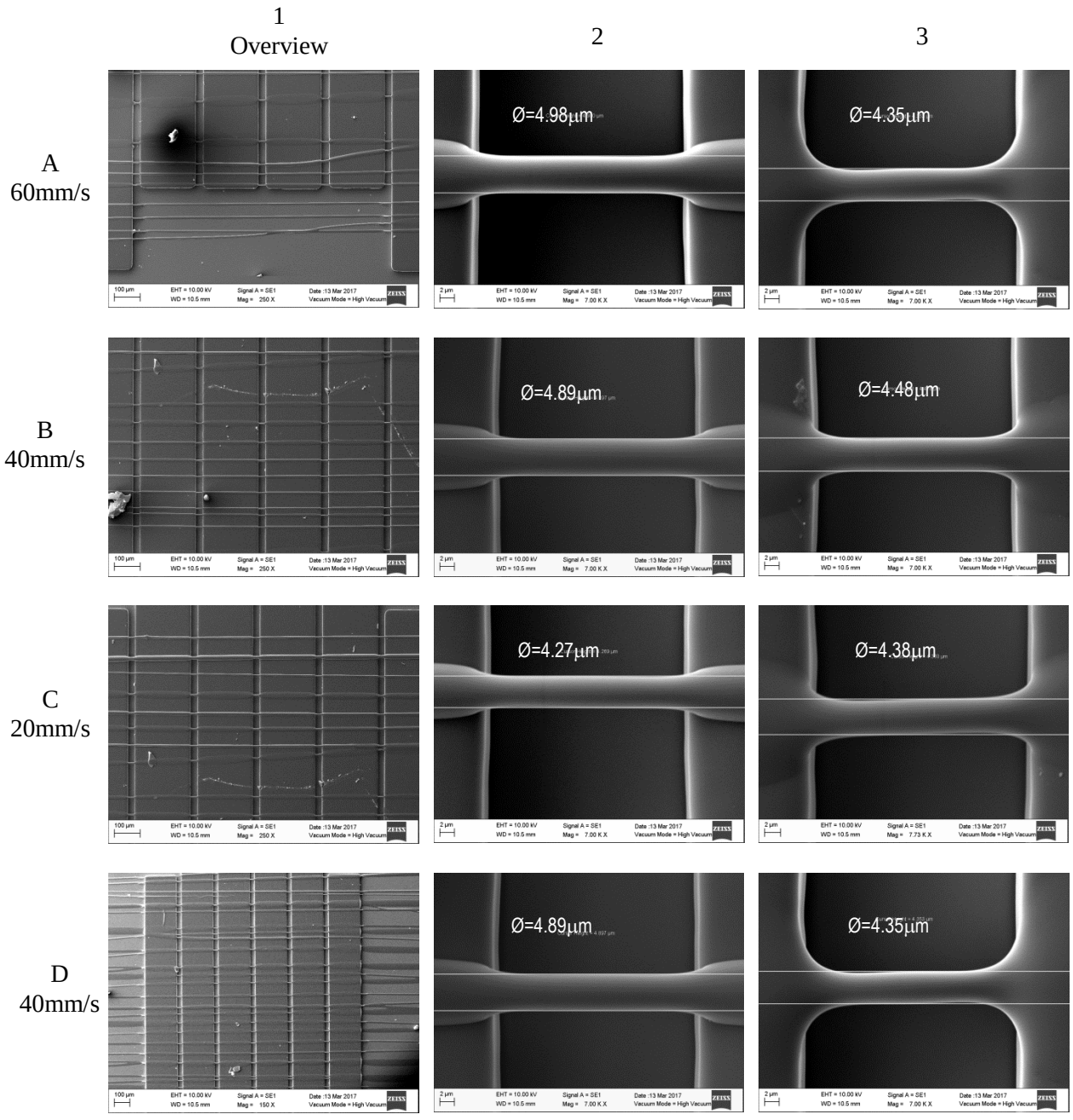

Figure 5.3-1Fiber deposited by EMS of SU-8 2002:PEO:TBATFB=99:0.5:0.5 wt%. solution. Rows A, B, and C are depositions of 10 fibers at fabrication velocities of 60, 40, and 20 mm/s ($\dot{\varepsilon}$=300, 200, 100 s^{-1}). Row D is a deposition of 30 fibers at 40mm/s ($\dot{\varepsilon}$=200s^{-1}). Column 1 is an overview of the deposition. Column 2 and 3 are the diameter of fibers at each speed.

In Figure 5.3-1 is showed the deposition of the fibers following the two explained methods in the experimental section. The solution used was 99:0.5:0.5wt%. Because this one is the reference for the all experimentations, due to its reproducibility on EMS process during depositions in the UCI.

The first method was the deposition of ten fibers at three different fabrication velocities, v_f. This method is presented in the rows A, B, and C. In row A at v_f=60 mm/s the average diameter, đ, of the fibers is 4.6 mm, in B at vf=40 mm/s đ=4.7 mm and for C at v_f=20mm/s đ=4.3mm. In row D a deposition of 30 fibers was done. The v_f used was 40mm/s and the đ founded was 4.6mm. These results indicate that the range of vf from 20 to 60mm/s does not affect considerably the diameter of the fibers. The smallest fibers were those from v_f=20mm/s.

In Column 1 are presented the overviews of each deposition. It can be seen that the deposition resolution and quality are not high. The separation between fibers must be 50μm but presents a large variation. The size of the fibers deposited over the posts also varies. Besides, the deposition was not always a straight line, in some cases there are inclined depositions. A possible explanation is that the depositions were made on the threshold of accuracy of the EMS platform.

Column 2 and 3 are showed the measurement of two fibers for each velocity of fabrication. Column 2 shows fibers that seem to be over the electrodes while, in Column 3, the fibers looks like they are fused with the posts. A possible explanation is that during some depositions, the SU-8 solvent (cyclopentanone) of the fibers does not evaporate completely causing a coalescence of the fiber and the electrode, since the posts are also SU-8. On the other hand, when less amount of solvent is present, the fibers are more solid and are deposited over the posts.

Figure 5.3-2 shows exactly the same methodology explained in Figure 5.3-1 but for a solution of 98.5:0.75:0.75 wt%. The quality of the deposition neither is high. In fact, the sloping depositions are more evident as it can be seen in SEM images B1 and C1 from 5.3-2.

Once these fiber depositions were made, it was found that the speeds used have not enough effect on the diameter of the fibers and it is more difficult to program the patterns and to start the deposition when velocity of fabrication has to be varied. For this

reason the rest of the depositions were carried out following the second methodology, that is, 30 fibers at 40 mm/s for each dispositive. As figure 5.3-3 displays.

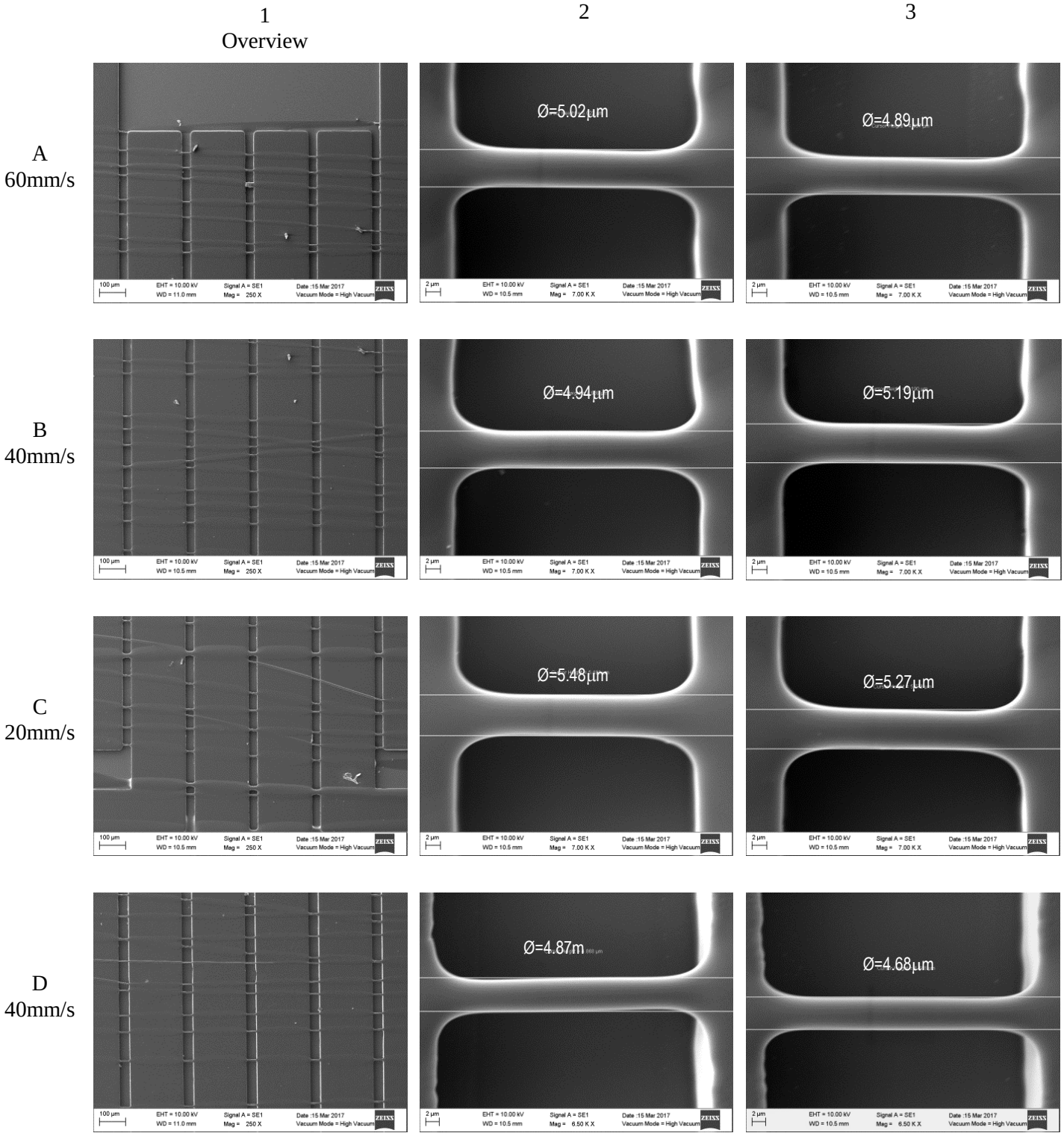

Figure 5.3-2 Fiber deposited by EMS of SU-8 2002:PEO:TBATFB=98.5 :0.75:0.75 wt%. solution Rows A, B, and C are depositions of 10 fibers at fabrication velocities of 60, 40, and 20 mm/s ($\dot{\varepsilon}$=300, 200, 100 s^{-1}). Row D is a deposition of 30 fibers at 40mm/s ($\dot{\varepsilon}$=200s^{-1}). Column 1 is an overview of the deposition. Column 2 and 3 are the diameter of fibers at each speed

Table 5.3-1 is a summary of the measurements of the diameters from the depositions displayed in Figure 5.3-3 and the elongational viscosity. All the depositions were made at 40mm/s and the concentration of both additives were varied from 0.25wt% to 1wt%. Depositions of pure SU-8 2002 were not successful.

It is evident that increasing the amount of additives the diameters becomes bigger. For concentration of 0.25wt% the obtained fibers have diameters around 4μm while for the concentration of 1wt% the average diameter of the fibers was 5.12μm. The difference between diameters for 0.25wt% and 0.5wt% is about 600 nm, that is almost the same difference for concentrations 1wt%. and 0.5wt%. this means that the concentration reduction from 0.5wt% can significantly decrease the diameter of the fibers while, if the concentration is higher than 5wt% there is an increase the diameter with a smaller effect of increase than the decreasing effect.

Table 5.3-1 Average fiber diameters for solutions from Serie A deposited at 40 mm/s ($\acute{\varepsilon}$ =200s^{-1}) at steady state

$\acute{\varepsilon}$=200s^{-1}	Solution from Serie A [PEO]=[TBATFB] variable wt%.			
	0.25	0.50	0.75	1.00
Diameter, μm	3.95	4.56	4.77	5.12
η_e, Pa-s	4E^{-4}	0.0030	0.0038	0.0068

As it can be seen from Table 5.3-1, the smallest the amount of additives the smallest the elongational viscosity and, therefore the diameter. The cause of these effects is related to the internal structure of the solution. The polymer chains for the smallest concentrations do not form enough entanglements, consequently there is less resistance to flow in a shear or elongational flow, this low interaction between polymer chains can promote also a smaller relaxation time allowing the polymer to be stretched to a finer threads. Besides, as can be seen in Table 5.2-24, the elements from the relaxation spectra, a_i, for low concentrated solutions are the smallest of all the set of concentrations this points out that the elastic behavior for this samples are minimum, therefore, if the solution is more viscous than elastic, it is expected that the solution will tend to flow rather than resist the elongational flow. On the other hand, for higher

concentrations, when the formed entanglements are stretched, the internal structure tries to pull all the connected polymer chains; this favors the widening of the fibers. Besides, the relaxation time is bigger and the elasticity of the solution increases making the solution to resists the elongational flow.

Serie A [PEO]=[TBATFB] variable	1 Overview	2
A 0.25wt%	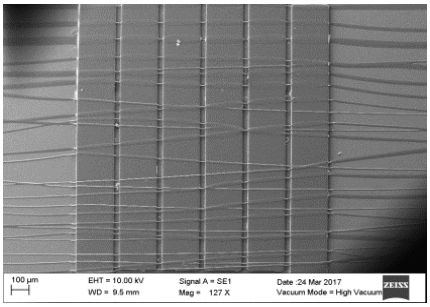	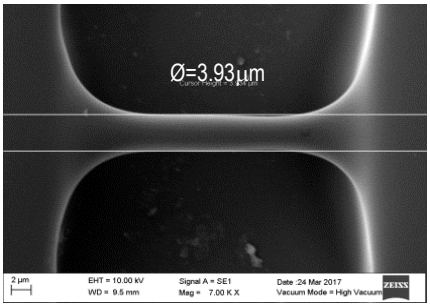
B 0.50 wt%	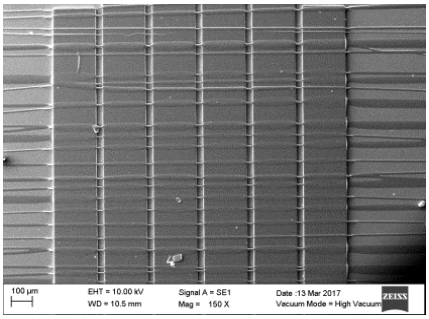	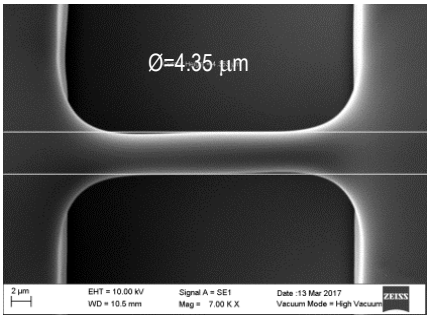
C 0.75 wt%	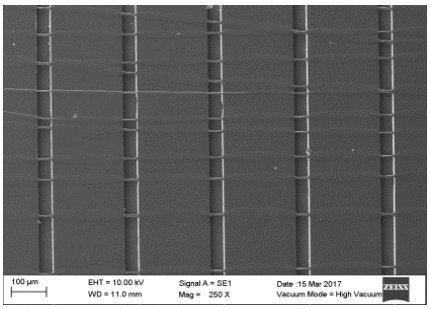	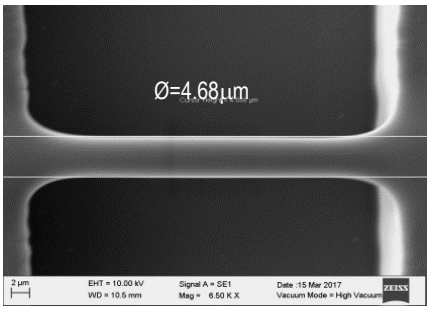
D 1.0 wt%	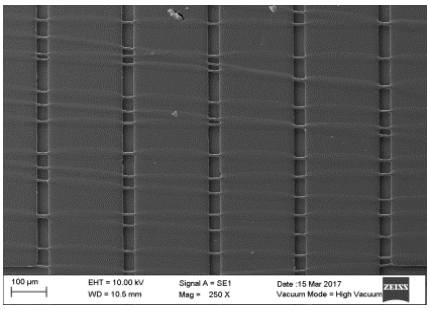	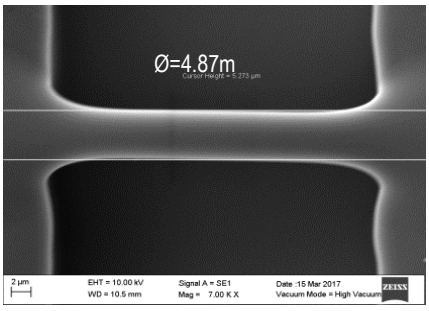

Figure 5.3-3 Depositon of 30 fibers at 40mm/s ($\dot{\varepsilon}$=200s^{-1}). by EMS for Serie A where [PEO]=[TBATFB] varies from 0wt% to 1wt%. Rows A, B, C, and D are deposition of solutions 0.25, 0.50, 0.75, and 1.0 wt% solutions respectively. Column 1 is an overview of the deposition. Column 2 are the diameters of fibers at each concentration

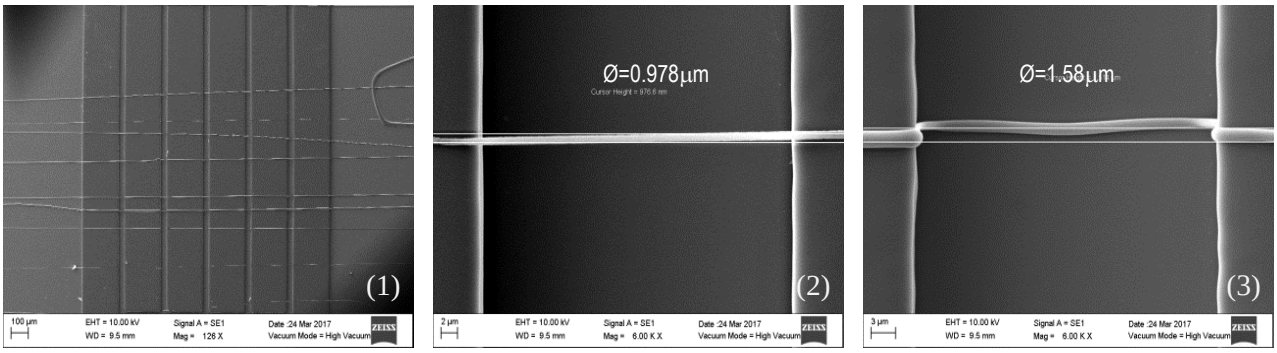

Figure 5.3-4 Fibers deposited in manual mode of the EMS platform. 1. Overview of deposited fibers 2. Suspended fiber 3. Non-suspended fiber. Solution with 0.25% of both additives.

Finally, Figure 5.3-4 shows an experiment where fibers were deposited in the stage manual mode at very low speed compared with the rest of the deposition. This speed is approximately 0.21mm/s and the extensional rate is $\dot{\varepsilon} \approx 1 s^{-1}$. By doing an extrapolation on the graph from Figure 5.2-14 (η_e vs $\dot{\varepsilon}$ at steady state for Serie A), the value of the elongational viscosity is $\eta_e \approx 20$ Pa·s. As it can be seen the diameter was reduced drastically. Using this method the smallest fiber (978nm) of all depositions was produced. In figure 5.3-4 there is an overview of the manual deposition (1) suspended fiber of 978nm of diameter (2) and a non-suspended fiber. The cause of the dropped fiber could be that there is a relatively a long distance from post to post, the effects of the voltage and its own weight. The elongational process is slower than those where velocities were varied from 20mm/s to 60mm/s, this means that the material has enough time to dissipate the energy related to the applied deformation, therefore the entanglement rate is smaller than the rupture entanglement rate.

CHAPTER VI CONCLUSIONS AND FUTURE WORK

A series of experimentations were carried out in order to correlate the rheological properties of a polymer solution used in an electro mechanical spinning process for the production of carbon micro electromechanical systems.

Shear flow and dynamic oscillatory measurements tests such as Flow Curves, Amplitude Sweeps and Frequency Sweeps and calculations were carried in a oscillatory rheometer out in order to study in a reproducible and quantitative way the rheological behavior of polymeric solutions of SU-8 2002, an epoxy-based negative photoresist, Poly(ethylene) oxide, a flexible, non-ionic polymer, and Tetrabutylammonium tetrafluoroborate that acts as an electrolyte.

Since the formulation of 99:0.5:0.5 wt% of SU8-2002:PEO:TBATFB shown the thinnest fibers on experiments from the University of California in Irvine research group. The concentrations of additives were varied from 0%wt to 1.0%wt with increments of 0.25% in order to perform a fine tune around the concentration reported by UCI. To observe the effects of each additive it was proposed a set of concentrations where both additives were equally varied (Serie A), TBATFB was constant the only PEO was varied (Serie B), and PEO was constant a TBATFB was varied (Serie C).

It was found that the variation of the additives (PEO and TBATFB) affects the rheological behavior of the solution. Generally, the addition of PEO increase the elongational and shear viscosities while the addition of TBATFB modifies this property but in a non-predictable manner. The solutions does not present yield stress as can be seen in Amplitude Sweeps and Frequency Sweeps.

From oscillatory data, the elongational viscosity, η_e, was estimated by using the Wagner model for uniaxial deformation. It was founded that the lower concentrations of PEO reduce the values of elongational viscosity in the whole range of extensional rate while concentrations of TBATFB does not have direct predictions, for example Serie C 1wt% has an $\eta_e \approx 1 Pa \cdot s$ at $\dot{\varepsilon} \approx 8 s^{-1}$ while Serie C 0.25wt% has an $\eta_e \approx 10 Pa \cdot s$ at the same extensional rate. For all solutions was found a thinning behavior of the elongational viscosity. The highest values of η_e are those obtained from Serie C 0.75wt% with a

maximum of $\eta_e \approx 80 Pa \cdot s$ at the lowest extensional rate $\dot{\varepsilon} \approx 8 s^{-1}$. The minimum values of η_e were those obtained from Serie C 1%wt. ($\eta_e \approx 1 Pa \cdot s$) and Serie A 0.25%wt ($\eta_e \approx 2 Pa \cdot s$) at $\dot{\varepsilon} \approx 8 s^{-1}$. Practically the rest of the concentrations are placed in the range of η_e between 2 to 12 $Pa \cdot s$ at $\dot{\varepsilon} \approx 8 s^{-1}$. Therefore, is possible to conclude that polymer chains have a similar response to an extensional deformation. Even when the effects of the salt or the PEO presents small differences for each solution, generally during uniaxial and extensional deformation the entanglement transient network of the solutions have a similar behavior. Nonetheless, the calculations of elongational viscosity were done with differences from the original procedure since the data was not adjustable to Wagner model in first instance. The shear viscosity estimated by Wagner was fitted with the experimental complex viscosity not with the experimental shear viscosity. It is recommended in future works to make modifications to the Wagner model for slow viscosity polymer solutions. Even so, the estimations of elongational viscosity presented in this work elucidate the general behavior of the solutions tested. May be the values obtained in an adequate rheometer will differs from the values presented, but no in its trend and behavior.

Depositions of fibers in SU-8 interdigitated electrodes were done at different fabrication velocities, therefore at different elongational rates, for Serie A ([PEO]=[TBATFB]) solutions in order to correlate its rheological behavior with the final diameter of the fibers. The parameters such as tip-to-collector distance, voltage, inter fabrication velocity and acceleration of the stage were kept constant at 200μm, 100v (400v for 0.75wt% and 1wt%), 500mm/s and $500 mm/s^2$ respectively, the higher voltages used in concentrated solutions were required because of lower voltages were unable to promote deposition of the fibers. The velocities of fabrication (deposition) were 60, 40, and 20 mm/s for an automatic deposition where a pattern is programed and the platform use it to perform the deposition. Also, a fiber deposition at velocity of 0.21mm/s on manual mode of the platform was made. For these velocities the extensional rates are $\dot{\varepsilon} = 300, 200, 100$ and $1 s^{-1}$respectively. Depositions of solutions Serie A of 0.50wt% and 0.75wt% with these parameters were performed but was not found conclusive information to correlate the velocity of fabrication in the ranges from 60 to 20 mm/s. For

this reason the concentrations from Serie A of 0.25wt%, 0.5 wt%, 0.75 wt%, and 1 wt% were deposited at 40mm/s which had, at least, less variance in the fiber diameters. It was found that the smallest fibers where obtained at the lowest velocities and concentrations of additives. The thickest average fiber diameter for 1wt% was 5.12μm ($\eta_e \approx 5.12$Pa·s at steady state) while the thinnest was 3.95μm ($\eta_e \approx 0$Pa·s at steady state) fo 0.25wt%. It was a found a direct relation with concentration, diameter and elongational viscosity for this solutions from Serie A. Furthermore, other finding of high importance was found. For manual deposition (v_f=0.21 mm/s, $\dot{\varepsilon} \approx 1s^{-1}$ and $\eta_e \approx 20$) the thinnest fiber was obtained.

We can conclude that the best concentration in order to obtain the thinnest fibers is Serie A 0.25wt%, in which the behavior is more viscous than elastic, and the fabrication velocities must be set around 0.2mm/s where the elongational process is slow enough to dissipate the energy applied by the deformation. The electrodes separation recommended for the depositions with the new parameters are those lower than 40mm to assure that the fibers will not fall from the electrodes.

Finally it was proved that it is possible to modify the process parameters to obtain the smallest fibers using simple and easy attainable rheological information.

APPENDIX I FREQUENCY SWEEPS FOR SERIES A, B, AND C SHOWING COMPLEX VISCOSITY AND BOTH STORAGE AND LOSS MODULUS

I. SERIE A

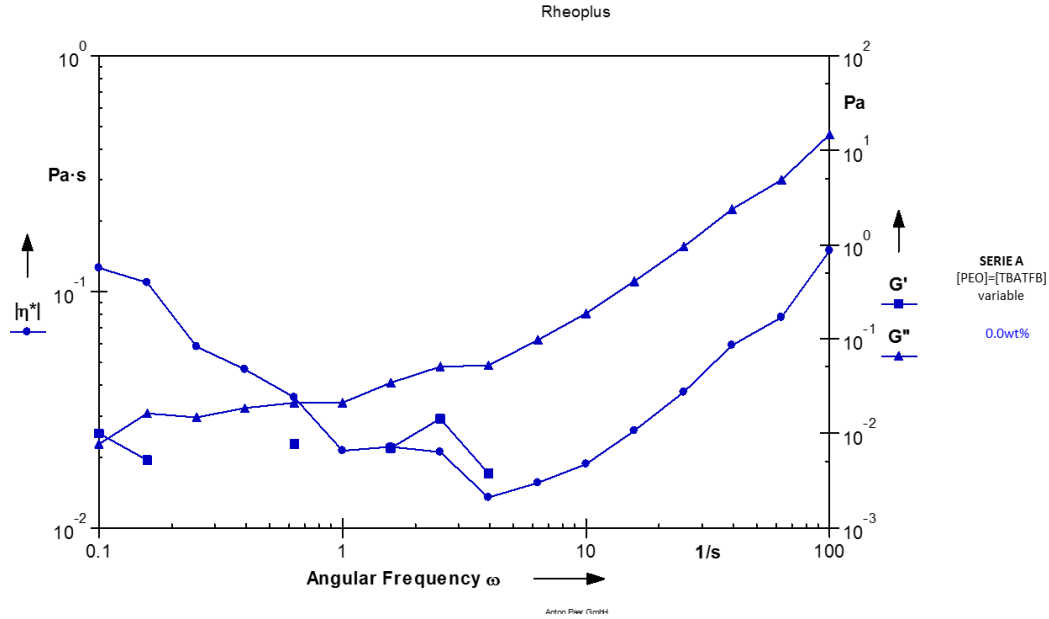

Figure I-1 Frequency Sweep for solutions from Serie A, where [PEO]=[TBATFB]=0.0wt%. Constant ammplitude gamma, %γ=20

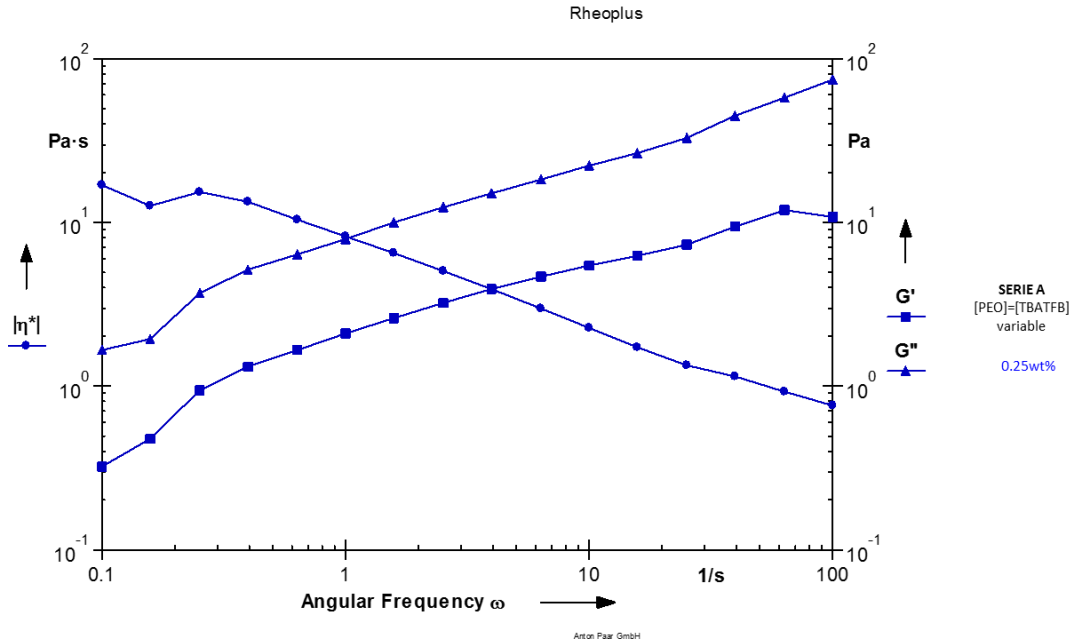

Figure I-2 Frequency Sweep for solutions from Serie A, where [PEO]=[TBATFB]=0.25wt%. Constant ammplitude gamma, %γ=20

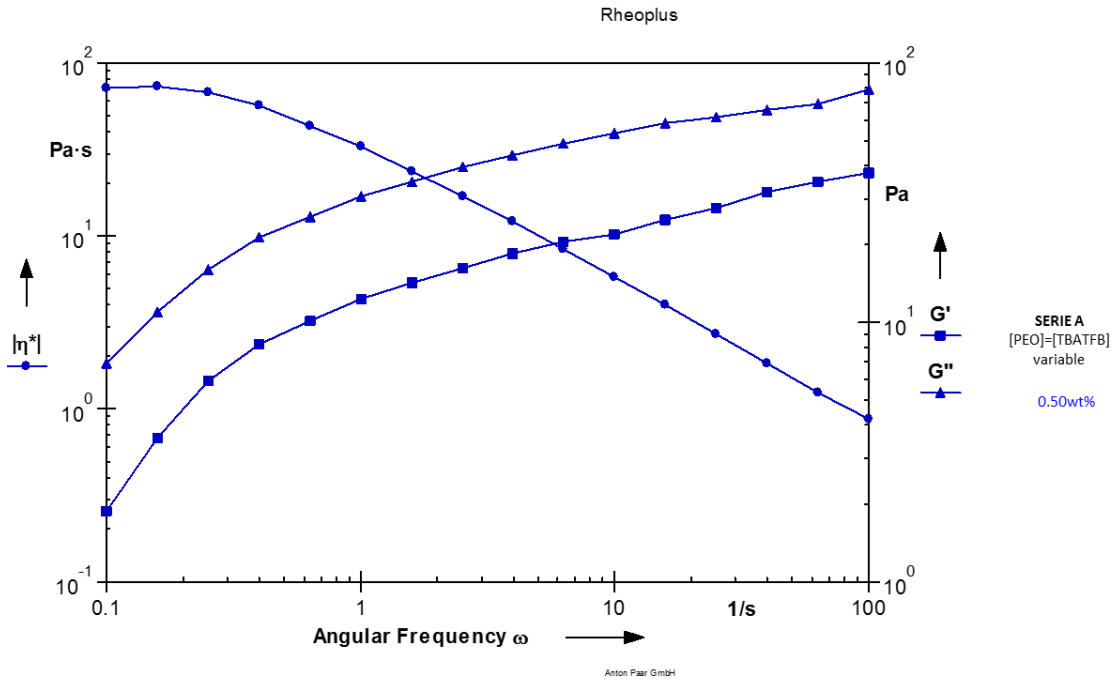

Figure I-3 Frequency Sweep for solutions from Serie A, where [PEO]=[TBATFB]=0.50wt%. Constant ammplitude gamma, %γ=20

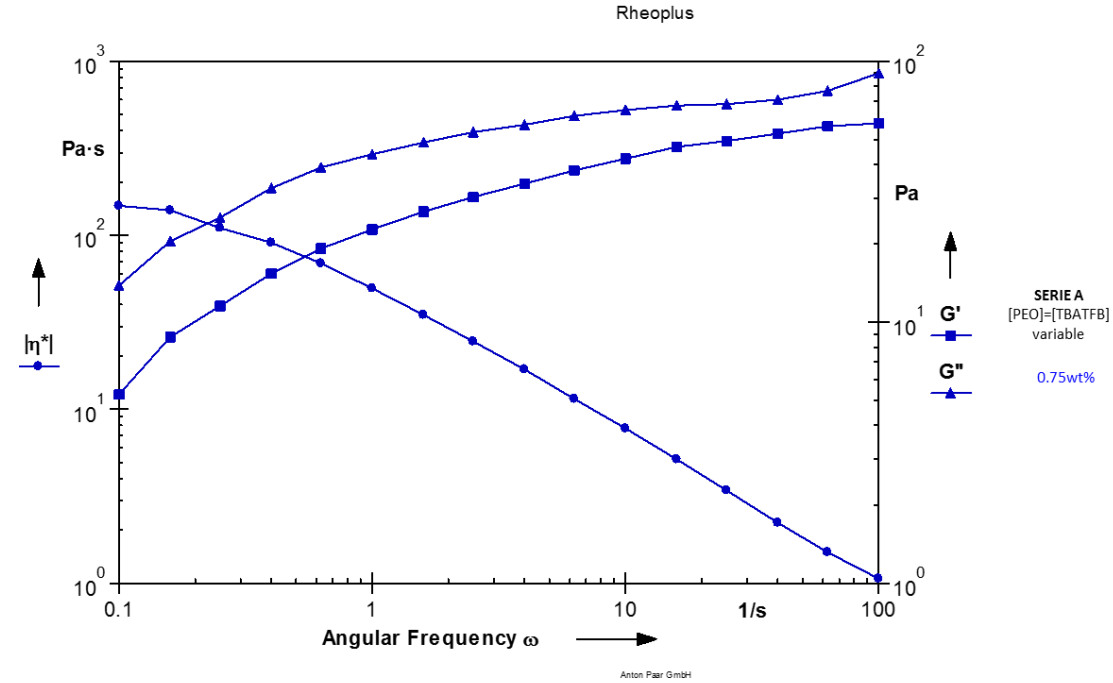

Figure I-4 Frequency Sweep for solutions from Serie A, where [PEO]=[TBATFB]=0.75wt%. Constant ammplitude gamma, %γ=20

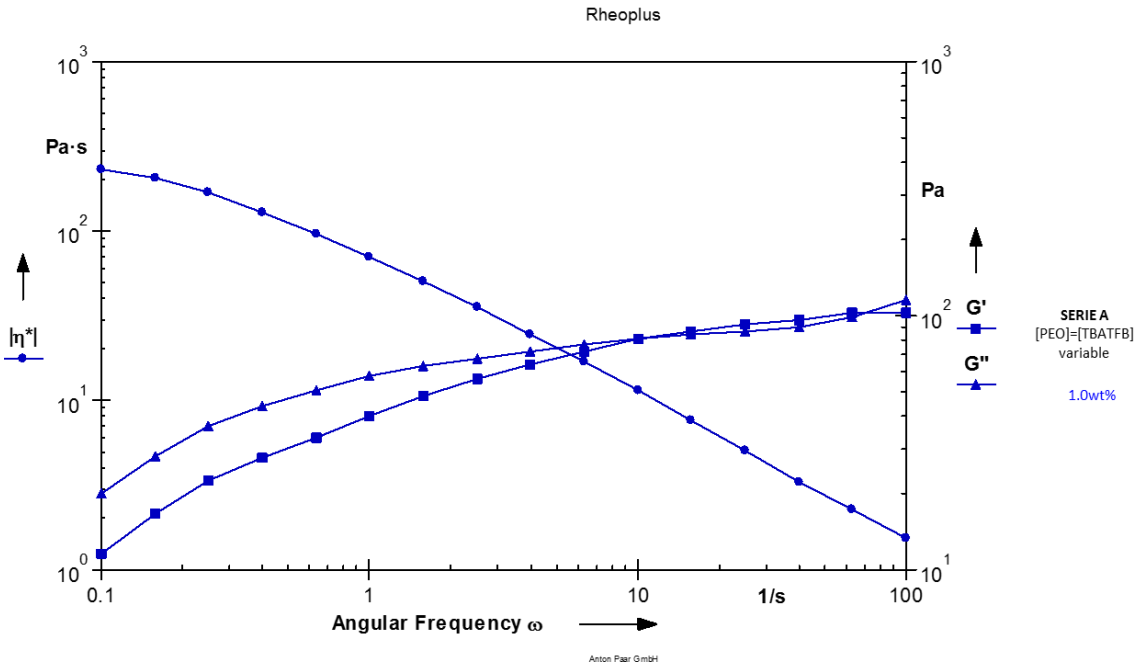

Figure I-5 Frequency Sweep for solutions from Serie A, where [PEO]=[TBATFB]=1.0wt%. Constant ammplitude gamma, %γ=20

II. SERIE B

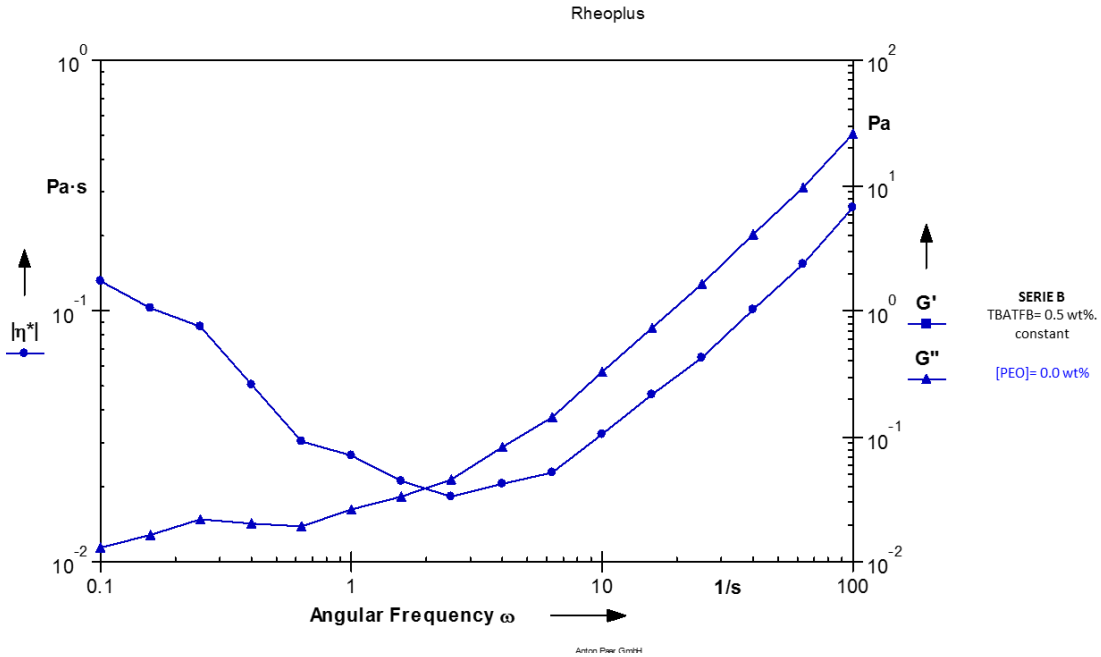

Figure II-1 Frequency for solutions from Serie B, where [PEO]=0.0wt% Constant ammplitude gamma, %γ=20

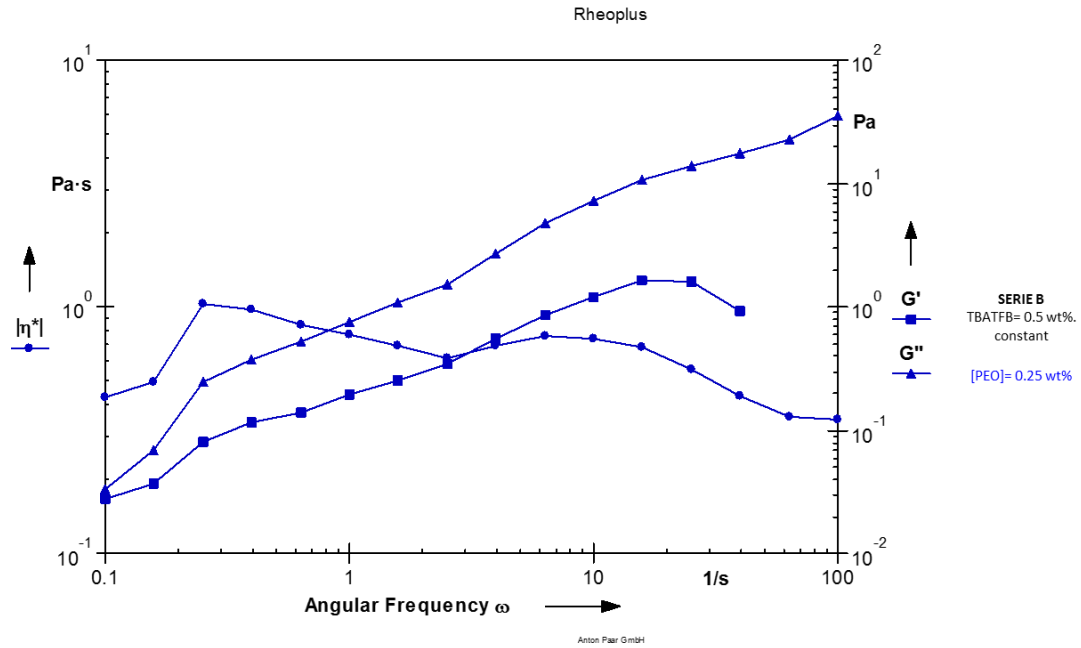

Figure II-2 Frequency for solutions from Serie B, where [PEO]=0.25wt% Constant ammplitude gamma, %γ=20

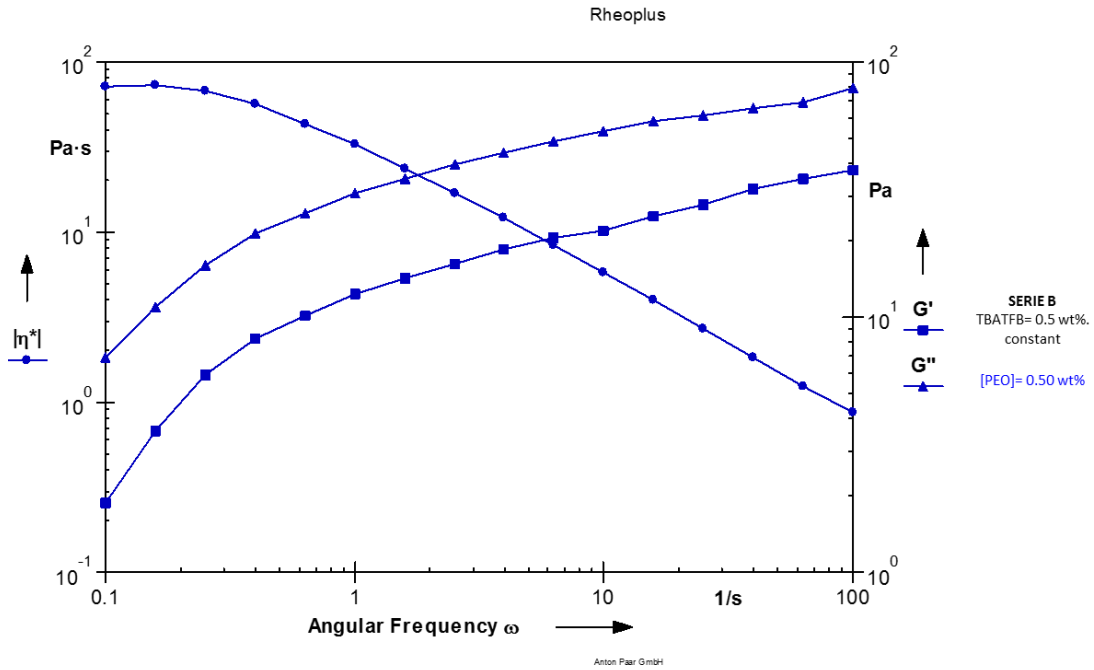

Figure II-3 Frequency for solutions from Serie B, where [PEO]=0.50wt% Constant ammplitude gamma, %γ=20

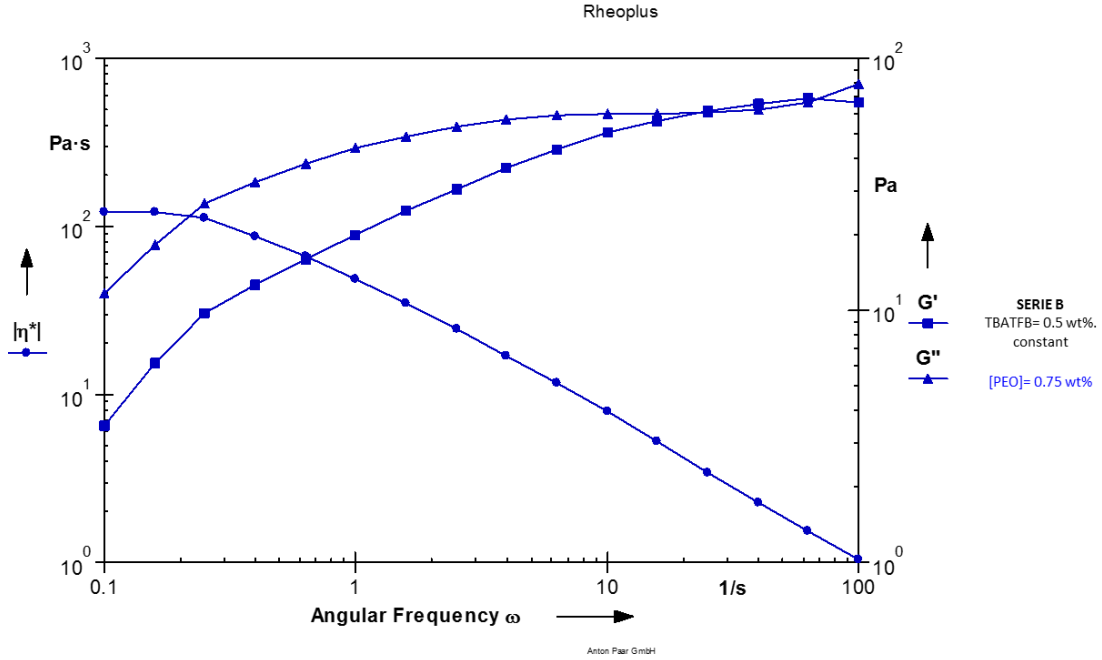

Figure II-4 Frequency for solutions from Serie B, where [PEO]=0.75wt% Constant ammplitude gamma, %γ=20

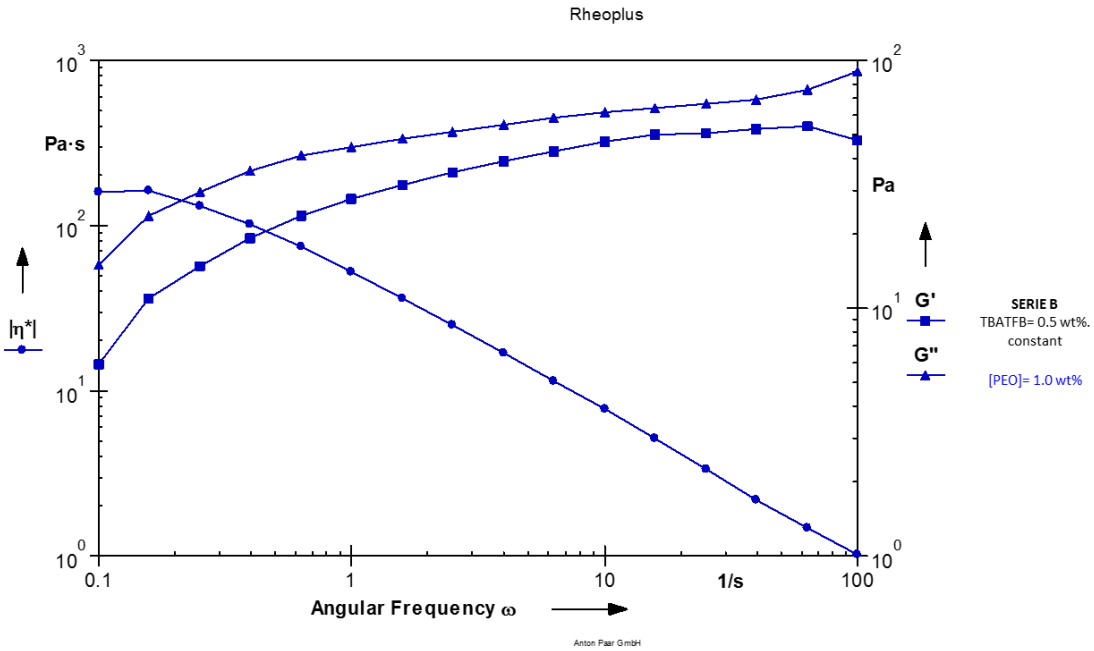

Figure II-5 Frequency for solutions from Serie B, where [PEO]=1.0wt% Constant ammplitude gamma, %γ=20

III. SERIE C

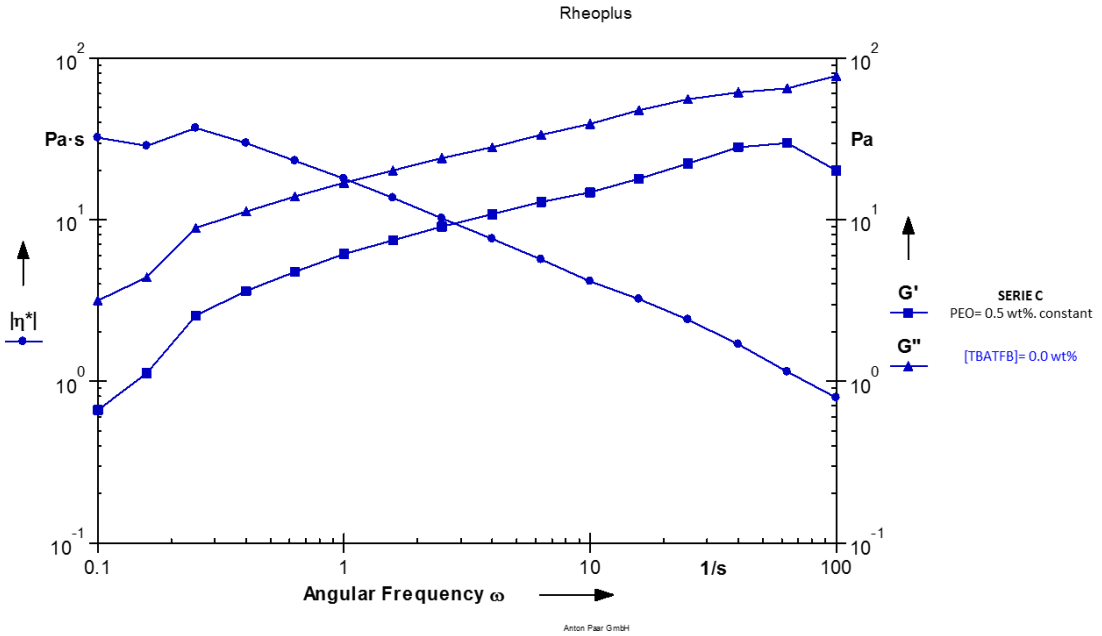

Figure III-1 Frequency Sweep for solutions from Serie C, where [TBATFB]=0.0wt%. Constant ammplitude gamma, %γ=20

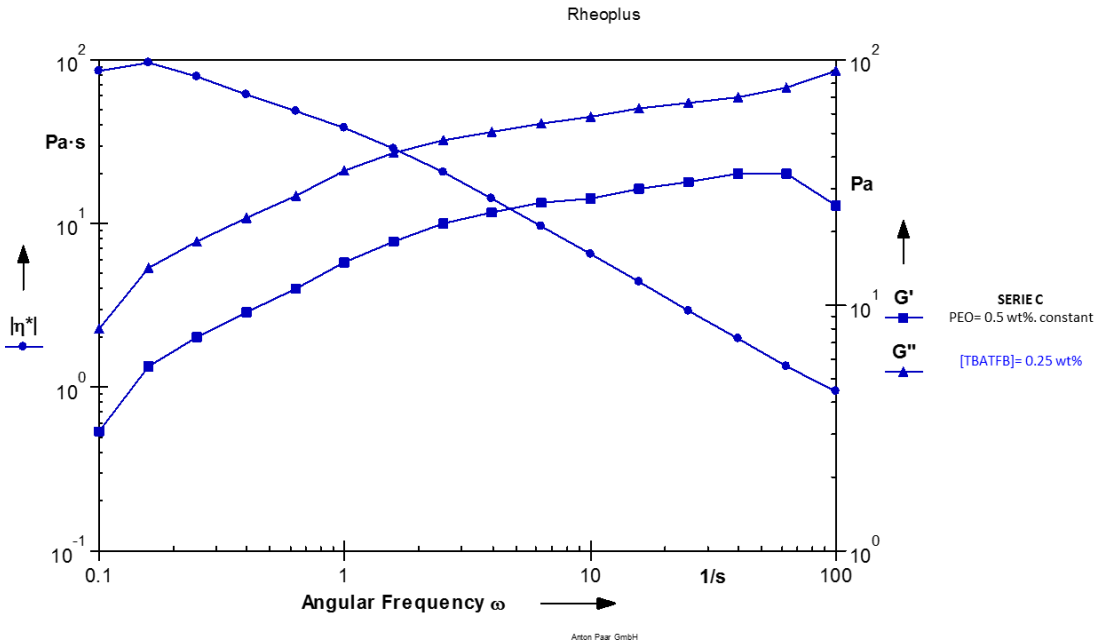

Figure III-2 Frequency Sweep for solutions from Serie C, where [TBATFB]=0.25wt%. Constant ammplitude gamma, %γ=20

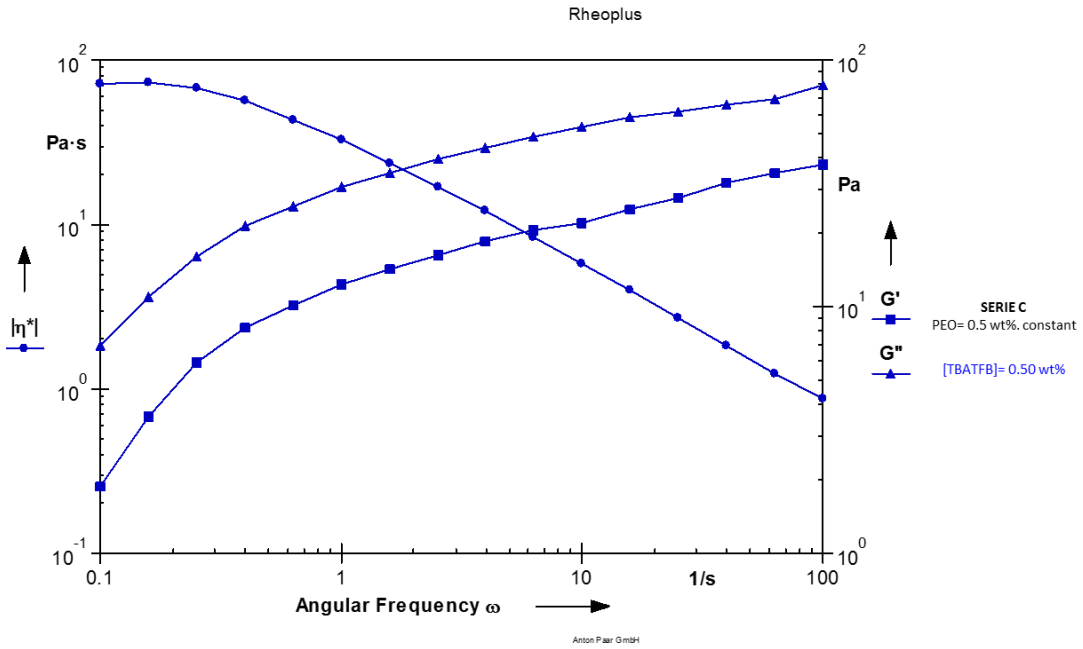

Figure III-3 Frequency Sweep for solutions from Serie C, where [TBATFB]=0.50wt%. Constant ammplitude gamma, %γ=20

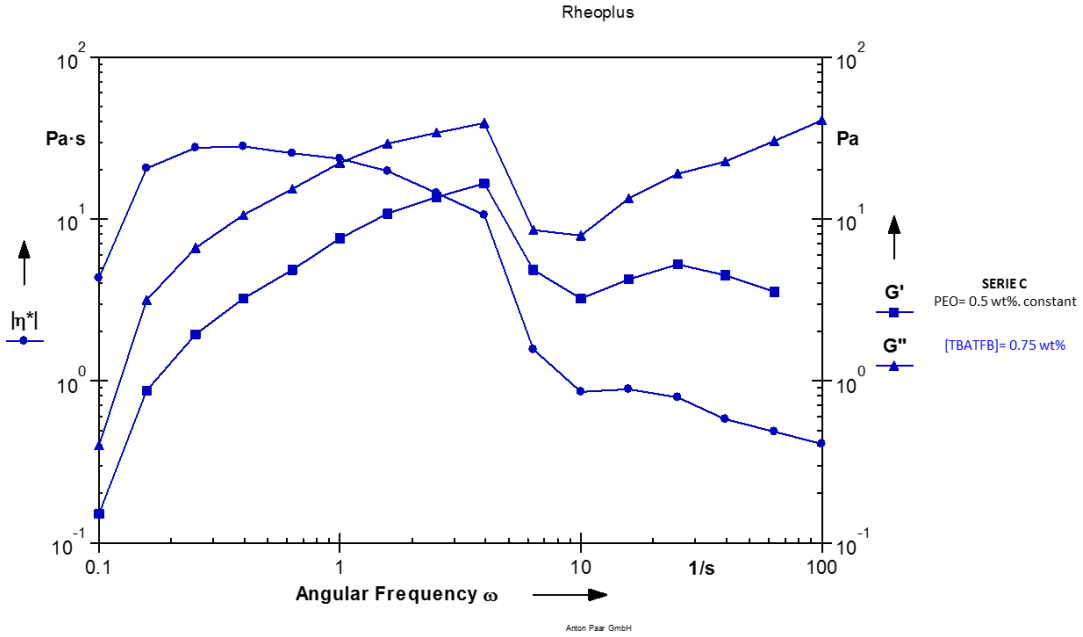

Figure III-4 Frequency Sweep for solutions from Serie C, where [TBATFB]=0.75wt%. Constant ammplitude gamma, %γ=20

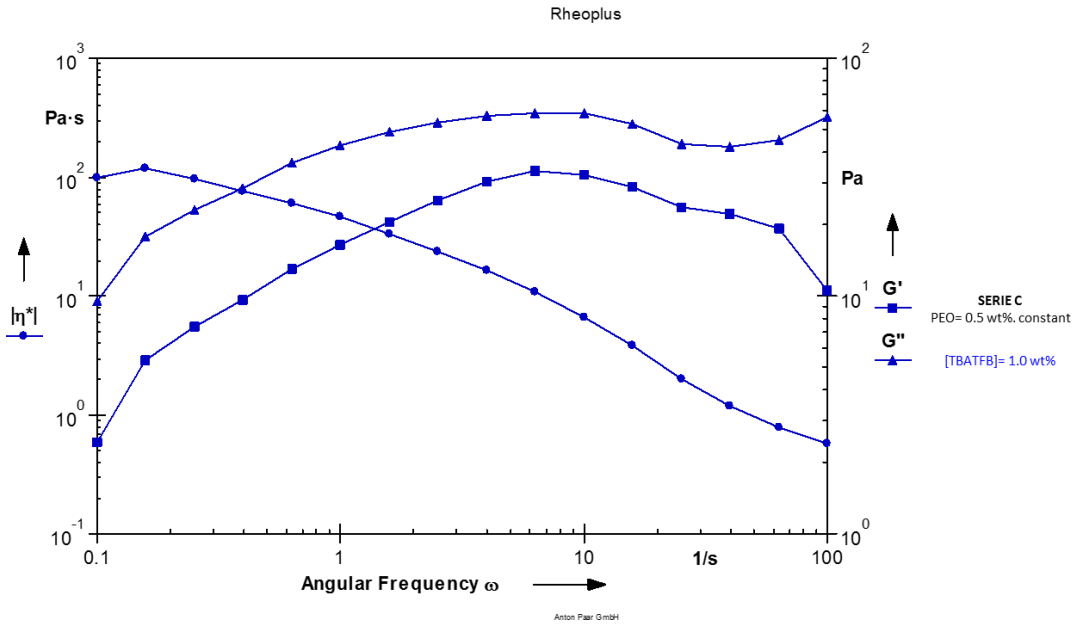

Figure III-5 Frequency Sweep for solutions from Serie C, where [TBATFB]=1.0wt%. Constant ammplitude gamma, %γ=20

APPENDIX II GRAPHS FOR ELONGATIONAL VISCOSITY IN FUNCTION OF TIME ESTIMATED AT DIFFERENT STEADY ELONGATIONAL RATES BY WAGNER MODEL FOR UNIAXIAL DEFORMATION

IV. SERIE A

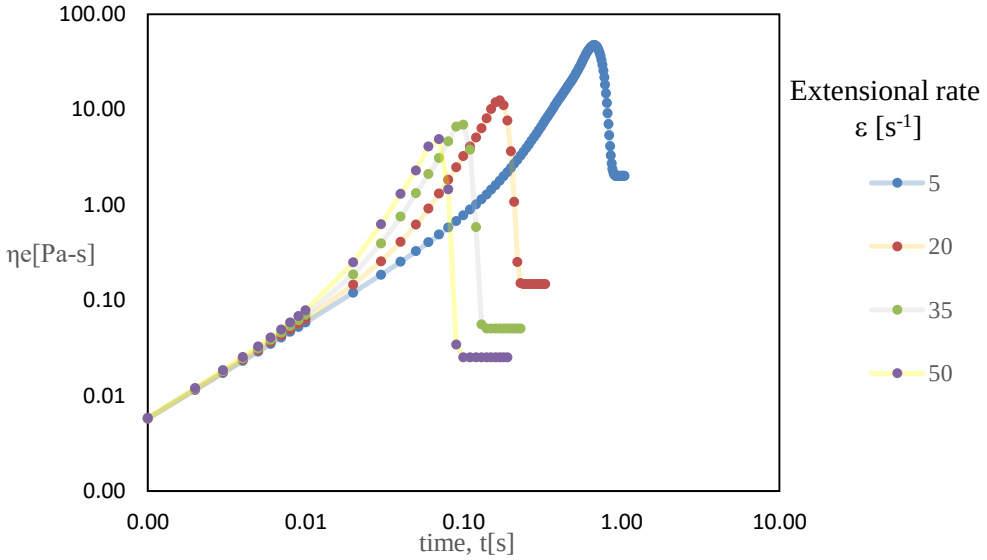

Figure IV-1Elongational viscosity in function of time for solutions from Serie A, where [PEO]=[TBATFB]=0.25wt% at different steady elongational rates

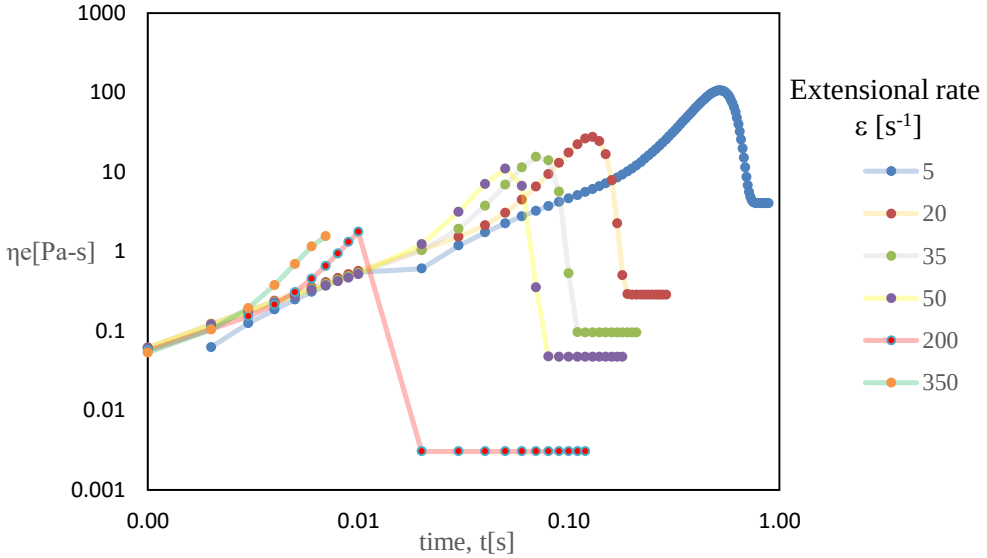

Figure IV-2Elongational viscosity in function of time for solutions from Serie A, where [PEO]=[TBATFB]=0.50wt% at different steady elongational rates

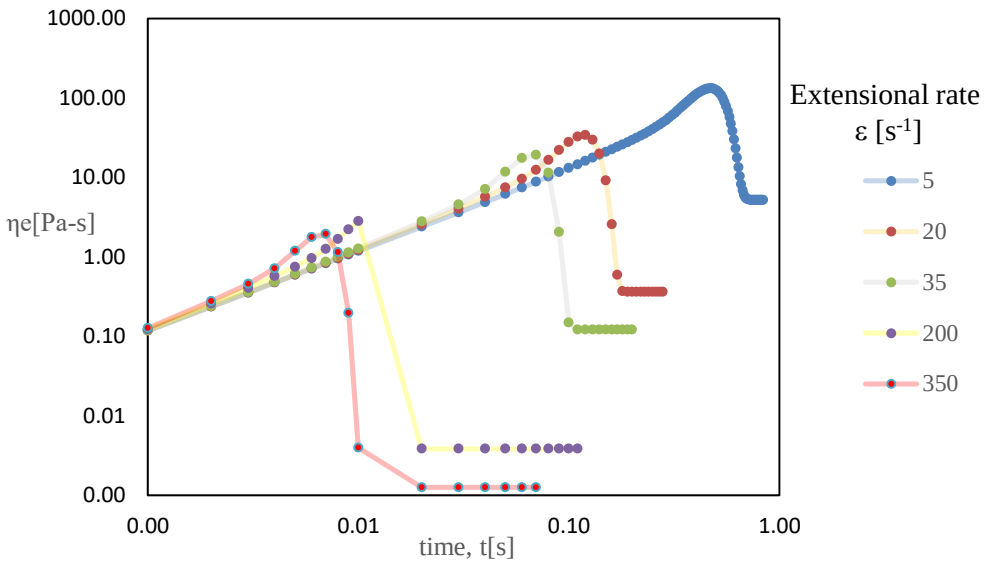

Figure IV-3Elongational viscosity in function of time for solutions from Serie A, where [PEO]=[TBATFB]=0.75wt% at different steady elongational rates

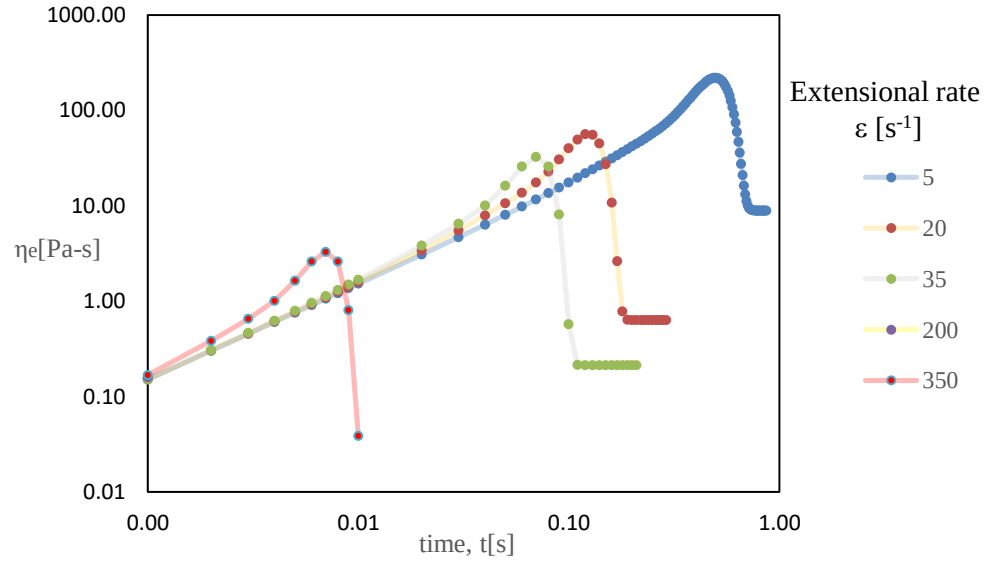

Figure IV-4Elongational viscosity in function of time for solutions from Serie A, where [PEO]=[TBATFB]=1.0wt% at different steady elongational rates

V. SERIE B

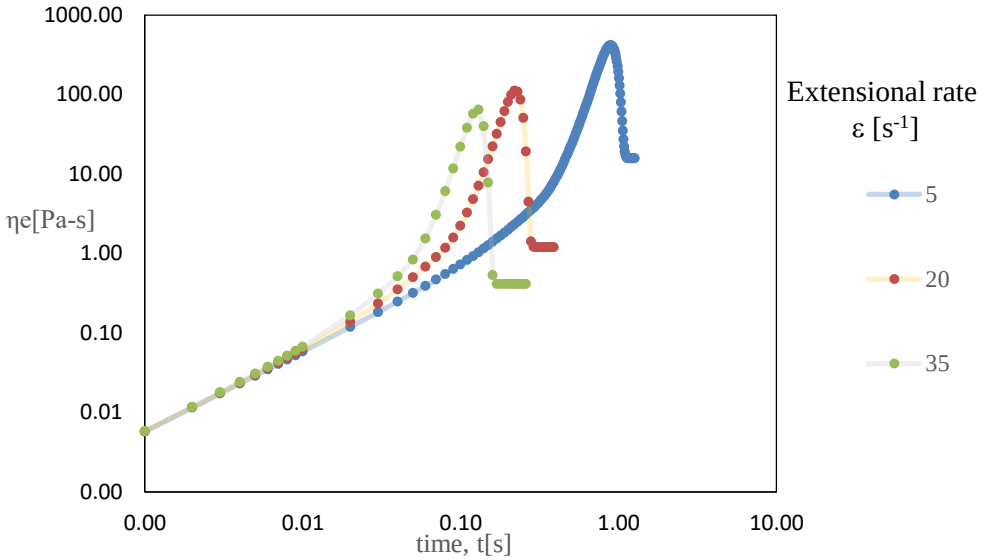

Figure V-1 Elongational viscosity in function of time for solutions from Serie B, where [PEO]=0.25wt% and [TBATFB]=0.5wt% at different steady elongational rates

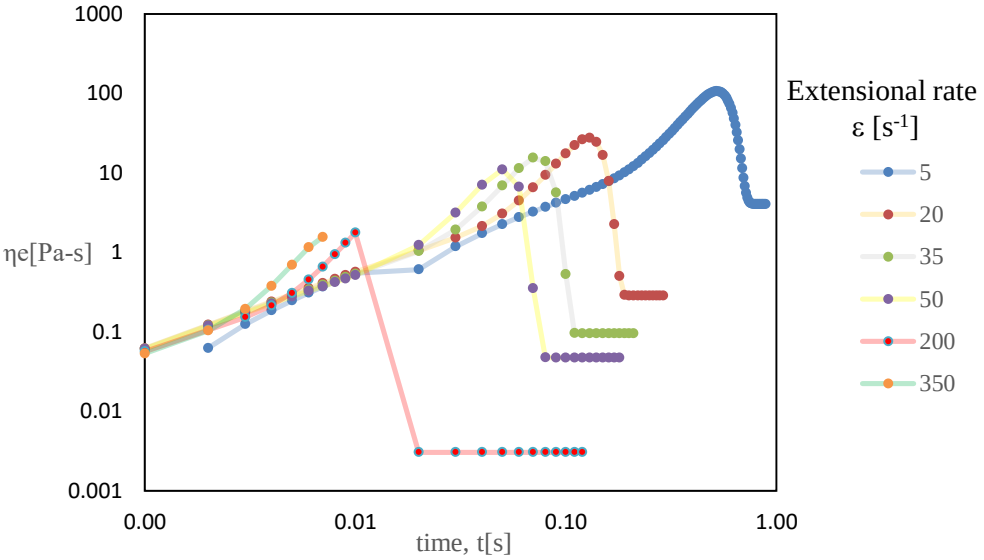

Figure V-2 Elongational viscosity in function of time for solutions from Serie B, where [PEO]=0.50wt% [TBATFB]=0.5wt% at different steady elongational rates

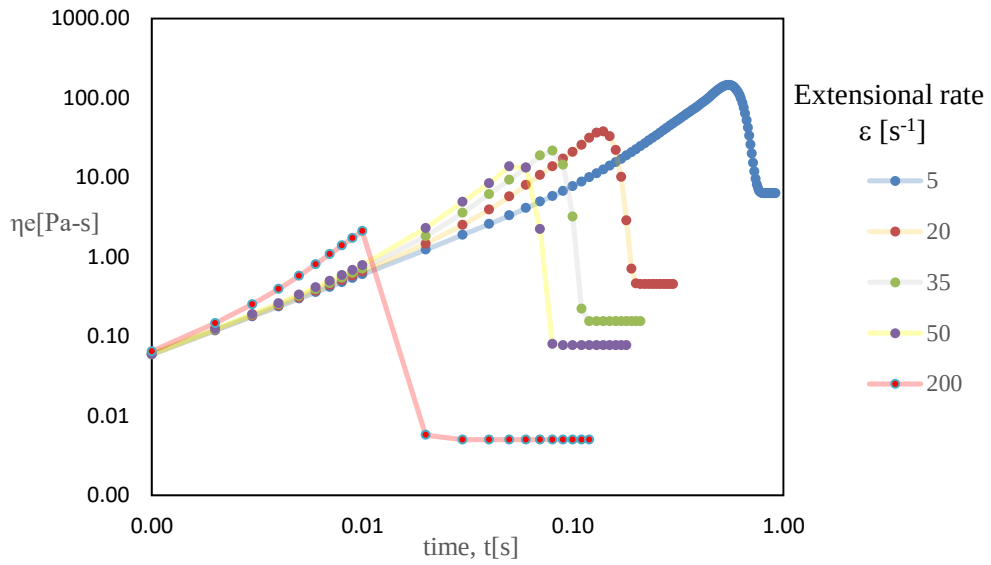

Figure V-3 Elongational viscosity in function of time for solutions from Serie B, where [PEO]=0.75wt% [TBATFB]=0.5wt% at different steady elongational rates

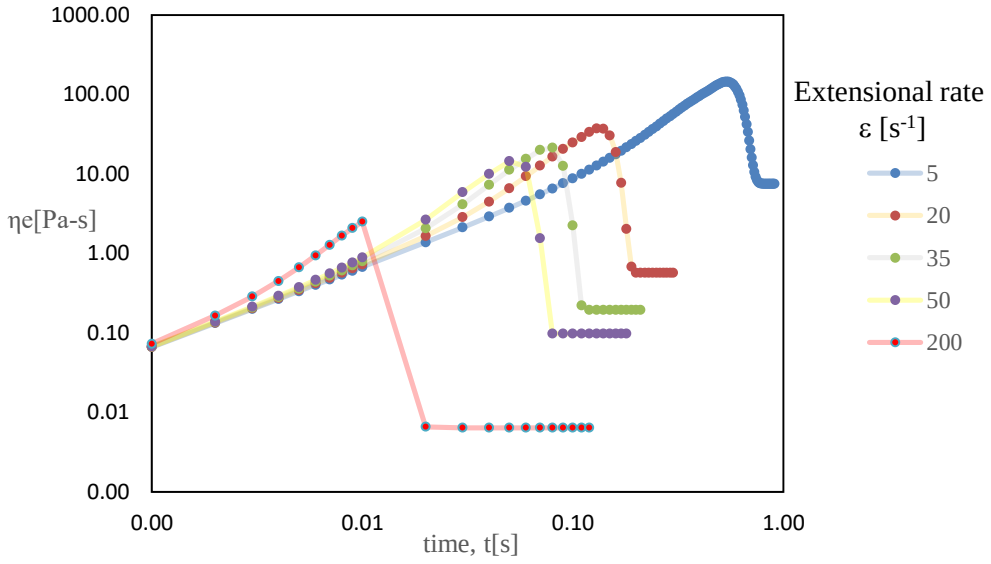

Figure V-4 Elongational viscosity in function of time for solutions from Serie B, where [PEO]=1.0wt% [TBATFB]=0.5wt% at different steady elongational rates

VI. SERIE C

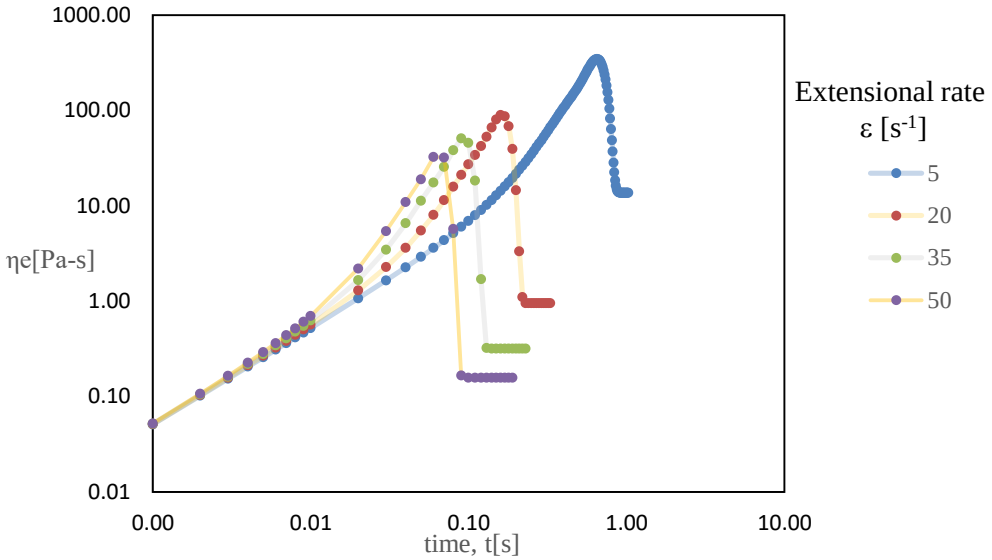

Figure VI-1 Elongational viscosity in function of time for solutions from Serie C, where [TBATFB]=0.0wt% [PEO]=0.5wt% at different steady elongational rates

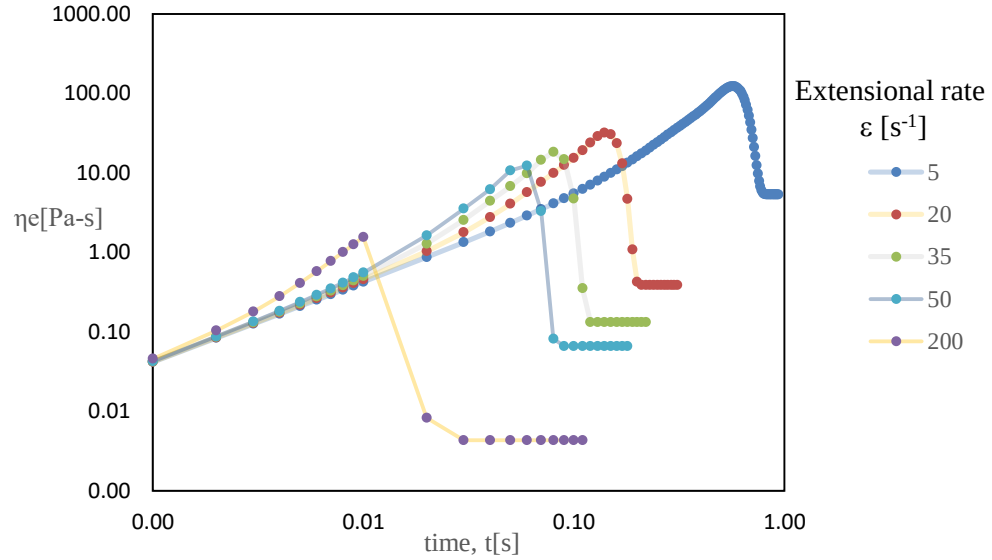

Figure VI-2 Elongational viscosity in function of time for solutions from Serie C, where [TBATFB]=0.25wt% [PEO]=0.5wt% at different steady elongational rates

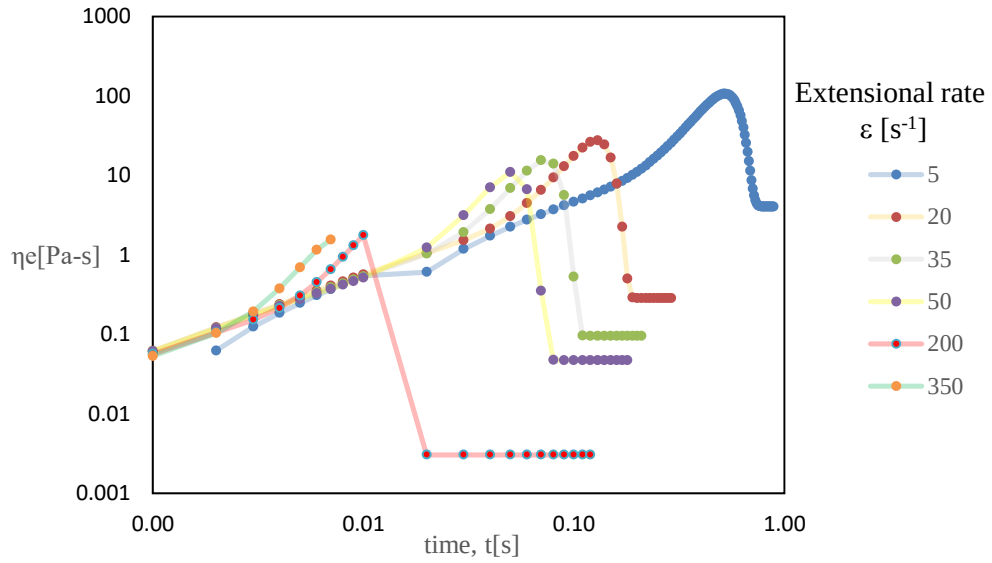

Figure VI-3 Elongational viscosity in function of time for solutions from Serie C, where [TBATFB]=0.50wt% [PEO]=0.5wt% at different steady elongational rates

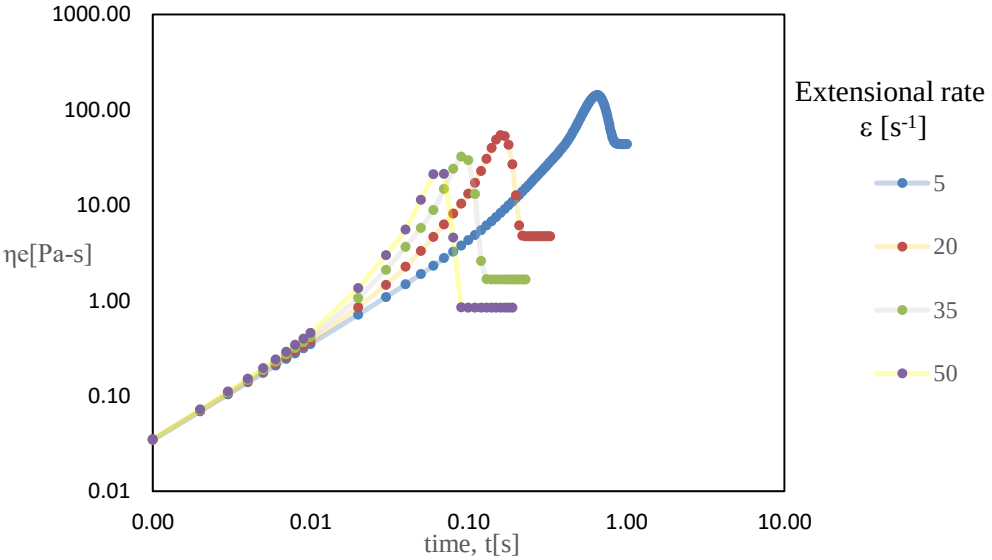

Figure VI-4 Elongational viscosity in function of time for solutions from Serie C, where [TBATFB]=0.75wt% [PEO]=0.5wt% at different steady elongational rates

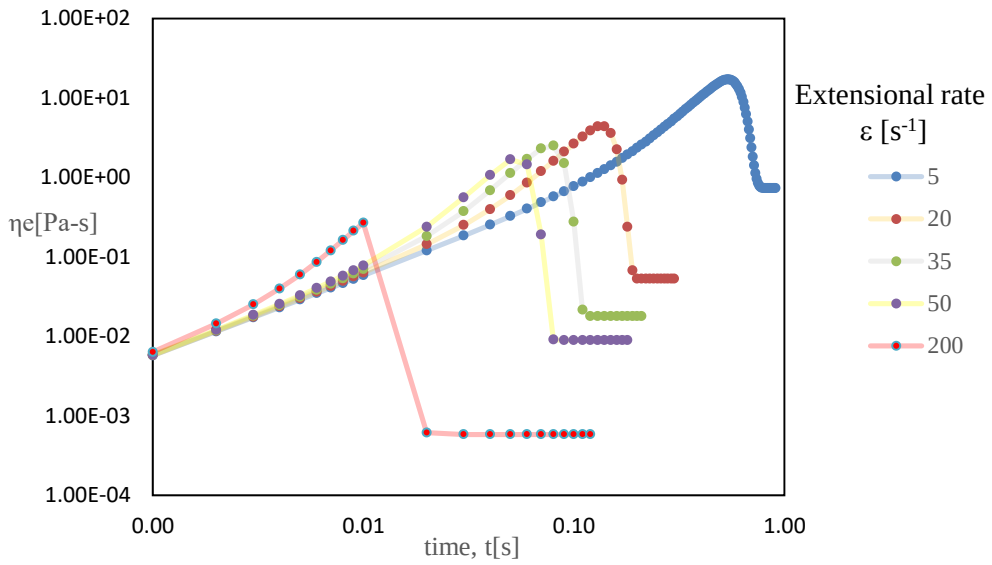

Figure VI-5 Elongational viscosity in function of time for solutions from Serie C, where [TBATFB]=1.0wt% [PEO]=0.5wt% at different steady elongational rates

REFERENCES

[1] Y. Yang, Z. Jia, Q. Li, and Z. Guan, "Experimental investigation of the governing parameters in the electrospinning of polyethylene oxide solution," *IEEE Trans. Dielectr. Electr. Insul.*, vol. 13, no. 3, pp. 580–584, 2006.

[2] M. Nascimento and U. Federal, "A Literature Investigation about Electrospinning and Nanofibers : Historical Trends , Current Status and Future Challenges A Literature Investigation about Electrospinning and Nanofibers : Historical Trends , Current Status and Future Challenges," no. JANUARY, 2015.

[3] L. Persano, A. Camposeo, C. Tekmen, and D. Pisignano, "Industrial upscaling of electrospinning and applications of polymer nanofibers: A review," *Macromol. Mater. Eng.*, vol. 298, no. 5, pp. 504–520, 2013.

[4] N. Bhardwaj and S. C. Kundu, "Electrospinning: A fascinating fiber fabrication technique," *Biotechnol. Adv.*, vol. 28, no. 3, pp. 325–347, 2010.

[5] J. Kristl, "The role of rheology of polymer solutions in predicting nanofiber formation by electrospinning," vol. 48, pp. 1374–1384, 2012.

[6] A. L. Yarin, S. Koombhongse, D. H. Reneker, and I. Introduction, "Taylor cone and jetting from liquid droplets in electrospinning of nanofibers," vol. 90, no. 9, pp. 4836–4846, 2001.

[7] Z. M. Huang, Y. Z. Zhang, M. Kotaki, and S. Ramakrishna, "A review on polymer nanofibers by electrospinning and their applications in nanocomposites," *Compos. Sci. Technol.*, vol. 63, no. 15, pp. 2223–2253, 2003.

[8] J. Doshi and D. H. Reneker, "Electrospinning Process and applications of electrospun fibers," *J. Electrostat.*, vol. 35, pp. 151–160, 1995.

[9] S. Megelski, J. S. Stephens, D. Bruce Chase, and J. F. Rabolt, "Micro- and nanostructured surface morphology on electrospun polymer fibers," *Macromolecules*, vol. 35, no. 22, pp. 8456–8466, 2002.

[10] C. Zhang, X. Yuan, L. Wu, Y. Han, and J. Sheng, "Study on morphology of electrospun poly(vinyl alcohol) mats," *Eur. Polym. J.*, vol. 41, no. 3, pp. 423–432, 2005.

[11] J. M. Deitzel, J. Kleinmeyer, D. Harris, and N. C. B. Tan, "The effect of processing variables on the morphology of electrospun nanofibers and textiles," vol. 42, pp. 261–272, 2001.

[12] C. Guo, L. Zhou, and J. Lv, "Effects of expandable graphite and modified ammonium polyphosphate on the flame-retardant and mechanical properties of wood flour-polypropylene composites," *Polym. Polym. Compos.*, vol. 21, no. 7, pp. 449–456, 2013.

[13] X. Geng, O. H. Kwon, and J. Jang, "Electrospinning of chitosan dissolved in concentrated acetic acid solution," *Biomaterials*, vol. 26, no. 27, pp. 5427–5432, 2005.

[14] A. Greiner and J. H. Wendorff, "Electrospinning : A Fascinating Method for the Preparation of Ultrathin Fibers Angewandte," pp. 5670–5703, 2007.

[15] G. S. Bisht, G. Canton, A. Mirsepassi, L. Kulinsky, S. Oh, D. Dunn-rankin, and M. J. Madou,

"Controlled Continuous Patterning of Polymeric Nanofibers on Three-Dimensional Substrates Using Low-Voltage Near-Field Electrospinning," 2011.

[16] S. P. Rwei and C. C. Huang, "Electrospinning PVA solution-rheology and morphology analyses," *Fibers Polym.*, vol. 13, no. 1, pp. 44–50, 2012.

[17] C. Mit-uppatham, M. Nithitanakul, and P. Supaphol, "Ultrafine Electrospun Polyamide-6 Fibers : Effect of Solution Conditions on Morphology and Average Fiber Diameter," vol. 6, pp. 2327–2338, 2004.

[18] C. L. Casper, J. S. Stephens, N. G. Tassi, D. B. Chase, and J. F. Rabolt, "Controlling Surface Morphology of Electrospun Polystyrene Fibers : Effect of Humidity and Molecular Weight in the Electrospinning Process," pp. 573–578, 2004.

[19] H. Kim, Y. Joo, S. Lee, and C. Kim, "Characteristics of Photoresist-derived Carbon Nanofibers for Li-ion Full Cell Electrode," vol. 15, no. 5, pp. 265–269, 2014.

[20] J. Huang and T. You, "Electrospun Nanofibers : From Rational Design , Fabrication to Electrochemical Sensing Applications," 2013.

[21] S. Saito, "Salt Effect on Polymer Solutions," *J.Poly.Sci., Part A-1*, vol. 7, no. 7, pp. 1789–1802, 1969.

[22] I. Teraoka, *Polymer Solutions: An introduction to physical properties*, vol. 3. 2002.

[23] A. K. Haghi and M. Akbari, "Trends in electrospinning of natural nanofibers," vol. 1834, no. 6, pp. 1830–1834, 2007.

[24] H. Fong, I. Chun, and D. H. Reneker, "Beaded nanofibers formed during electrospinning," *Polymer (Guildf).*, vol. 40, no. 16, pp. 4585–4592, 1999.

[25] Q. P. Pham, U. Sharma, and A. G. Mikos, "Electrospun poly (??-caprolactone) microfiber and multilayer nanofiber/microfiber scaffolds: Characterization of scaffolds and measurement of cellular infiltration," *Biomacromolecules*, vol. 7, no. 10, pp. 2796–2805, 2006.

[26] W. Zuo, M. Zhu, W. Yang, H. Yu, Y. Chen, and Y. Zhang, "Experimental study on relationship between jet instability and formation of beaded fibers during electrospinning," *Polym. Eng. Sci.*, vol. 45, no. 5, pp. 704–709, 2005.

[27] M. M. Hohman and G. Rutledge, "Electrospinning and electrically forced jets . II . Applications," vol. 13, no. 8, pp. 2221–2236, 2001.

[28] C. J. Thompson, G. G. Chase, a. L. Yarin, and D. H. Reneker, "Effects of parameters on nanofiber diameter determined from electrospinning model," *Polymer (Guildf).*, vol. 48, no. 23, pp. 6913–6922, 2007.

[29] N. M. Thoppey, R. E. Gorga, L. I. Clarke, and J. R. Bochinski, "Control of the electric fi eld e polymer solution interaction by utilizing ultra-conductive fl uids," vol. 55, pp. 6390–6398, 2014.

[30] A. F. Spivak, "Asymptotic decay of radius of a weakly conductive viscous jet," 1998.

[31] K. W. Ebagninin, A. Benchabane, and K. Bekkour, "Rheological characterization of

poly(ethylene oxide) solutions of different molecular weights," *J. Colloid Interface Sci.*, vol. 336, no. 1, pp. 360–367, 2009.

[32] C. Tzoganakis, J. Vlachopoulos, a E. Hamielec, and D. M. Shinozaki, "Effect of molecular weight distribution on the rheological and mechanical properties of polypropylene," *Polym. Eng. Sci.*, vol. 29, no. 6, pp. 390–396, 1989.

[33] Y. Zhang, J. Qian, Z. Ke, X. Zhu, and H. Bi, "Viscometric study of poly (vinyl chloride)/ poly (vinyl acetate) blends in various solvents," vol. 38, pp. 333–337, 2002.

[34] J. Ferguson, K. Walters, and C. Wolff, "Shear and extensional flow of polyacrylamide solutions," *Rheol. Acta*, vol. 29, no. 6, pp. 571–579, 1990.

[35] P. Gupta, C. Elkins, T. E. Long, and G. L. Wilkes, "Electrospinning of linear homopolymers of poly (methyl methacrylate): exploring relationships between fiber formation , viscosity , molecular weight and concentration in a good solvent," vol. 46, pp. 4799–4810, 2005.

[36] D. Sun, C. Chang, S. Li, and L. Lin, "Near-Field Electrospinning," 2006.

[37] G. Bisht, G. Canton, A. Mirsepassi, D. Dunn-rankin, L. Kulinsky, and M. Madou, "NOVEL POLYMERIC INKS FOR PRECISION PATTERNING OF CARBON MICRO / NANO-FIBERS USING NEAR-FIELD ELECTROSPINNING," pp. 2–5.

[38] N. Martinez-prieto and M. Abecassis, "Feasibility of Fiber-Deposition Control by Secondary Electric Fields in Near-Field Electrospinning," vol. 3, no. December 2015, pp. 1–6, 2016.

[39] S. Park and G. Heo, *Carbon Fibers*. 1985.

[40] S. Imaizumi, H. Matsumoto, K. Suzuki, M. Minagawa, M. Kimura, and A. Tanioka, "Phenolic Resin-Based Carbon Thin Fibers Prepared by Electrospinning: Additive Effects of Poly(vinyl butyral) and Electrolytes," *Polym. J.*, vol. 41, no. 12, pp. 1124–1128, 2009.

[41] J. Bauer, A. Schroer, R. Schwaiger, and O. Kraft, "Approaching theoretical strength in glassy carbon nanolattices.," *Nat. Mater.*, vol. 15, no. 4, pp. 438–443, 2016.

[42] B. Ding, M. Wang, J. Yu, and G. Sun, "Gas sensors based on electrospun nanofibers," *Sensors*, vol. 9, no. 3, pp. 1609–1624, 2009.

[43] X. Yang, V. Salles, Y. Valentino, M. Liu, M. Maillard, C. Journet, X. Jiang, and A. Brioude, "Sensors and Actuators B : Chemical Fabrication of highly sensitive gas sensor based on Au functionalized WO 3 composite nanofibers by electrospinning," *Sensors Actuators B. Chem.*, vol. 220, pp. 1112–1119, 2015.

[44] I. D. Kim, A. Rothschild, B. H. Lee, D. Y. Kim, S. M. Jo, and H. L. Tuller, "Ultrasensitive chemiresistors based on electrospun TiO 2 nanofibers," *Nano Lett.*, vol. 6, no. 9, pp. 2009–2013, 2006.

[45] D. H. Reneker and A. L. Yarin, "Electrospinning jets and polymer nanofibers," *Polymer (Guildf).*, vol. 49, no. 10, pp. 2387–2425, 2008.

[46] T. Han, A. L. Yarin, and D. H. Reneker, "Viscoelastic electrospun jets: Initial stresses and

elongational rheometry," *Polymer (Guildf).*, vol. 49, no. 6, pp. 1651–1658, 2008.

[47] G. C. Rutledge and S. V Fridrikh, "Formation of fibers by electrospinning," vol. 59, pp. 1384–1391, 2007.

[48] C. J. Thompson, G. G. Chase, a. L. Yarin, and D. H. Reneker, "Effects of parameters on nanofiber diameter determined from electrospinning model," *Polymer (Guildf).*, vol. 48, no. 23, pp. 6913–6922, 2007.

[49] S. a. Theron, a. L. Yarin, E. Zussman, and E. Kroll, "Multiple jets in electrospinning: Experiment and modeling," *Polymer (Guildf).*, vol. 46, no. 9, pp. 2889–2899, 2005.

[50] M. M. Hohman and G. Rutledge, "Electrospinning and electrically forced jets . I . Stability theory," vol. 13, no. 8, pp. 2201–2220, 2001.

[51] J. Eggers, "Nonlinear dynamics and breakup of free-surface flows," *Rev. Mod. Phys.*, vol. 69, no. 3, pp. 865–929, 1997.

[52] C. D. Han, R. R. Lamonte, and Y. T. Shah, "Studies on melt spinning. III. Flow instabilities in melt spinning: Melt fracture and draw resonance," *J. Appl. Polym. Sci.*, vol. 16, no. 12, pp. 3307–3323, 1972.

[53] S. V Fridrikh, J. H. Yu, M. P. Brenner, and G. C. Rutledge, "Controlling the Fiber Diameter during Electrospinning," no. APRIL, pp. 1–4, 2003.

[54] D. H. Reneker and A. L. Yarin, "Bending Instability of Electrically Charged Liquid Jets of Polymer Solutions in Electrospinning," 2000.

[55] H. A. Barnes, *A handbook of elemntary rheology*, 1st ed., vol. 6, no. 4. Wales, 2000.

[56] A. N. Semenov, "Dynamics of concentrated solutions of rigid-chain polymers. Part 1. Brownian motion of persistent macromolecules in isotropic solution," *J. Chem. Soc. Faraday Trans. 2*, vol. 82, no. 3, p. 317, 1986.

[57] M. V. S. Rao, "Viscosity of dilute to moderately concentrated polymer solutions," *Polymer (Guildf).*, vol. 34, no. 3, pp. 592–596, 1993.

[58] T. M. Kulicke Chemic and T. Universit, "The shear viscosity dependence on concentration , molecular weight , and shear rate of polystyrene solutions *)," vol. 83, pp. 75–83, 1984.

[59] S. L. Shenoy, W. D. Bates, H. L. Frisch, and G. E. Wnek, "Role of chain entanglements on fiber formation during electrospinning of polymer solutions: Good solvent, non-specific polymer-polymer interaction limit," *Polymer (Guildf).*, vol. 46, no. 10, pp. 3372–3384, 2005.

[60] T. O. Kashmola and E. S. Kamil, "Structure Rheology of[1] T. O. Kashmola and E. S. Kamil, 'Structure Rheology of Polyethylene Oxide Solution,' Iraqi J. Chem. Pet. Eng., vol. 15, no. 1, pp. 23–32, 2014. Polyethylene Oxide Solution," *Iraqi J. Chem. Pet. Eng.*, vol. 15, no. 1, pp. 23–32, 2014.

[61] P. Sorlier, *Electrospinning and nanofibers*. 2007.

[62] "Measuring_Polymers_using_a_Rotational_Rheometer_in_Oscillatory_Mode.pdf." .

[63] H. Jiang, D. Fang, B. Hsiao, B. Chu, and W. Chen, “Journal of Biomaterials Science , Polymer Edition Preparation and characterization of ibuprofen- loaded poly (lactide-co-glycolide)/ poly (ethylene glycol) -g-chitosan electrospun membranes,” no. October 2013, pp. 37–41, 2012.

[64] C. J. Buchko, K. M. Kozloff, and D. C. Martin, “Surface characterization of porous, biocompatible protein polymer thin films,” *Biomaterials*, vol. 22, no. 11, pp. 1289–1300, 2001.

[65] S. Sukigara, M. Gandhi, J. Ayutsede, M. Micklus, and F. Ko, “Regeneration of Bombyx mori silk by electrospinning - Part 1: Processing parameters and geometric properties,” *Polymer (Guildf).*, vol. 44, no. 19, pp. 5721–5727, 2003.

[66] M. Berta, J. Wiklund, R. Kotzé, and M. Stading, “Correlation between in-line measurements of tomato ketchup shear viscosity and extensional viscosity,” *J. Food Eng.*, vol. 173, pp. 8–14, 2016.

[67] J. Piermar??a, C. Bengoechea, A. G. Abraham, and A. Guerrero, “Shear and extensional properties of kefiran,” *Carbohydr. Polym.*, vol. 152, pp. 97–104, 2016.

[68] C. E. Wagner and G. H. McKinley, “The importance of flow history in mixed shear and extensional flows,” *J. Nonnewton. Fluid Mech.*, vol. 233, pp. 133–145, 2015.

[69] L. M. Smitter, J. C. Ruiz, M. E. Torres, A. J. Müller, and A. E. Sáez, “Elongational flow of solutions of poly(ethylene oxide) and sulfonated surfactants,” *J. Colloid Interface Sci.*, vol. 251, no. 2, 2002.

[70] P. K. Bhattacharjee, D. A. Nguyen, Y. Masubuchi, and T. Sridhar, “Extensional Step Strain Rate Experiments on an Entangled Polymer Solution,” *Macromolecules*, p. acs.macromol.6b00823, 2016.

[71] G. Strobl, *The Physics of Polymers*, vol. 53, no. 9. 2013.

[72] S. O. Deville, Michel (Institute of Mechanical Engineering Swiss Federal Institute of Technology EPFL Lausanne and E. and A. S. B. Gatski, Thomas (Center for Coastal Physical Oceanography and Ocean, *Mathemathical Modelong for Complex Fluids and Flows*, 1st ed. Sroinger-Verlag, 2010.

[73] L. M. Smitter, J. F. Guedez, A. J. Muller, and A. E. Saez, “Interactions between poly(ethylene oxide) and sodium dodecyl sulfate in elongational flows,” *J. Colloid Interface Sci.*, vol. 236, no. 2, pp. 343–353, 2001.

[74] M. Padmanabhan and C. W. Macosko, “Extensional viscosity from entrance pressure drop measurements,” *Rheol. Acta*, vol. 36, no. 2, pp. 144–151, 1997.

[75] D. Sarkar and M. Gupta, “Estimation of Elongational Viscosity,” *Polymer (Guildf).*, vol. 90, 2000.

[76] G. H. Mckinley, S. L. Anna, A. Tripathi, and M. Yao, “Extensional rheometry of polymeric fluids and the uniaxial elongation of viscoelastic filaments,” *Int. Polym. Process. Soc.*, no. June, pp. 1–14, 1999.

[77] N. J. Kim, C. J. Pipe, K. H. Ahn, S. J. Lee, and G. H. McKinley, “Capillary breakup extensional

rheometry of a wormlike micellar solution," *Korea Aust. Rheol. J.*, vol. 22, no. 1, pp. 31–41, 2010.

[78] S. Formenti, R. Castagna, R. Momentè, C. Bertarelli, and F. Briatico-vangosa, "The relevance of extensional rheology on electrospinning : the polyamide / iron chloride case," *Eur. Polym. J.*, vol. 75, pp. 46–55, 2016.

[79] O. Arnolds, H. Buggisch, D. Sachsenheimer, and N. Willenbacher, "Capillary breakup extensional rheometry (CaBER) on semi-dilute and concentrated polyethyleneoxide (PEO) solutions," *Rheol. Acta*, vol. 49, no. 11, pp. 1207–1217, 2010.

[80] H. Winter, "Capillary Rheometry," pp. 1–11, 2008.

[81] S. S. Vadodaria and R. J. English, "Extensional rheometry of cellulose ether solutions: flow instability," *Cellulose*, vol. 23, no. 1, pp. 339–355, 2016.

[82] A. Lindner, J. Vermant, and D. Bonn, "How to obtain the elongational viscosity of dilute polymer solutions?," *Phys. A Stat. Mech. its Appl.*, vol. 319, pp. 125–133, 2003.

[83] J. J. Feng, "Stretching of a straight electrically charged viscoelastic jet," vol. 116, pp. 55–70, 2003.

[84] A. R. Y. R.-M. María Guadalupe Neira-Velásquez, María Teresa Rodríguez-Hernández, Ernesto Hernández-Hernández, "Polymer molecular weight measurement," *Handb. Polym. Synth. Charact. Process.*, pp. 355–366, 2013.

e